HYDRODYNAMICS AND SOLIDS MIXING BEHAVIOUR OF FLUIDIZED BEDS WITH INCLINED-HOLE DISTRIBUTOR

by

Alhussain Bakhurji

B.Sc., The Pennsylvania State University, 2004

A THESIS SUBMITTED IN PARTIAL FULFILLMENT OF
THE REQUIREMENTS FOR THE DEGREE OF

MASTER OF APPLIED SCIENCE

in

THE FACULTY OF GRADUATE AND POSTDOCTORAL STUDIES

(Chemical and Biological Engineering)

THE UNIVERSITY OF BRITISH COLUMBIA

(Vancouver)

June 2017

Abstract

Most research on the hydrodynamics and solids mixing of swirling fluidized beds has targeted applications relate to drying and combustion processes, with large mean particle diameters. A potential use of such reactors is in the area of catalyst regeneration to improve mixing. In the present study, the hydrodynamics and solids mixing behaviour of swirling fluidized beds were investigated for particles in Groups A and B of the Geldart classification. Three distributors were designed and fabricated in-house. They shared the same specifications, but differed in the orifice inclination angle (30°, 45° and 90° to the horizontal).

The effect of orifice angle on the hydrodynamics of a fluidized bed of glass beads was investigated. The study showed that, in an empty bed, the distributor pressure drop was lower for the inclined-hole distributors compared to the 90°-hole distributor by a factor of 10%. In addition, bed pressure drop increased with the inclined-hole distributors as well with static bed height. Bed expansion was also investigated and found that in a shallow bed, the inclined-hole distributor led to less expansion compared to the 90°-hole distributor. However, in a deep bed, the orifice angle had negligible influence on bed expansion. The minimum fluidization velocity was found to change with static bed height for the inclined-hole distributors, and it was also higher for steeper angles.

Solids mixing was also explored, axial mixing for the 90°-hole distributor and tangential mixing for all three distributors. Residence time distribution studies were conducted using phosphorescent tracer particles belonging to Group A, activated by ultraviolet light. The turnover time was estimated using the bubbling bed model and found to match the experimental results well. It was found that the probes installed at the walls of the fluidization column reduced the dense phase downward velocity. The tangential particle velocity was also estimated and was found to be highest for the 30°-hole distributor, decreasing with increasing orifice angle. A dispersion model was used to describe tangential mixing for all three distributors which showed that the dispersion coefficient for the inclined-hole distributors was twice that for the 90°-hole in a shallow bed.

Lay Summary

This work is intended to gain better understanding of the hydrodynamics and solids mixing in a fluidized bed reactor with swirling gas flow. Swirling gas flow was achieved by fabricating two distributors with inclined holes, with the results compared with one distributor with vertical holes. The effect of the inclination angle on several hydrodynamic properties of the fluidized bed was then investigated. The hydrodynamic properties included bed pressure drop in an empty reactor, bed pressure drop in a reactor filled with glass beads, bed pressure drop fluctuations and minimum fluidization velocity. The solids mixing was also investigated using phosphorescent particles that emit light when activated. The vertical solids mixing was described in terms of the turnover time, defined as the time required to turn the particles of the bed over once. The tangential solids mixing was described by adopting a one-dimensional dispersion model.

Preface

This dissertation is original, unpublished, independent work by the author, A. Bakhurji.

Table of Contents

Abstract ii

Lay Summary iii

Preface iv

Table of Contents v

List of Tables viii

List of Figures ix

List of Symbols and Abbreviations xiii

Acknowledgements xvi

Dedication xvii

Chapter 1: Introduction 1

1.1 Swirling fluidized bed 1

1.2 Research objectives 3

1.3 Thesis layout 3

Chapter 2: Literature Review 4

2.1 Distributor design 4

2.2 Flow regimes in a swirling fluidized bed 6

2.3 Effect of orifice angle on distributor pressure drop 6

2.4 Effect of orifice angle on bed pressure drop and minimum fluidization velocity 7

2.5 Effect of orifice angle on particle velocity 8

2.6 Effect of bed inventory and height on hydrodynamics 8

2.7 Effect of particle size on hydrodynamics 9

2.8 Centrifugal fluidized bed 9

2.9 Solids residence time distribution 10

2.10 Solids mixing models 11

Chapter 3: Experimental Design and Methods 13

3.1 Experimental plan 13

3.1.1 Hydrodynamic study 13

3.1.2 Solids mixing study 14
3.2 Properties of bed materials 16
3.2.1 Particle size distribution 16
3.2.2 Bulk density 18
3.3 Distributor design 18
3.4 Instrumentation 19
3.4.1 Pressure transducers 19
3.4.2 Flow and superficial gas velocity 20
3.4.3 Bed height 20
3.4.4 Residence time distribution (RTD) 21
3.5 Data analysis 22
Chapter 4: Hydrodynamic Study 25
4.1 Effects of orifice angle on hydrodynamics 25
4.1.1 Effect on distributor pressure drop (empty bed) 25
4.1.2 Effects on bed pressure drop 26
4.1.3 Effects on pressure drop fluctuations 30
4.1.4 Effects on bed expansion 32
4.1.5 Effects on minimum fluidization velocity 38
4.2 Effects of static bed depth on hydrodynamics 41
4.2.1 Effects on bed pressure drop 41
4.2.2 Effects on pressure drop fluctuations 44
4.2.3 Effects on minimum fluidization velocity 47
4.3 Effects of windbox packing on pressure drop 50
Chapter 5: Solids Mixing Study 58
5.1 Introduction 58
5.2 Measurement system, tracer particles activation and detection 58
5.3 Axial solids mixing 61
5.4 Tangential solids mixing 67
Chapter 6: Conclusions 80
6.1 Major conclusions 80
6.2 Suggestions for future work 82
References 83

Appendices **87**

Appendix A: Distributor designs 87

Appendix B: Pressure transducers calibration procedure 89

Appendix C: Graphical determination of U_{mf} 91

List of Tables

Table 2.1 Advantages and disadvantages of different types of distributor 5
Table 3.1 Hydrodynamic study plan summary 13
Table 3.2 Solids mixing study plan summary 15
Table 3.3 Particle size properties summary 17
Table 3.4 Bulk density measurements for glass beads 18
Table 3.5 Bulk density measurements for phosphorescent particles 18
Table 3.6 Fitting data for distributor pressure drop (empty bed) 23
Table 4.1 Minimum fluidization velocity from empirical equation of Wen and Yu (1966) 39
Table 5.1 Geldart (1997) turnover time estimation 63
Table A.1 Distributor design calculations 88

List of Figures

Figure 3.1 Equipment set-up for hydrodynamics study 14
Figure 3.2 Equipment set-up for solids mixing study 15
Figure 3.3 Particle size distribution for glass beads 16
Figure 3.4 Particle size distribution for phosphorescent tracer particles 17
Figure 3.5a Photo of 30° distributor 19
Figure 3.5b Orifice inclination angles 19
Figure 3.6 Camera set-up for bed height measurement 20
Figure 3.7 Time decay curve for phosphorescent tracer particles 24
Figure 4.1 Effect of orifice angle on distributor pressure drop (empty bed) 25
Figure 4.2 Effects of orifice angle on bed pressure drop for a static bed height of 40 mm 27
Figure 4.3 Effects of orifice angle on bed pressure drop for a static bed height of 60 mm 28
Figure 4.4 Effects of orifice angle on bed pressure drop for a static bed height of 90 mm 29
Figure 4.5 Effects of orifice angle on bed pressure drop for a static bed height of 120 mm 30
Figure 4.6 Orifice angle effect on pressure drop fluctuations for a static bed height of 40 mm 31
Figure 4.7 Orifice angle effect on pressure drop fluctuations for a static bed height of 60 mm 32
Figure 4.8 Bed expansion at both inner and outer walls 33
Figure 4.9 Bed expansion at outer wall for bed height of 40 mm 33
Figure 4.10 Bed expansion at inner wall for bed height of 40 mm 34
Figure 4.11 Bed expansion difference between outer and inner walls for bed height of 40 mm … ……...35
Figure 4.12 Bed expansion at outer wall for bed height of 120 mm 36
Figure 4.13 Bed expansion at inner wall for bed height of 120 mm 37

Figure 4.14 Bed expansion difference between outer and inner walls for bed height of 120 mm…..……..38
Figure 4.15 Minimum fluidization velocity for static bed height of 40 mm 40
Figure 4.16 Minimum fluidization velocity for static bed height of 120 mm 41
Figure 4.17 Normalized bed pressure drop vs. superficial gas velocity for different static bed depths and 30°-hole distributor..... 42
Figure 4.18 Normalized bed pressure drop vs. superficial gas velocity for different static bed depths and 45°-hole distributor..... 43
Figure 4.19 Normalized bed pressure drop vs. superficial gas velocity for different static bed depths and 90°-hole distributor..... 44
Figure 4.20 Pressure drop fluctuations for 30°-hole distributor for different static bed depths..... 45
Figure 4.21 Pressure drop fluctuations for 45°-hole distributor for different static bed depths..... 46
Figure 4.22 Pressure drop fluctuations for 90°-hole distributor for different static bed depths..... 47
Figure 4.23 Effect of static bed depth on minimum fluidization velocity based on two methods for 90°-hole distributor..... 48
Figure 4.24 Effect of static bed depth on minimum fluidization velocity based on two methods for 45°-hole distributor..... 49
Figure 4.25 Effect of static bed depth on minimum fluidization velocity based on two methods for 30°-hole distributor..... 50
Figure 4.26 Photo of 25 mm plastic pall rings packing 51
Figure 4.27 Effect of windbox packing on distributor pressure drop (empty bed) for 90°-hole distributor 52
Figure 4.28 Effect of windbox packing on distributor pressure drop (empty bed) for 45°-hole distributor 53
Figure 4.29 Effect of windbox packing on distributor pressure drop (empty bed) for 30°-hole distributor 54

Figure 4.30 Effect of windbox packing on bed pressure drop for 90°-hole distributor for static bed depth of 60 mm..... 55
Figure 4.31 Effect of windbox packing on bed pressure drop for 45°-hole distributor for static bed depth of 60 mm..... 56
Figure 4.32 Effect of windbox packing on bed pressure drop for 30°-hole distributor for static bed depth of 60 mm..... 57
Figure 5.1 Decay curve fit 60
Figure 5.2 Axial solids mixing experiment diagram showing both axial and radial coordinates 61
Figure 5.3 Normalized corrected tracer concentration for U=0.29 m/s and r=50 mm 62
Figure 5.4 Measured turnover time for axial solids mixing vs. time predicted by Geldart (1997) equation (5-2) 64
Figure 5.5 Dense phase downward velocity measured vs. predicted 66
Figure 5.6 Dense phase downward velocity measured without probes vs. predicted..... 67
Figure 5.7 Top view of fluidized bed surface highlighting both radial and tangential coordinates 68
Figure 5.8 Normalized corrected tracer concentrations for 90°-hole distributor, U=0.17 m/s and r=50 mm 69
Figure 5.9 Normalized corrected tracer concentrations for 90°-hole distributor, U=0.24 m/s and r=50 mm 70
Figure 5.10 Normalized corrected tracer concentrations for 45°-hole distributor, U=0.17 m/s and r=50 mm 71
Figure 5.11 Normalized corrected tracer concentrations for 30°-hole distributor, U=0.17 m/s and r=50 mm 72
Figure 5.12 Tangential particle velocity profiles for 30°-hole distributor between θ = 0°and θ = 180°..... 73
Figure 5.12b Angular particle velocity profiles for 30°-hole distributor between θ = 0°and θ = 180°..... 74
Figure 5.13 Tangential particle velocity profiles for 45°-hole distributor between θ = 0°and θ = 180°..... 75

Figure 5.14 Effect of orifice angle on tangential particle velocity at r=50 mm and between θ = 0°and θ = 180° 76
Figure 5.15 Effect of orifice angle on tangential solids mixing 78
Figure 5.16 Comparison of our experimental tangential dispersion coefficient with horizontal dispersion coefficient from Kunii and Levenspiel (1991) with α=1 79
Figure B.1 Pressure transducer calibration for distributor pressure drop 89
Figure B.2 Pressure transducer calibration for orifice 90
Figure C.1 Illustration of U_{mf} graphical determination..... 91

List of Symbols and Abbreviations

A	Distributor Cross-Sectional Area, m^2
A/D	Analog-Digital
A_o	Orifice Area, m^2
AR	Aspect Ratio, -
C	Tracer Concentration, kg/ m^3
C_d	Orifice Discharge Coefficient, -
C_f	Flow Coefficient, -
CFB	Circulating Fluidized Bed
CSTR	Continuously Stirred Tank Reactor
D	Fluidized Column Inside Diameter, m
$\mathfrak{D}_a$	Dispersion Coefficient, m^2/s
D_b	Bubble Diameter, m
D_{be}	Maximum Bubble Diameter, m
D_{bo}	Initial Bubble Diameter, m
D_c	Fluidized Bed Middle Cylinder Diameter, m
$\mathfrak{D}_h$	Horizontal Dispersion Coefficient, m^2/s
d_h	Holes Diameter, m
d_p	Particle Diameter, m
D_T	Bed Diameter, m
$\mathfrak{D}_t$	Tangential Dispersion Coefficient, m^2/s
E(t)	Residence Time Distribution Function, -
f_w	Wake Fraction, -
g	Acceleration of Gravity, m^2/s
Ho	Static Bed Height, m
H_c	Bed Height at Central Wall, m
H_{mf}	Bed Height at Minimum Fluidization, m
H_w	Bed Height at Outer Wall, m
I	Intensity, volts
I_o	Initial Intensity, volts

K	Distributor Gas Entry Constant, -
L	Expanded bed height, m or tangential distance half way between inner and outer walls, m
L_h	Distributor Hole Pitch, m
n	Number of tanks, -
N	Number of holes, -
N_d	Number of holes' density, m^{-2}
N_{or}	Number of orifices, -
PDI	Pressure Differential Instrument
Pe	Peclet Number, -
PFR	Plug Flow Reactor
Q	Volumetric Flow Rate, m^3/s
r	Radial Coordinate, m
r'	Annulus width, m
RTD	Residence Time Distribution
SCR	Selective Catalytic Reduction
t	Time, s or Thickness, m
t_m	Mean Residence Time, s
U	Superficial gas velocity, m/s
U_b	Bubble Rise Velocity, m/s
U_h	Distributor Hole Velocity, m/s
U_{mf}	Minimum Fluidization Velocity, m/s
U_s	Dense Phase Downward Velocity, m/s
w	Annulus Width, m
Y	Visible Bubble Flow Rate, m^3/s
z	Axial Coordinate, m
ΔP	Differential Pressure, Pa
β_d	Drift Fraction, -
β_w	Wake Fraction, -
δ	Bubble Fraction, -
ε_{mf}	Voidage at Minimum Fluidization, -

μ	Air Viscosity, Pa.s
ρ	Gas Density, kg/ m^3
ρ_s	Particle Density, kg/ m^3
ρ_b	Bulk Density, kg/ m^3
θ	Tangential Coordinate, -
$\boldsymbol{\sigma}$	Variance, s^2
τ	Space Time, s
τ_T	Turnover Time, s
ϕ	Sphericity, -

Acknowledgements

I am thankful for both Dr. Grace and Dr. Bi for their support and supervision during my time working on this research project. They were very helpful and patient with me. I would like also to express my appreciation for Mr. Andrew Mezo from Coanda Research and Development for lending me the phosphorescent particles to use in my research project.

There were many modifications made to the fluidized bed at AMPEL. Without the support from the workshop, the project could not have happenned. Thank you to both Gordon and Doug for their help and support in doing the modifications.

I would like also to thank my colleagues in Chemical and Biological Engineering for their support and encouragement. A special thanks to Eric Dening and Farzam Fotovat. I would like also to thank my sponsoring company Saudi Aramco for approving my sponsorship to UBC and covering all financial obligations.

A special appreciation goes to my family. To my wife Sara, my sons Yusuf, Ibrahim, Salih and to my lovely daughter Arwa. With your smiles and support, I was spiritually inspired to achieve this great work.

Dedication

To my Father and all families who lost a loved one from Cancer

Chapter 1: Introduction

Fluidization is a process in which solid particles are suspended in a fluid-like form subject to several forces acting on them. These forces include gravity, buoyancy and drag. Particles are grouped according to their mean particle size and density in a classification proposed by Geldart (1973) who classified these particles into four different groups (A, B, C and D) for particle densities of typical particles under room temperatures and pressure. Group A (Aeratable) has an average particle size of ~30-100 microns. Group B (Bubbling) has an average particle size of ~100-1000 microns, whereas Group C (Cohesive) has an average particle size of less than ~30 microns and Group D (Spoutable) has an average particle size of more than ~1000 microns.

Fluidized bed reactors can have many configurations, depending on the process being applied. There is the circulating fluidized bed reactor in which solids mixing is improved by circulating the solids back to the bottom of the reactor after passing through a riser. Such processes usually operate at high superficial gas velocity in the fast fluidization flow regime. It is also considered to be a type of reactor with good fluid to particle heat and mass transfer.

In the configuration of the annular fluidized bed, particles are fluidized between concentric outer and inner columns. This type of reactor can combine the benefits of conventional fluidized beds (long residence time) and the circulating fluidized bed (good heat and mass transfer) (Collin et al., 2009).

1.1 Swirling fluidized bed

Another interesting type of fluidized beds is the swirling fluidized bed, where the fluidizing gas is introduced at an inclined angle at the distributor so that there is a tangential component, and the gas swirls inside the fluidization zone. The gas flow can then be divided into two components, a vertical component, that is responsible for supporting the particles

weight-minus-buoyancy, and a horizontal component that induces swirling motion (Sreenivasan et al., 2002). Such reactors typically have a central cone or cylinder that limits the utilization of volume inside the reactor. It is like the annular fluidized bed except for the distributor design in which there can be inclined holes or an annular spiral distributor or any other type with an angle other than 90° to the horizontal axis. Some applications of swirling fluidized beds include drying and combustion processes using Geldart type D particles (Mohideen et al., 2012).

In a swirling fluidized bed, the bed height is an important factor in determining the bed behaviour. A shallow bed usually swirls as a single mass, whereas a deep bed behaves differently. As the bed height increases, two layers of fluidization occur; a bottom layer that is swirling and a top layer that is bubbling (Kaewklum et al., 2009).

A swirling fluidized bed has some advantages over conventional fluidized beds in which there is no swirl. In a swirling bed, due to the inclined angle of gas injection, the process can operate at higher superficial velocity with less elutriation compared to a conventional bed. This is due to the gas injection angle that reduces the vertical component of the gas flow compared to a conventional fluidized bed in which all entering gas flows vertically. The centrifugal force also pushes particles to the outer wall of the column, where the upward gas velocity is lower (Sreenivasan et al., 2002). A disadvantage of the swirling bed is that with increasing air velocity, the swirling affects the particle movement where the particles migrate from the centre to the outer wall. This may create an empty space adjacent to the inner wall of the column in which gas bypassing can occur.

An application that could benefit from the swirling fluidized bed is the decoupled adsorption-reduction selective catalytic reduction (SCR) process for Nitrogen Oxides (NOx). In this process, the flue gas enters the reactor in one region, while the reductant gas enters in an adjacent region in such a way that catalyst particles flow tangentially from an area of adsorption to an area of reduction. An issue found in this application (Yang, 2009) is that

the reactor performance was limited by the catalyst adsorption capacity since the overall NOx conversion increased with decreasing gas velocity in the annulus. Therefore, to improve the catalyst performance, a low gas velocity in the region for adsorption (increasing the catalyst residence time) could be used (Yang, 2009).

1.2 Research objectives

Most previous research on swirling fluidized bed reactors did not use Group A/B particles that are common in catalytic reaction applications. My research on swirling fluidized beds with Group A/B particles focused on investigating the impact of introducing gas flow at an angle at the distributor on the overall residence time and mixing of the particles in the reactor. Specifically, how would changing the inclination angle of orifices in the distributor affect the pressure drop across the distributor and over the bed, the minimum fluidization velocity, the tangential and vertical mixing of particles and the bed expansion?

1.3 Thesis layout

A literature review is presented in Chapter 2 summarizing previous research on the hydrodynamics of swirling fluidized bed, which includes the effects of inclined orifice angle, static bed height and mean particle size on the hydrodynamic behaviour. It also reviews measurement techniques used to determine minimum fluidization velocity, bed expansion and particle residence time. Chapter 3 presents the experimental design, including the distributor design and fabrication, and the instruments used to determine the pressure, residence time and bed height. In addition, the particulate materials used and their properties such as the particle size distribution and bulk density are presented. Chapter 4 reports the results obtained from the hydrodynamics study and discussions, while the results from the solids mixing study are given in Chapter 5. Overall conclusions, as well as recommendations for future work, are presented in Chapter 6.

Chapter 2: Literature Review

There has been limited research on the hydrodynamics and solids mixing of swirling fluidized beds. In this chapter, a detailed review of previous work on swirling bed hydrodynamics is presented. Also, techniques for determining solids residence time distributions in fluidized beds that could be useful when applied to a swirling bed are summarized.

2.1 Distributor design

The design of the gas distributor is very important for fluidized beds. Karri (2003) summarized the purposes of gas distributors as follows:

- Induce fluidization over the bed.
- Prevent dead areas in the bed where no fluidization occurs.
- Increase operation time without plugging.
- Minimize weepage of particles into the windbox.
- Minimize attrition of bed materials.
- Support the bed weight both during operation and during shutdowns.

Advantages and disadvantages of several different geometries of distributors are summarized in Table 2-1.

Table 2-1 Advantages and disadvantages of different types of distributor (Karri, 2003)

Types of Grids	Advantages	Disadvantages
Perforated Plates 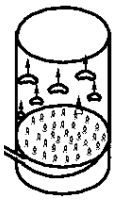	1. Easy to make. 2. Cheap. 3. Easy to change and modify hole size. 4. Easy to scale. 5. Easy to clean.	1. Weepage. 2. Thermal distortion.
Bubble Caps and Nozzles 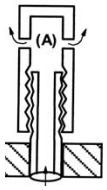	1. Less weepage. 2. Good turndown. 3. Internals support.	1. Expensive. 2. May have stagnant regions. 3. Hard to clean. 4. Hard to modify.
Spargers 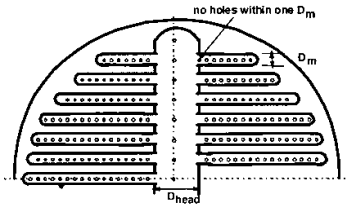	1. Minimum weeping. 2. Good turndown. 3. Low pressure drop. 4. Good internals support. 5. Can withstand thermal expansion.	1. Solids defluidization under the grid.
Conical Grids 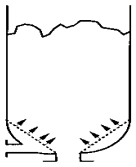	1. Promote solids mixing. 2. Prevent stagnant zones. 3. Minimize segregation of particles.	1. Difficult to fabricate. 2. Difficult to design. 3. High pressure drop.
Pierced Sheet Grids 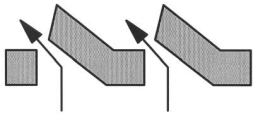	1. Promote solids mixing. 2. Prevent stagnant zones. 3. Good for solids discharge. 4. Prevent weeping.	1. Difficult to fabricate. 2. Small holes size only. 3. Requires more support underneath to support bed materials.

Different distributor designs can be used in a swirling fluidized bed. Ouyang et al. (1986) proposed a new design of distributor called the spiral distributor and evaluated its performance in comparison to the sintered-plate distributor. The spiral distributor was made of overlapping plates with variable gaps inbetween. The gap length was highest at the wall and zero at the centre. This way, an angle was formed that caused the gas to swirl as it entered the bed.

Other interesting types have inclined blades in three rows and a perforated plate with inclined holes. Kumar et al. (2011) studied the dynamic behaviour of these types of distributors in terms of the variation of bed pressure drop with varying air velocity.

2.2 Flow regimes in a swirling fluidized bed

Several researchers studied the flow regimes in swirling fluidized beds (Sreenivasan et al. 2002, Kaewklum et al. 2009, 2010). Their studies identified four distinct regimes of operation. With increasing gas velocity, the first regime is the bubbling regime which starts when the first bubbles appear in the bed. With increasing superficial velocity, the bed becomes wavelike, with dunes forming on the surface; within this flow regime, localized swirling occurs randomly in the bed. It is sometime also called a slugging regime. The third regime is the two-layer fluidization that can be seen only in deep beds with bed height exceeding 45 mm, according to Sreenivasan et al. (2002). In this case, two distinct layers are visible, a bottom swirling layer and a top bubbling layer. The fourth flow regime is stable swirling; in this regime, the bed behaves as a rotating fluid with the bed height varying in the radial direction (higher near the outer wall and lower near the inner wall or centre).

2.3 Effect of orifice angle on distributor pressure drop

Ouyang et al. (1986) plotted the pressure drop across the distributor against the superficial gas velocity for spiral and sintered plate distributors. They found that the pressure drop for the spiral distributor was 1 to 2 orders of magnitude smaller than for the sintered plate.

Kumar et al. (2011) also studied the variation of distributor pressure drop with superficial gas velocity for spiral distributors, inclined blades in three rows and perforated plates with inclined holes. They found that the pressure drop was highest for the perforated plate with inclined holes due to its high thickness and low open area ratio.

2.4 Effect of orifice angle on bed pressure drop and minimum fluidization velocity

Sreenivasan et al. (2002) studied the performance of a spiral distributor in terms of bed pressure drop versus the superficial gas velocity for two sizes of PVC particles and two bed heights. They found that, unlike conventional fluidized beds, the bed pressure drop always increased with increasing superficial gas velocity in the swirling fluidized bed. This indicated that there was an additional force acting on the bed in addition to its weight. The magnitude of this force is proportional to the centrifugal force and increases with increasing superficial gas velocity.

Unlike a conventional bed, Sreenivasan et al. (2002) also found that the minimum fluidization velocity, which, by definition, is also identical to the minimum bubbling velocity of the swirling fluidized bed of group B particles, increased with increasing static bed height. Yudin et al. (2016) studied the effect of distributor configuration on the pressure drop across the bed and the minimum fluidization velocity. They used three different distributor configurations, a conventional perforated plate with 11% opening ratio, a 45-degree inclined slots and a 90-degree inclined slots with 13% opening ratio each. They discovered that the pressure drop was lowest for the 90-degree inclined slots, followed by the 45-degree inclined slots, and highest for the conventional perforated plate. They also found that the minimum fluidization velocity was lowest in the case of a perforated plate, followed by the 45-degree inclined slots, and then the 90-degree inclined slots.

Naz et al. (2016) studied the particle movement on the top and side of a swirling fluidized bed with 12-degree inclination angle to the horizontal by particle tracking velocimetry. They did not find any effect of increasing the superficial gas velocity on the bed pressure drop.

Kumar et al. (2011) also studied the variation of bed pressure drop with superficial gas velocity for three types of distributors with Group D particles of average diameter 7.8 mm. They found that bed pressure drop was almost constant after reaching the minimum fluidization velocity for both inclined-blade single-row and inclined-blade three-row distributors. However, for the case of the inclined-holes distributor, the bed pressure drop continued to increase with increasing superficial velocity. Unfortunately, they did not report the behaviour at fluidization velocities beyond 0.1 m/s for the inclined-holes perforated plate distributor.

2.5 Effect of orifice angle on particle velocity

Some researchers have studied the hydrodynamics of swirling fluidized beds in terms of particle motion in the bed. Miin et al. (2015) used particle imaging velocimetry to observe particle motion in the swirling flow regime for three distributor angles (12, 15 and 18 degrees to the horizontal) and PVC particles of average diameter 3.9 mm. Their results showed that tangential particle velocity decreased with increasing blade angle. They concluded that a 3 degree increase in blade angle caused an 18% reduction in tangential particle velocity. Naz et al (2016) did work similar to that of Miin et al. (2015). However, their work focused primarily on the top and side sections of the swirling bed. They used three different blade angles (10, 15 and 20 degrees to the horizontal). They also found that the average particle velocity decreased with increasing blade angle.

2.6 Effect of bed inventory and height on hydrodynamics

Researchers focused on the effect of bed inventory, while others reported the effects of bed height on the dynamic behaviour of swirling beds. Both properties of the bed usually come together since a lower solids inventory in a given bed corresponds to a lower bed height. Kaewklum et al. (2009, 2010) studied the effect of static bed height for a 14-degree inclined annular spiral distributor. They concluded that increasing the static bed height caused an increase in both the minimum fluidization velocity and bed pressure drop. Research of Yudin et al. (2016) on the effect of aspect ratio (ratio between bed height and diameter) on the bed pressure drop and minimum fluidization velocity showed that, unlike a conventional bed, the

minimum fluidization velocity changes with changing aspect ratio (height/diameter). They found that with increasing aspect ratio, the minimum fluidization velocity increased.

Miin et al. (2015) studied the effect of bed weight on tangential particle velocity using PVC particles with an average diameter of 3.9 mm. They found that tangential particle velocity decreased with increasing bed weight. Kumar et al. (2011), on the other hand, compared the performance of three distributors in terms of bed expansion with increasing superficial gas velocity. Their work showed that bed expansion started at lower superficial gas velocities for shallow beds with an inclined-holes distributor.

2.7 Effect of particle size on hydrodynamics

Sreenivasan et al. (2002) tested two diameters of PVC particles, 2.5 and 3.5 mm. Their work showed minimal impact of particle size on the bed pressure drop. Yudin et al. (2016) investigated the effect of particle size on the degree of solids mixing for three average particle sizes: 177, 520 and 756 microns. They concluded that the degree of mixing increased with decreasing particle size. Miin et al. (2015) reported that the particle size had less influence on tangential particle velocity than the solids inventory.

2.8 Centrifugal fluidized bed

Note that the centrifugal fluidized bed is another type of fluidized bed in which the bed rotates around its axis of symmetry. Particles are fluidized because of high centrifugal forces controlled by the speed of the rotor. This type of fluidized bed system may be useful in applications where high superficial velocities are needed, but without large bubbles to improve gas-solid contact. Kroger et al. (1979) predicted the pressure drop in this system along with the radial flow distribution. Takahashi et al. (1984) used a horizontal rotating fluidized bed to study bed pressure drop. They concluded that the bed pressure drop reached a maximum value at minimum fluidization and, with further increase in the superficial velocity, the bed pressure drop slightly decreased.

2.9 Solids residence time distribution

The residence time distribution (RTD) portrays the time each particle or fluid element spends inside a chemical reactor. It is a very important parameter in characterizing chemical reactors. The RTD gives information regarding mixing inside the reactor. For example, in a continuously stirred tank reactor (CSTR), the system is considered perfectly mixed compared to a plug flow reactor (PFR) where no mixing takes place. The RTD can be measured experimentally by introducing a tracer and then measuring the tracer concentration at the exit as a function of time (Fogler, 2006). There are two main methods of tracer injection in the literature: pulse and step-change inputs. The pulse input, as the name suggests, introduces a high concentration of tracer in a very short time. On the other hand, the step-change input introduces the tracer at a constant concentration and flow beginning at time zero. In both cases, one then measures the concentration at the exit as a function of time.

Several experimental methods have been used by researchers to determine the RTD of different reactors. Harris et al. (2002) used phosphorescent tracer particles that can be activated using high-intensity light to measure the RTD in a circulating fluidized bed (CFB) riser. They activated the tracer at a known location at the base of the riser and detected the tracer at the outlet of the riser in order to measure the RTD of the riser. Kojima et al. (1989) investigated the solids behaviour in a fast fluidized bed. They used tracer particles with fluorescent dye. Ran et al. (2001) used phosphor tracer to determine the lateral solids dispersion in a high-density CFB riser, with the phosphor particles illuminated by a flashlight. The particles then emitted light while moving and were detected by a light detector. The concentration was then adjusted by subtracting the decay of phosphor from the detected signal. Ghaly et al. (2012) used a simple method to determine the RTD. Colored Styrofoam balls were injected at the centre of the bed containing sand particles. They used an electronic stop-watch to measure the time it took each ball to appear at the surface of the bed. Morooka et al. (1989) measured local fines movement in a fluidized bed by means of a fluorescent tracer. They coated the catalyst particles with fluorescent dye which was then used as the tracer.

Fluorescent dye only emits light while being activated. Therefore, a special optical fiber probe is used to measure local concentration. The probe itself sends out ultraviolet light and receives signals from the dye at the same location. This fluorescent dye tracer technique was used previously by Baba et al. (1984) to determine the flow patterns of solid particles at arbitrary locations. Pallares et al. (2006) developed a technique to track particles in a cold 2-dimensional fluidized bed to simulate fuel dispersion. They used phosphorescent tracer particles that were video recorded and digitally analyzed to determine the concentration profiles. Alternative methods have been used by other researchers. Goswami et al. (2014) measured the mixing time of solids using a radiotracer, Gold-198 radioisotope, to label sand particles. On the other hand, Liu et al. (2012) used a thermal tracing technique to quantify lateral solids mixing, with sand particles as bed material and as tracers. The tracer particles were heated and then injected into the bed resulting in a stepwise increase of temperature inside the bed, where magnitude as a function of time was used to determine the RTD.

2.10 Solids mixing models

After looking at the RTD techniques, prediction of flow pattern and mixing behaviour is needed in non-ideal reactors. Such predictions are usually based on modelling. There are several types of models. There are one-parameter models such as the tanks-in-series model or the dispersion model. Two-parameter models include reactors with dead volume or bypassing. The RTD data are used to test the validity of these models.

The most common one-parameter model is the tanks-in-series model in which the parameter is the number of tanks. Dispersion models are widely used also, where the parameter is the dispersion coefficient. Usually, the RTD data is analyzed from pulse tracer tests to estimate model parameters. The RTD function for a series of n equi-size CSTRs is given by (Fogler, 2006):

$$\boldsymbol{E(t) = \frac{t^{n-1}}{(n-1)!\tau_i^n} e^{-t/\tau_i}} \qquad (2\text{-}1)$$

Where τ_i is the space time (ratio of volume to flow rate) in one of the reactor, and since all reactors have the same volume, therefore, $\tau_i = \tau/n$. The number of tanks in series is then found using the variance of the RTD data as follows (Fogler, 2006):

$$n = \frac{\tau^2}{\sigma^2} \qquad (2\text{-}2)$$

Dispersion models assume axial dispersion of solids superimposed on the flow. The RTD data are used to estimate the dispersion coefficient. However, the dispersion model needs to be solved first, requiring clear understanding of the problem and the boundary conditions (Fogler, 2006).

$$\mathfrak{D}_a \frac{\partial^2 C}{\partial z^2} - \frac{\partial (UC)}{\partial z} = \frac{\partial C}{\partial t} \qquad (2\text{-}3)$$

Typical boundary conditions are the closed-closed and the open-open vessel. In a closed-closed vessel, it is assumed that there is no dispersion across both the entrance and exit, whereas in an open-open vessel, it is assumed that there is dispersion across both boundaries. The solution to the model equation differs in these two cases (Fogler, 2006).

Chapter 3: Experimental Design and Methods

3.1 Experimental plan

The experimental plan involves two parts: hydrodynamics study and solids mixing study.

3.1.1 Hydrodynamic study

The hydrodynamic study focused mainly on studying the effect of the distributor hole inclination angle on distributor pressure drop, bed pressure drop, bed height, minimum fluidization velocity and pressure fluctuations. The plan of the hydrodynamic study is summarized in Table 3-1.

Table 3-1 Hydrodynamic study plan summary

Distributor Hole Inclination Angle	Bed Material	Bed Height (mm)	Measured Variables
30	Glass beads	40, 60, 90 and 120	Bed and distributor pressure drop, air superficial velocity and bed expansion
45			
90			

Figure 3-1 presents the equipment set-up. In the figure, D is the fluidized column diameter measured to be 300 mm, D_c is the central cylinder diameter measured to be 90 mm and H_{mf} is the bed height at minimum fluidization which is selected to be 40, 60, 90 and 120 mm.

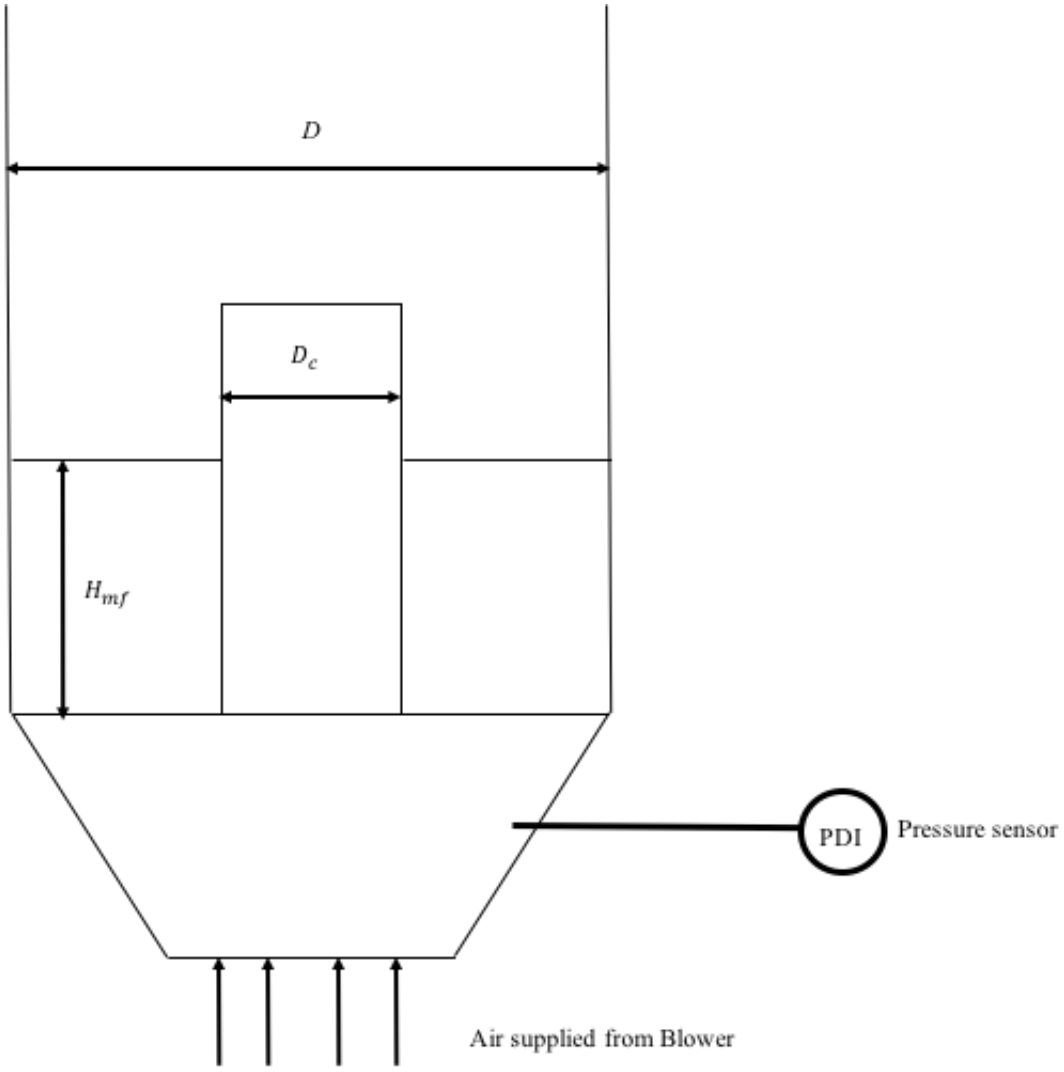

Figure 3-1 Equipment set-up for hydrodynamics study

3.1.2 Solids mixing study

The solids mixing study investigated the mixing behaviour of phosphorescent particles. First, using the vertical distributor, the residence time distribution (RTD) was measured and the turnover time was estimated based on the RTD data. Then, for all distributors and by assuming very fast axial mixing, the tangential dispersion coefficient was estimated using the dispersion model. Table 3-2 summarizes the experimental plan for the solids mixing study, while Figure 3-2 shows the equipment setup for the mixing study.

Table 3-2 Solids mixing study summary

Distributor Inclination Angle	Bed Material	Bed Height (mm)	Detectors Position	Measured Variables
30	Phosphorescent particles	100	Tangential and radial at same axial position	RTD and air superficial velocity
45				
90		100	Tangential, axial and radial at same tangential position	

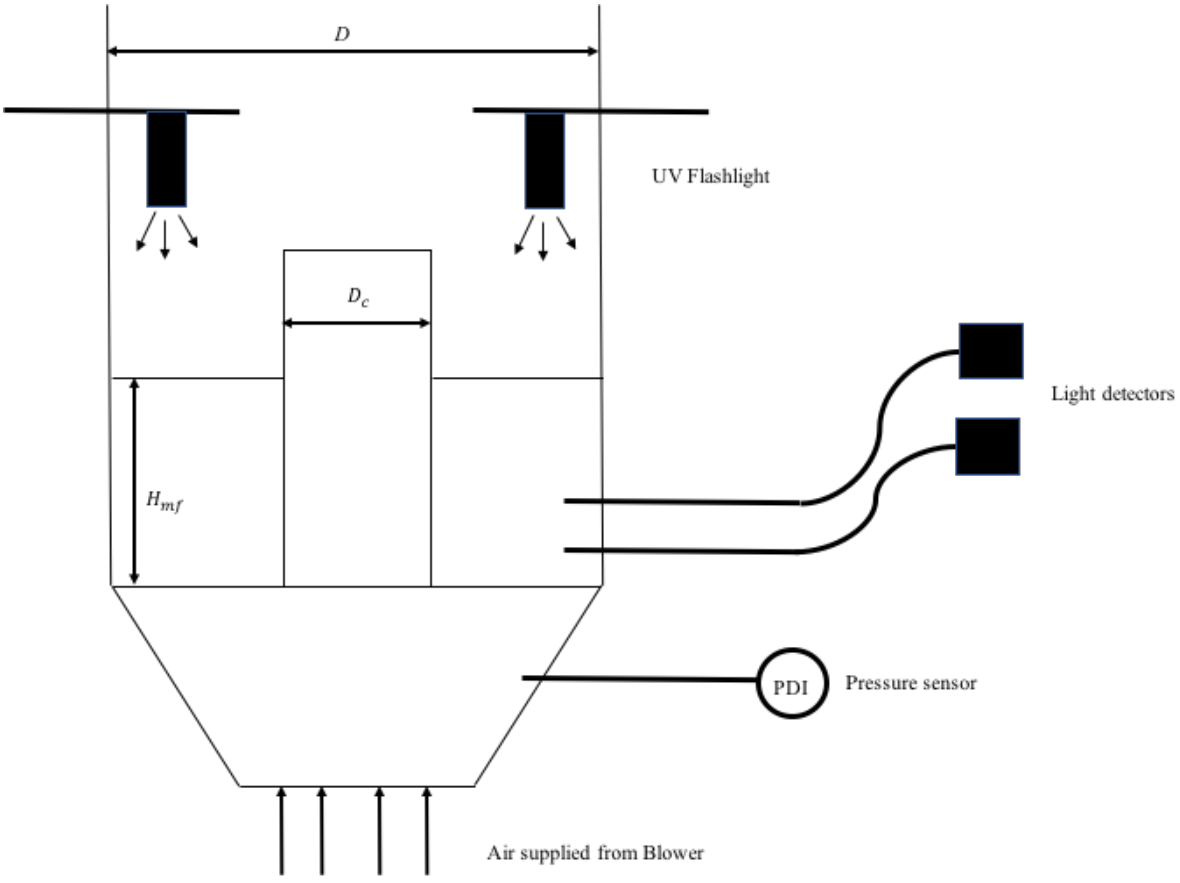

Figure 3-2 Equipment set-up for solids mixing study

3.2 Properties of bed materials

Two types of particles were used: Glass beads and Phosphorescent particles. Two major properties were determined: particle size distribution and bulk density.

3.2.1 Particle size distribution

The particle size distribution was determined using the laser diffraction equipment (Malvern Mastersizer 2000E). The volume mean particle size for glass beads was determined to be 154 microns, while for phosphorescent it was 76 microns. Figures 3-3 and 3-4 show the particle size distributions, while Table 3-3 summarizes key particle size properties.

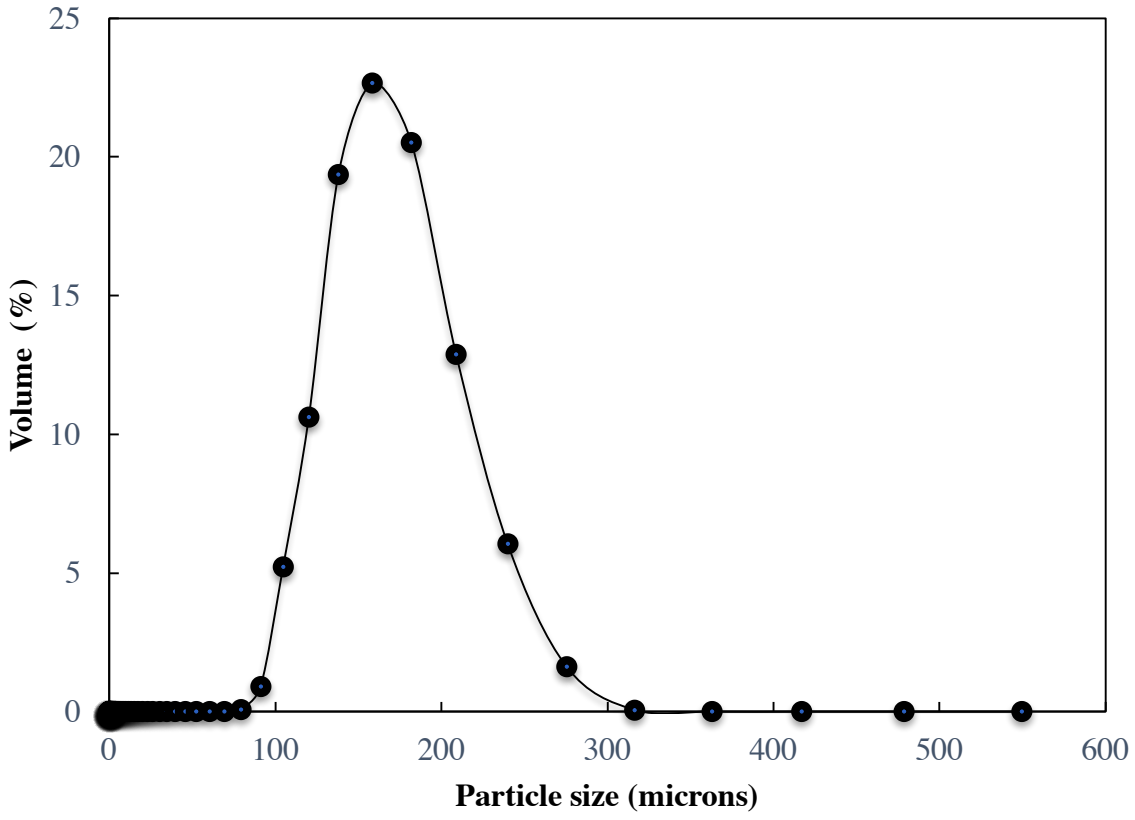

Figure 3-3 Particle size distribution for glass beads

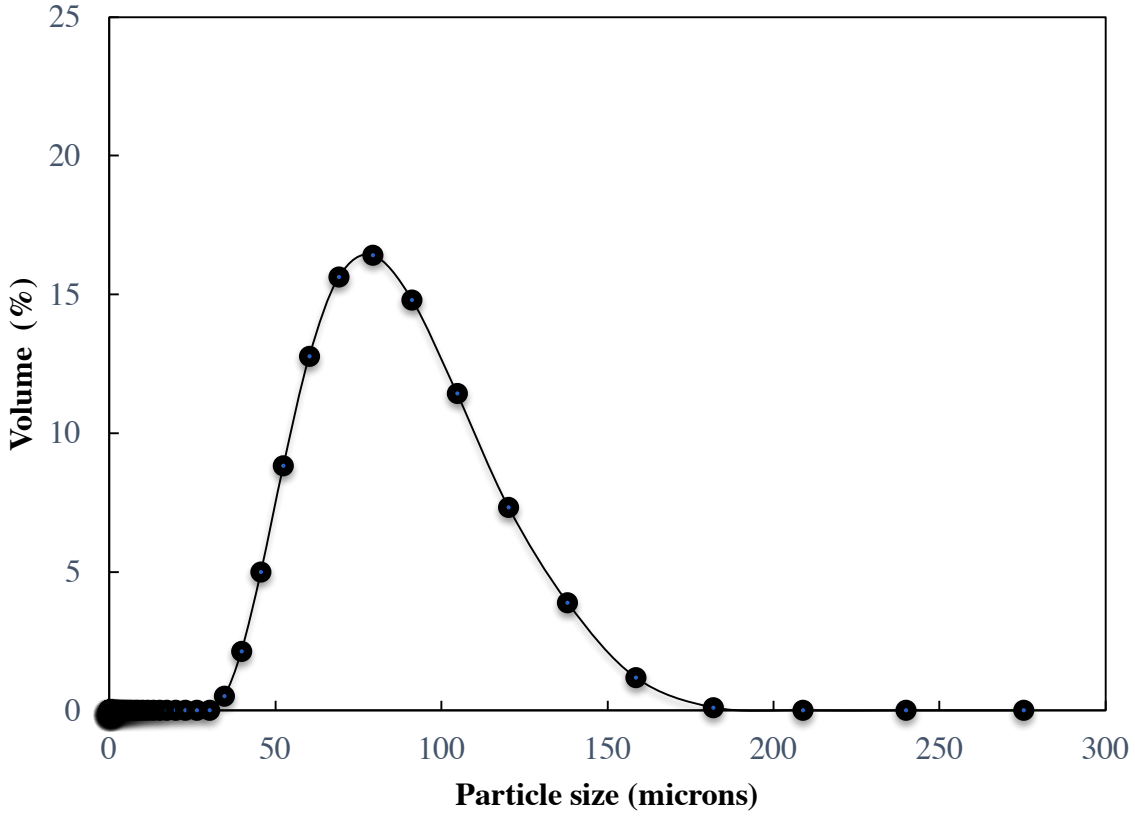

Figure 3-4 Particle size distribution for phosphorescent tracer particles

Table 3-3 Particle size properties summary

Property	Glass Beads	Phosphorescent particles
Volume-Weighted Mean (microns)	154	76
Surface-Weighted Mean (microns)	146	69
d(0.9) (microns)	202	109
d(0.5) (microns)	150	72
d(0.1) (microns)	111	48

3.2.2 Bulk density

Bulk density was determined by weighing the material in a volumetric flask and then measuring the volume it occupies. Three trials were performed and the average was recorded for each material. Tables 3-4 and 3-5 show the trial results for glass beads and phosphorescent particles, respectively.

Table 3-4 Bulk density measurements for glass beads

	Trial 1	Trial 2	Trial 3	Average
Mass (g)	20.9	41.8	70.8	
Volume (ml)	14	28	47	
Bulk Density (g/ml)	1.49	1.49	1.51	
Bulk Density (kg/m^3)	1493	1493	1506	1497

Table 3-5 Bulk density measurements for phosphorescent particles

	Trial 1	Trial 2	Trial 3	Average
Mass (g)	16	31.2	52.2	
Volume (ml)	10	20	35	
Bulk Density (g/ml)	1.6	1.56	1.49	
Bulk Density (kg/m^3)	1600	1560	1491	1550

3.3 Distributor design

Three distributors were fabricated in-house using Plexiglas. The distributor plate thickness was 9.5 mm, while the hole diameter was 3.2 mm. All three distributors had 60 holes in total. Refer to Appendix-A for details of distributor design calculations. The three distributors were

all the same except for the orifice inclination angle. Three inclination angles were chosen: 90°, 45° and 30° , all measured from the horizontal axis. Figure 3-5a shows a photo of one of the three distributors and Figure 3-5b shows a representation of the angle inclination.

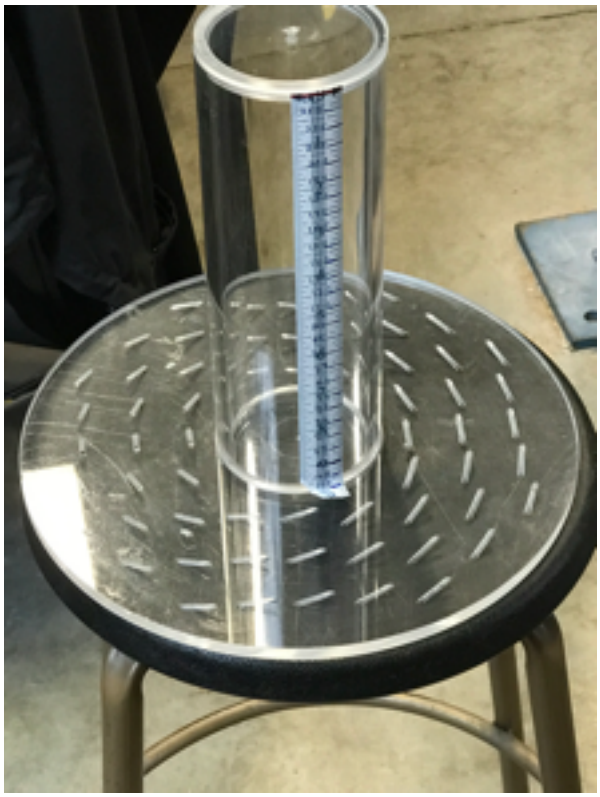

Figure 3-5a Photo of 30° distributor

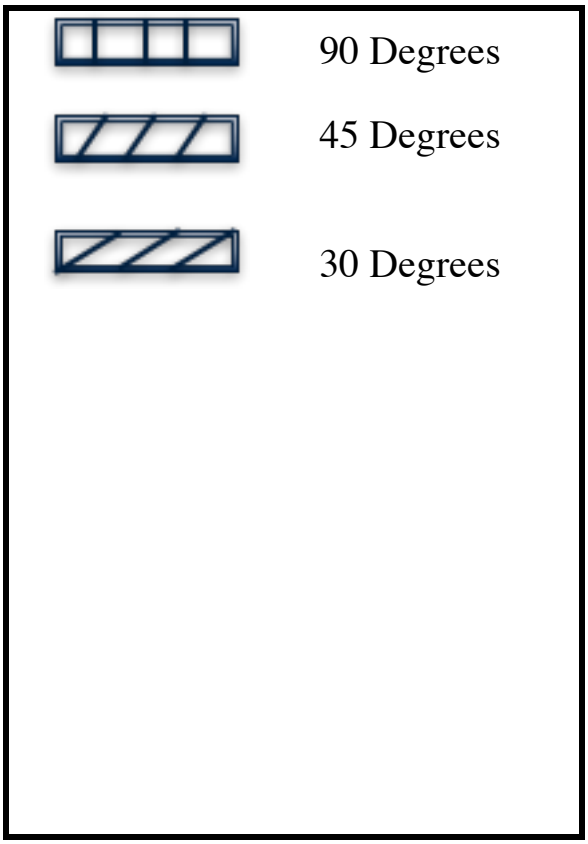

Figure 3-5b Orifice inclination angles

3.4 Instrumentation

3.4.1 Pressure transducers

Pressure was measured using pressure transducers of type OMEGA PX-140. Only one transducer was used to measure the overall pressure drop. One port of the transducer legs was connected to a port under the distributor, while the other port was connected to the freeboard region of the column.

3.4.2 Flow and superficial gas velocity

The air flow rate was measured using an orifice meter. The pressure drop across the orifice was measured using an OMEGA PX-140 pressure transducer. The flow rate was then calculated using the following formula (Karri, 2003):

$$Q = C_f A_o \sqrt{\frac{2\Delta P}{\rho}} \qquad (3\text{-}1)$$

where C_f is the flow coefficient and A_o is the orifice area. The flow coefficient is a function of Reynolds number and orifice-to-pipe diameter ratio. The value of the coefficient was calculated to be 0.61 according to Perry et al. (2008). The superficial gas velocity was then calculated by (Karri, 2003):

$$U = \frac{4Q}{\pi\left(D^2 - D_c^2\right)} \qquad (3\text{-}2)$$

3.4.3 Bed height

The bed height was measured visually from the transparent outer wall using a ruler. In addition, a web camera connected to a computer was installed inside the bed to capture the bed height at the central wall. Figure 3-6 shows the camera set-up.

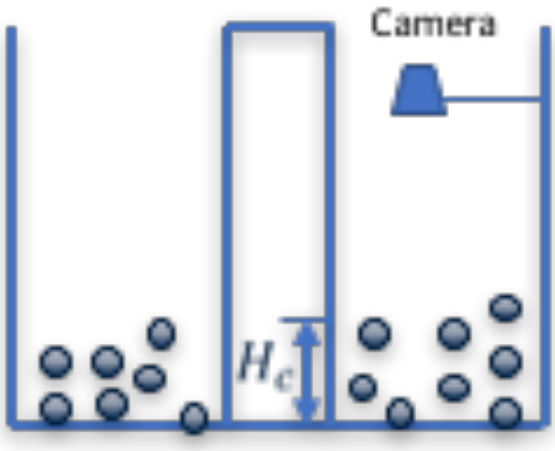

Figure 3-6 Camera set-up for bed height measurement

3.4.4 Residence time distribution (RTD)

The RTD was measured in the solids mixing study using light detectors. Two different methods were used to measure the RTD: one for the vertical (90°) hole distributor and the other for the inclined-hole (45° and 30°) distributors. Both methods required the activation of particles while the bed is stagnant. This was because the phosphorescent tracer particles took a long time to get activated, and using the UV light alone to activate the particles while the bed is fluidized was not possible since the intensity was too small to be detected.

For the vertical distributor, the intention was to measure the turnover time and dense phase downward velocity. Therefore, the light detector probes were placed at different heights, one at z = 80 mm and the other was directly below it at z = 50 mm. The bed was full of phosphorescent particles that were activated by two UV lamps at the top of the bed. Both lamps were turned on to ensure that the whole surface of the bed was illuminated. Then, once the particles were activated, the air flow valve was opened, causing the particles to travel from the top of the bed axially downward and then upward in a cyclic motion. The probe at z = 80 mm detected the first tracer followed by the probe at z = 50 mm. This way, the RTD was measured for the vertical distributor. In addition, the probes were also inserted to different radial positions from the inner wall. Three radial positions measured from the inner wall towards the outer wall across the annulus were tested: 25, 50 and 75 mm. The intention was to see whether the axial mixing varied with radial position.

To measure the tangential dispersion for the inclined distributors and the vertical one, the method was quite different. The probes were installed at the same height, but at different tangential and radial positions from the inner wall. Three tangential positions: 0° , 90° and 180° were chosen in addition to three radial positions: 25, 50 and 75 mm. The UV light was directed onto only one sector at the surface of the bed covering the tangential positions being tested. Therefore, only particles at the top section near the first probe were activated. The particles were assumed to move tangentially from 0° to 360° counter clockwise in the direction of the inclined angle of the distributor holes. Therefore, the first detector located at

$\theta = 0°$ for example detected the tracer signal first followed by the detector at $\theta = 90°$, where θ is the angle in a top view of the column.

3.5 Data analysis

The data captured during the hydrodynamic study were the pressure readings from the transducers. One pressure reading was captured at the distributor and one at the orifice meter. Calculations were made to determine other data such as the superficial gas velocity. Both pressure transducers were calibrated using a manometer. The calibration data and procedures are provided in Appendix-B. For every test, a confidence interval of 90% was used by repeating the experiment three times for the calculation of error bars reported in each graph.

The bed pressure drop was determined by subtracting the distributor pressure drop (empty bed) from the total pressure drop captured by the transducers. First, the column was operated empty and the distributor pressure drop was measured by the pressure transducers for different superficial gas velocities. The data captured were fitted to a 4^{th} order polynomial function. Then, once the column was operated with particulate materials, the transducer measured the total pressure drop. The bed pressure drop data were then obtained by subtracting the distributor data from the fitted 4^{th} order polynomial function from the data captured by the transducer. Table 3-6 presents the fitted functions for all three distributors, together with the corresponding R-squared values, where the superficial gas velocity ranged from 0 to 0.3 m/s and the pressure drop is in Pascals.

Table 3-6 Fitting data for distributor pressure drop (empty bed)

Distributor hole angle	Fitted Function	R-Squared Value	Range of U (m/s)
90 Degrees	$-9.7\times10^5u^4+2.97\times10^5u^3-1856u^2+2106u+10.3$	0.999	0 to 0.3
45 Degrees	$1\times10^6u^4-4.4\times10^5u^3+8.5\times10^4u^2-2121u-0.33$	0.999	0 to 0.3
30 Degrees	$6.7\times10^5u^4-2.4\times10^5u^3+54482u^2-561u-0.4$	0.999	0 to 0.3

The minimum fluidization velocity was determined from the bed pressure drop and superficial gas velocity curve. Once the bed materials are supported by their weight, the superficial gas velocity was determined to be the minimum fluidization velocity. This is achieved when the bed pressure drop flattens out. Another method for determining the minimum fluidization velocity utilized by Felipe et al. (2007) for Group B particles was by using the standard deviation of pressure fluctuations. They studied four types of particles that included both Groups A and B. They showed that the minimum bubbling velocity can be estimated with high accuracy by assuming a linear relationship between standard deviation of pressure and the superficial fluid velocity. Moreover, the minimum fluidization velocity was also observed visually, and it was also estimated based on the correlation of Wen and Yu (1966).

The data captured during the solids mixing study were the pressure readings from the orifice meter to find the superficial gas velocity and the readings from the light detectors to measure the signals from the tracer particles. The Phosphorescent tracer intensity decays with time. Therefore, a correction must be made to the measured signals. The same equipment set-up presented in Figure 3-2 was used for the decay experiment. Phosphorescent particles were loaded in the reactor, and the UV light was turned on for 12 minutes. When the UV light was turned off, the signal from the particles started to decay. The light detector then detected

the signal as the particles continued to decay. Figure 3-7 shows the decay curve for the phosphorescent particles.

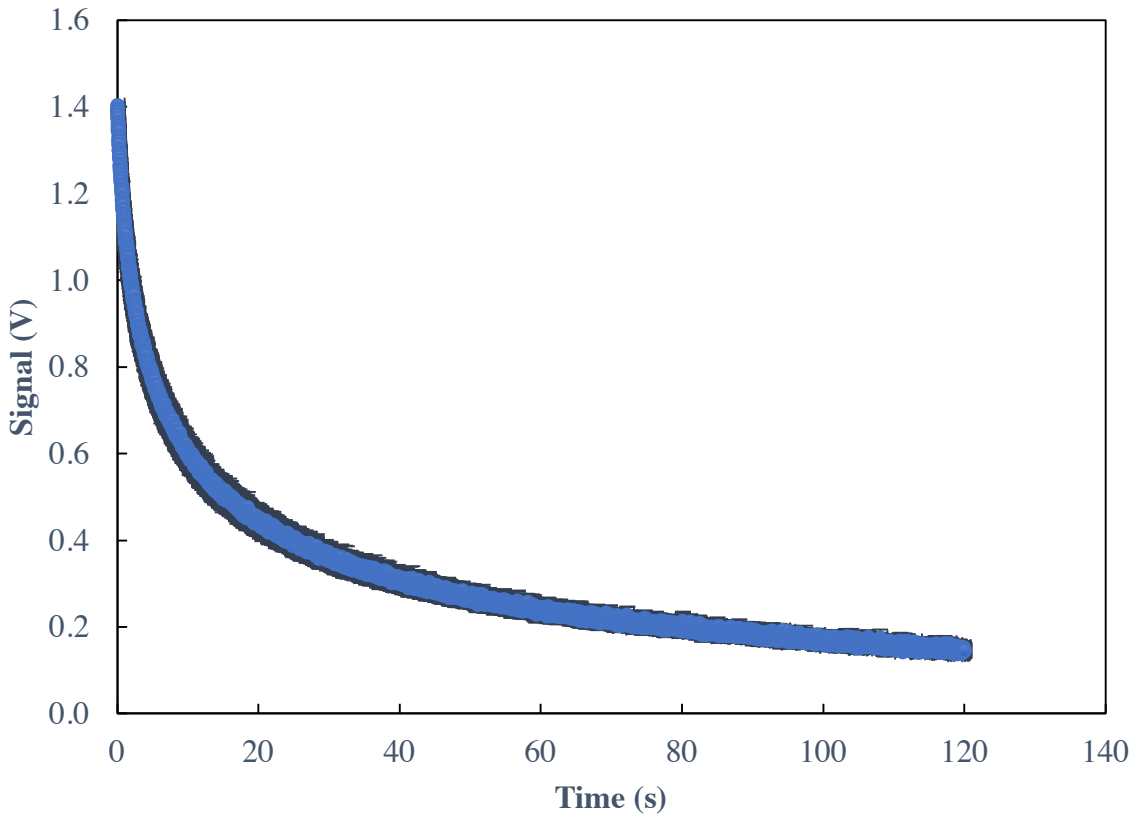

Figure 3-7 Time decay curve for phosphorescent tracer particles

Chapter 4: Hydrodynamic Study

This chapter presents the results from the hydrodynamic study. They include the effects of orifice angle, static bed height and windbox packing on the hydrodynamics of the fluidized bed. The hydrodynamic properties investigated were the distributor pressure drop, bed pressure drop, pressure fluctuations, bed expansion and minimum fluidization velocity.

4.1 Effects of orifice angle on hydrodynamics

The effects of orifice inclination angle on distributor pressure drop, bed pressure drop, pressure drop fluctuations, bed expansion and minimum fluidization velocity were examined.

4.1.1 Effect on distributor pressure drop (empty bed)

Figure 4-1 shows the effect of orifice angle on the distributor pressure drop.

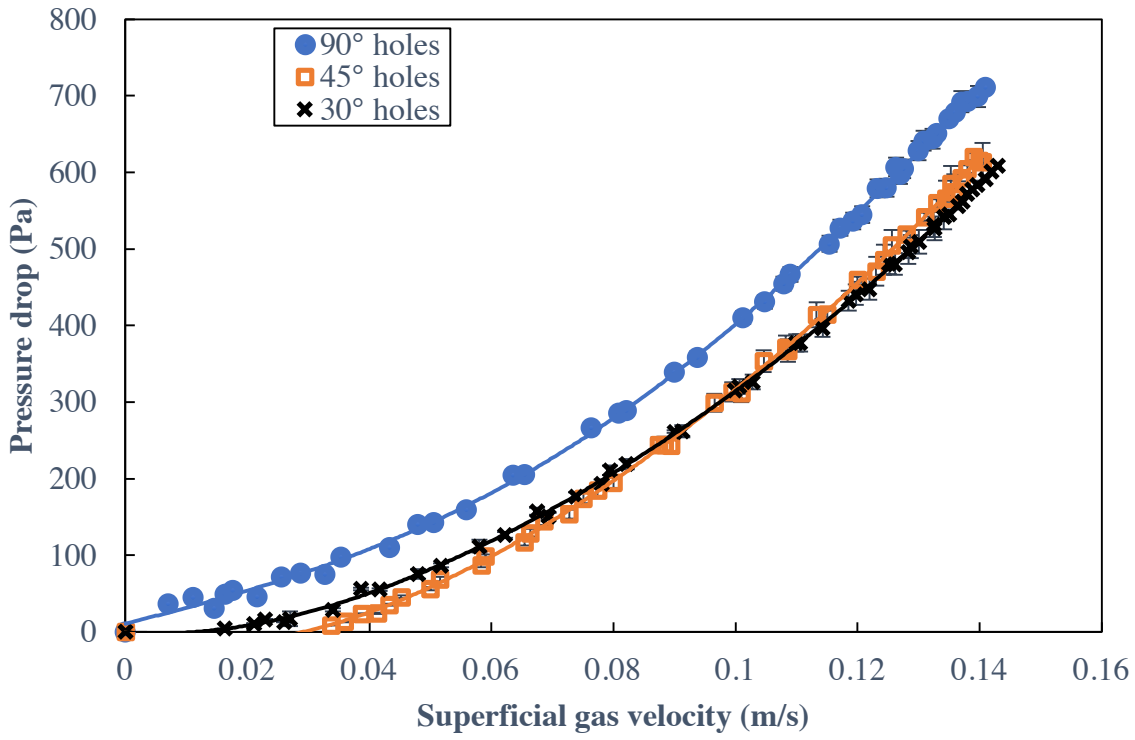

Figure 4-1 Effect of orifice angle on distributor pressure drop (empty bed)

In an empty bed, the 90°-hole distributor had the highest pressure drop compared to both the 30°-hole and 45°-hole distributors. For the 45°-hole distributor, the pressure drop was lowest for low superficial velocities, up to 0.1 m/s. Above this velocity, the 30°-hole distributor had the lowest pressure drop. However, the differences among the three distributors were small, with only 10% more pressure drop across the 90°-hole distributor compared to the others. The reason for having higher pressure drop for the 90°-hole distributor followed by the 45° and 30°-hole was because of the added cross-sectional hole area at the entrance to and exit from the inclined holes, providing an effective tapering. When looking at the drilled holes from a top view, it was clear that the inclined drilled holes had higher cross-sectional area at top and bottom, leading to lower pressure drop.

4.1.2 Effects on bed pressure drop

The effects of the orifice angle on bed pressure drop were also studied for four different static bed heights: 40, 60, 90 and 120 mm. Figure 4-2 presents the results for operation at a static height of 40 mm.

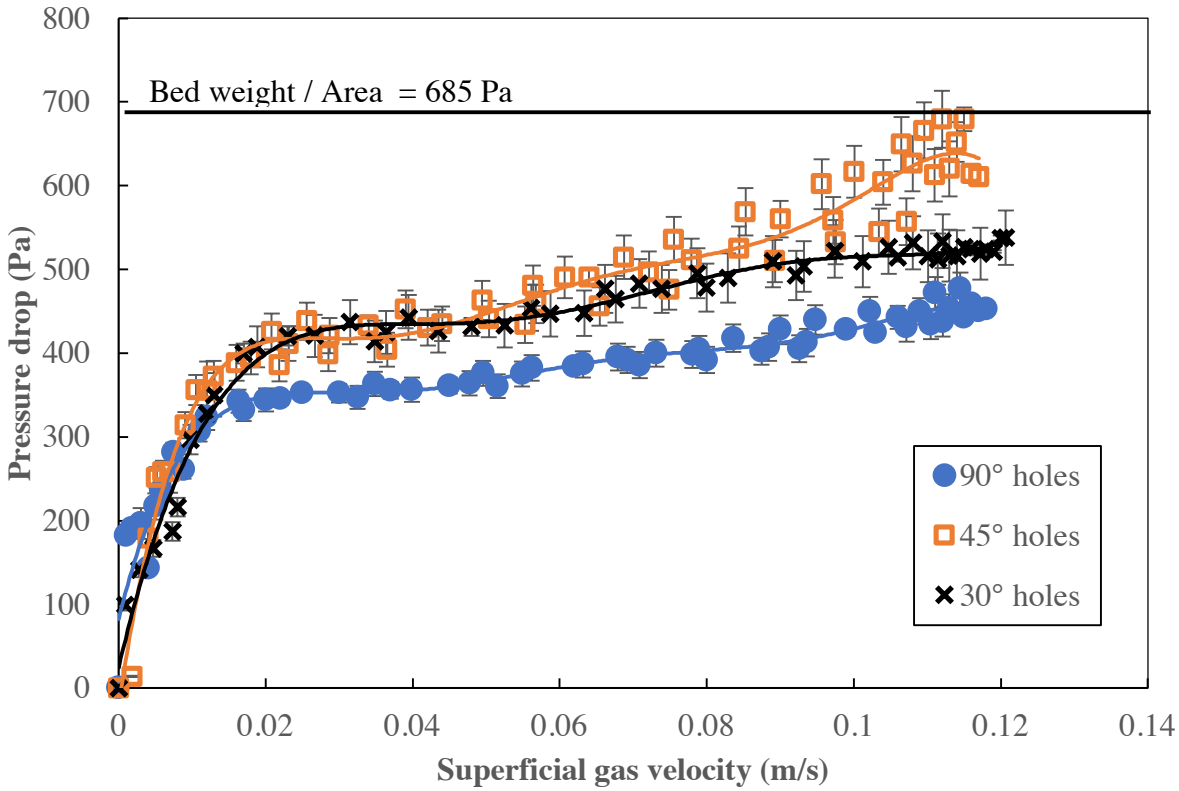

Figure 4-2 Effects of orifice angle on bed pressure drop for a static bed height of 40 mm

The bed pressure drop was lowest for the 90°-hole distributor. However, the bed pressure drop flattened out at a pressure of around 400 Pa compared to the bed pressure drop required to support the bed weight-minus-buoyancy of 685 Pa. There was a 40% difference between them. The difference was less for the 30° and 45°-hole distributors, around 34%. This indicated that there was possibly a large dead volume near the outer wall for the 90°-hole distributor that was not fluidized. The dead volume was much less for the 30°-hole and 45°-hole distributors with negligible differences between them.

Moreover, the bed was operated at a static bed height of 60 mm as in Figure 4-3. For this bed height, the effects were similar in that the 90°-hole distributor had the lowest bed pressure drop. However, dead volume was furthered reduced since the bed pressure drop was only around 200 Pa less than that required to support the bed weight-minus-buoyancy. The

difference reduced from 40% to 22%, which indicated that the dead volume was reduced. On the other hand, the difference was reduced for the 30°-hole distributor from 34% down to 15% and for the 45°-hole distributor from 34% down to 9%, indicating much less dead volume near the outer wall compared to the 90°-hole distributor.

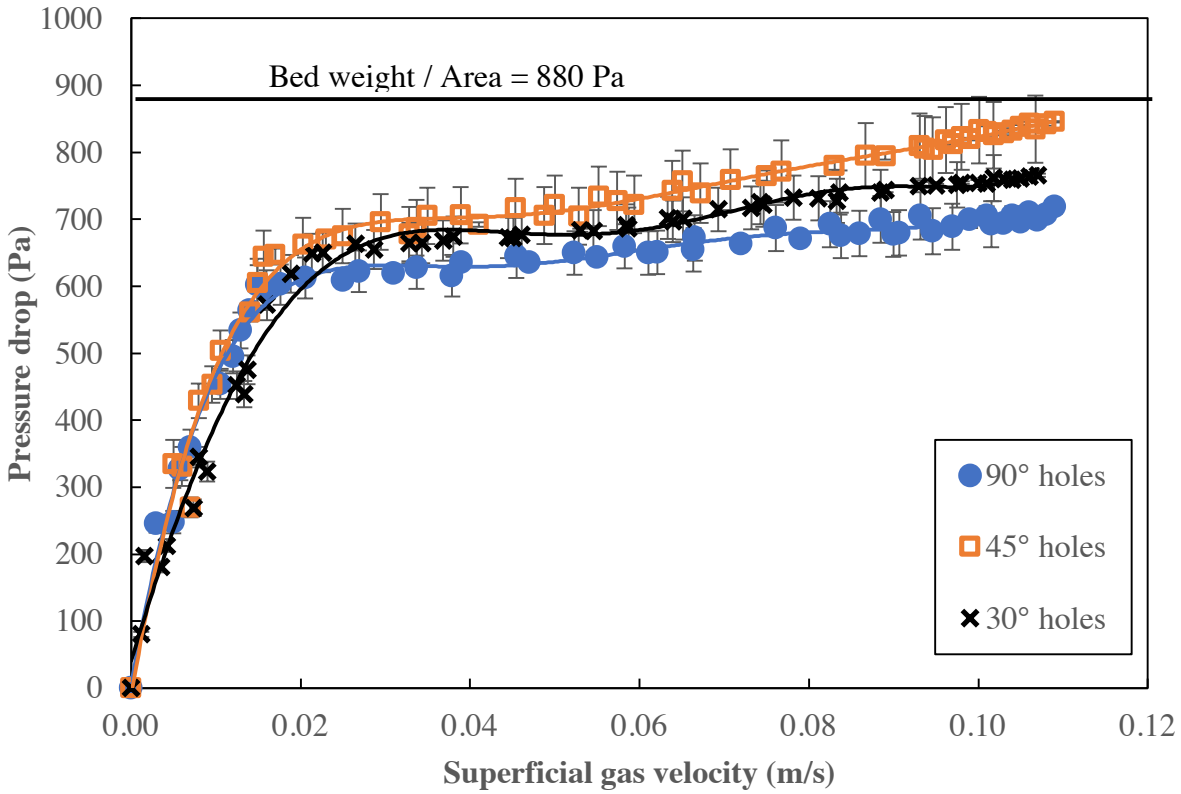

Figure 4-3 Effects of orifice angle on bed pressure drop for a static bed height of 60 mm

When the bed was operated at a static height of 90 mm, the behaviour was similar (Refer to Figure 4-4). However, the 30°-hole distributor had the highest bed pressure drop, and was very close to that of the 45°-hole distributor. In addition, dead volume for the 90°-hole distributor was still not reduced, with the same difference of 22% from the bed pressure drop required to support the bed weight-minus-buoyancy.

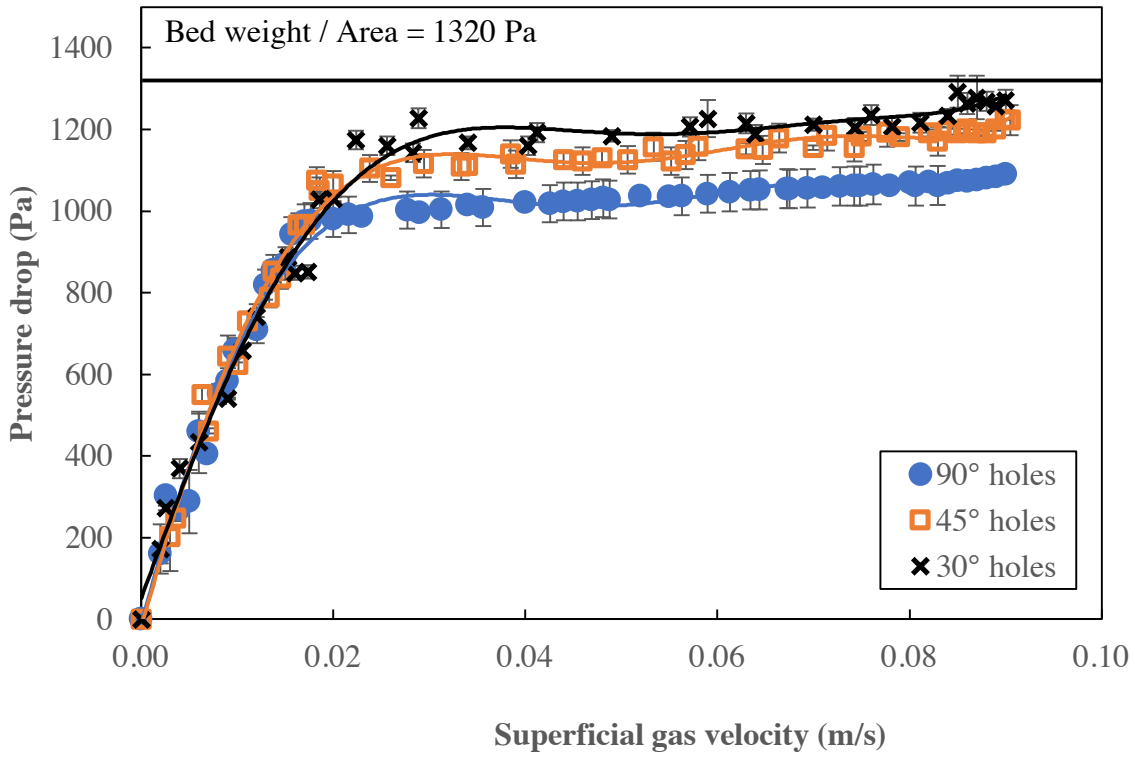

Figure 4-4 Effects of orifice angle on bed pressure drop for a static bed height of 90 mm

The dead volume was reduced for the 90°-hole distributor when the bed was operated at a static bed height of 120 mm. All three distributors performed in a similar manner as seen in Figure 4-5 with the 90°-hole distributor having the lowest bed pressure drop and the 45°-hole distributor with the highest bed pressure drop.

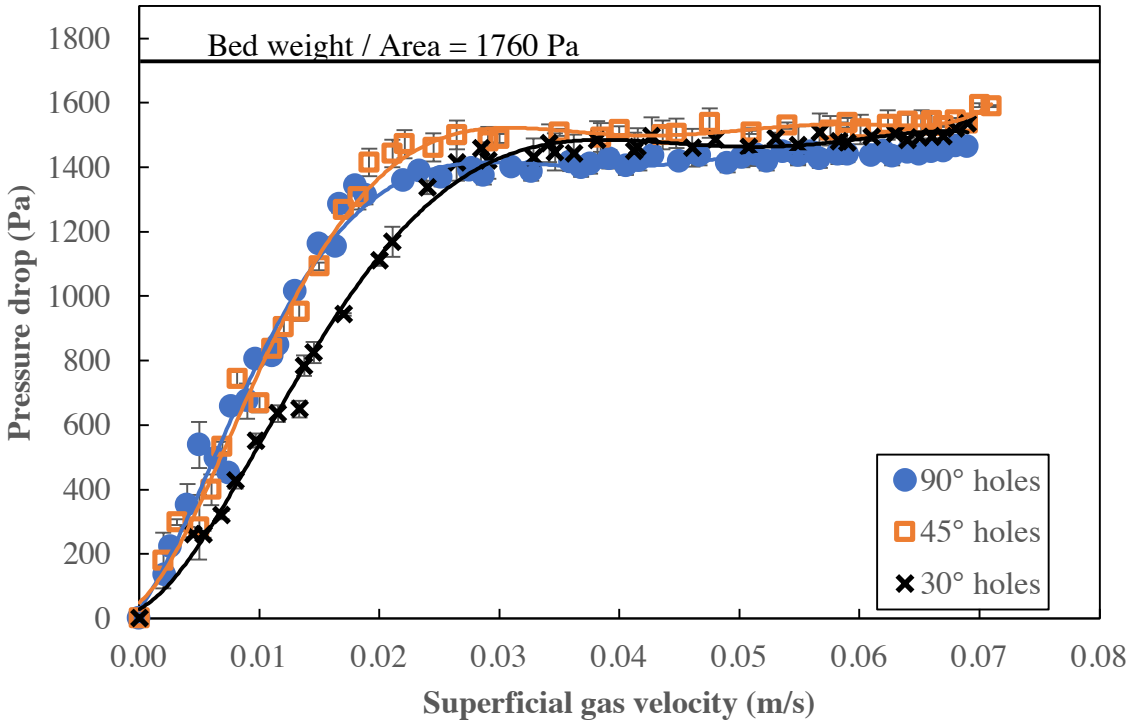

Figure 4-5 Effects of orifice angle on bed pressure drop for a static bed height of 120 mm

This indicated that the orifice angle alone was not enough to capture the hydrodynamics of the fluidized bed and that static bed height had also an impact on the bed pressure drop.

4.1.3 Effects on pressure drop fluctuations

The effect of orifice angle on the pressure drop fluctuations was also studied. Figure 4-6 shows its effects on pressure drop fluctuations for a static bed height of 40 mm. At this static bed height, the pressure fluctuations were highest for the 90°-hole distributor, followed by the 45°-hole and then the 30°-hole distributors. This indicated that there were larger bubbles forming and erupting for the 90°-hole distributor compared to the other distributors.

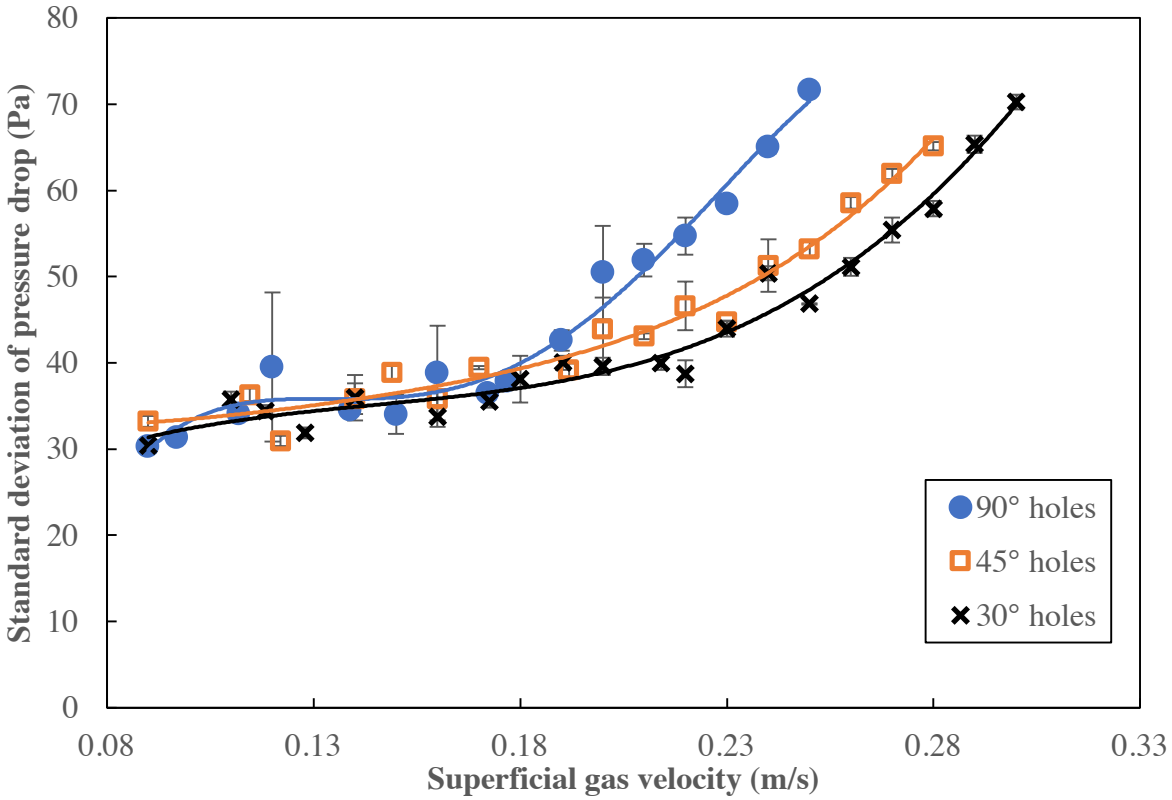

Figure 4-6 Orifice angle effect on pressure drop fluctuations for a static bed height of 40 mm

When the bed was operated at a static bed height of 60 mm, the effects on pressure drop fluctuations were virtually the same (see Figure 4-7).

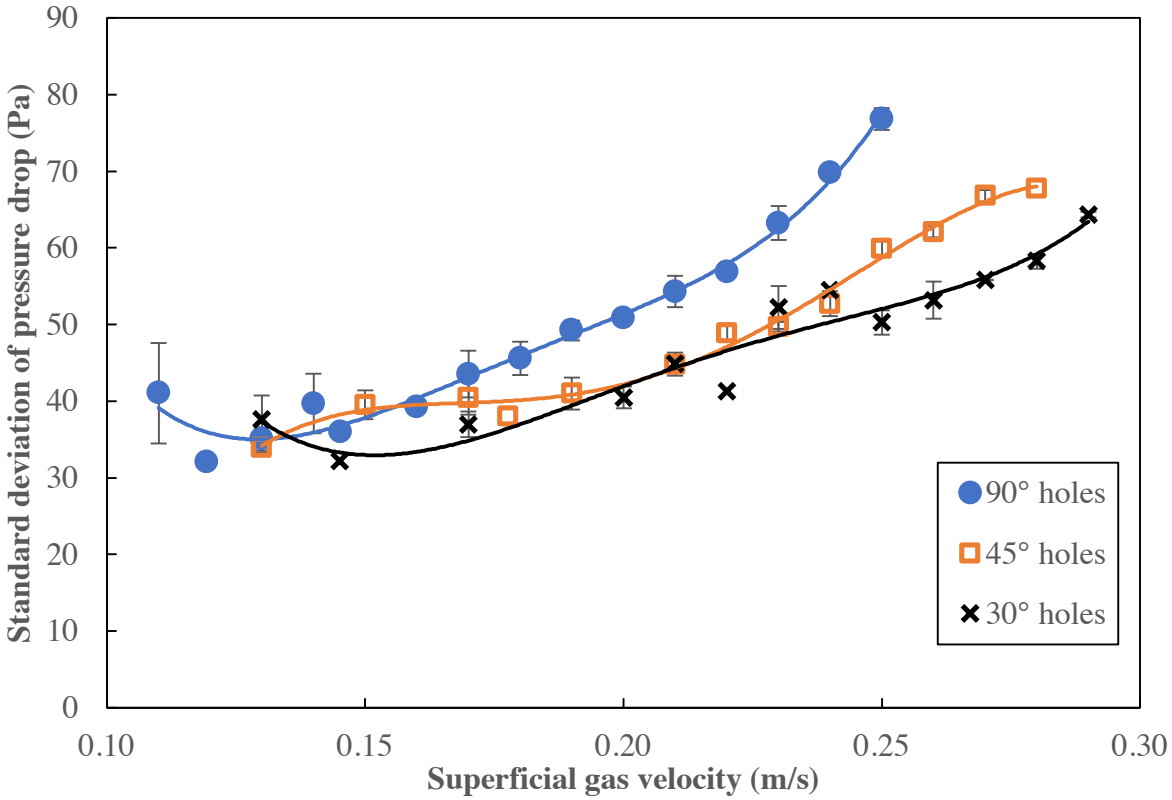

Figure 4-7 Orifice angle effect on pressure drop fluctuations for a static bed height of 60 mm

4.1.4 Effects on bed expansion

The orifice inclination angle effects on bed expansion was studied at two locations, at the outer wall (H_w) and at the central inner wall (H_c) (Figure 4-8). Two static bed heights were also investigated (40 mm and 120 mm).

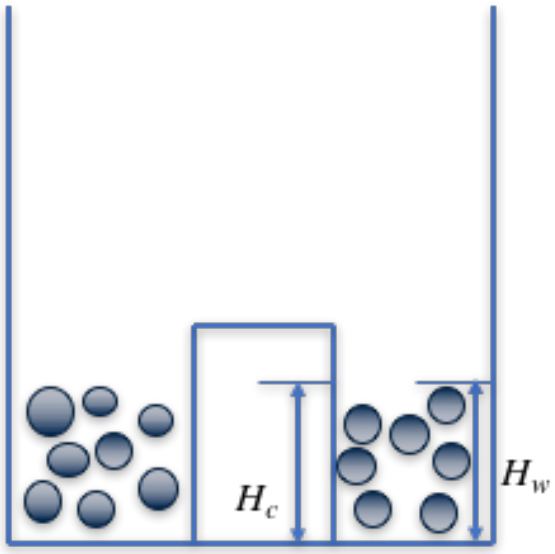

Figure 4-8 Bed expansion at both inner and outer walls

Figures 4-9 and 4-10 present the bed expansion for operation at a static bed height of 40 mm at both the outer wall and central wall.

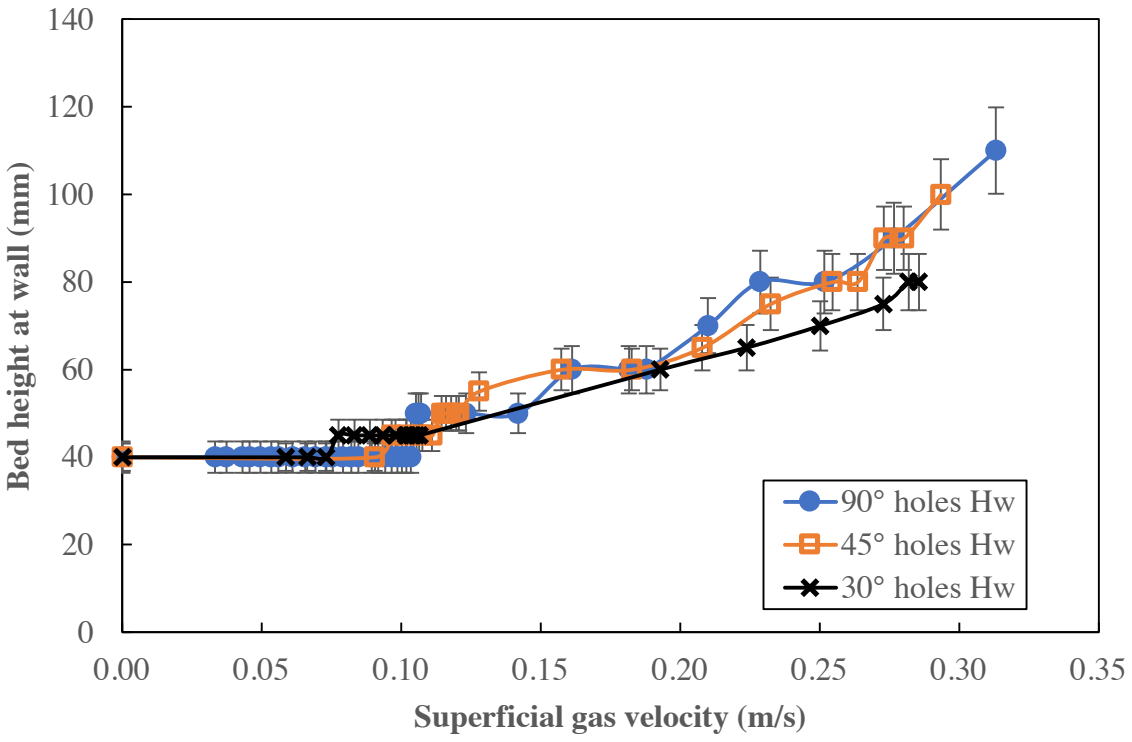

Figure 4-9 Bed expansion at outer wall for bed height of 40 mm

The 30°-hole distributor started to expand at lower superficial gas velocity compared to the other distributors. This was because of the jetting effects at the centre of the distributor which resulted in pushing the particles more towards the outer wall. This created a bed expansion gradient across the annulus, with less bed expansion at the inner wall and higher expansion at the outer wall. Note, however, that the error bars often overlap, meaning that the difference between inner and outer expansion may not always be significant.

Similar results were obtained by studying the bed expansion at the inner wall. However, the 90°-hole distributor showed no change in bed expansion between the outer wall and the inner wall compared to the changes observed for the inclined-holes distributors.

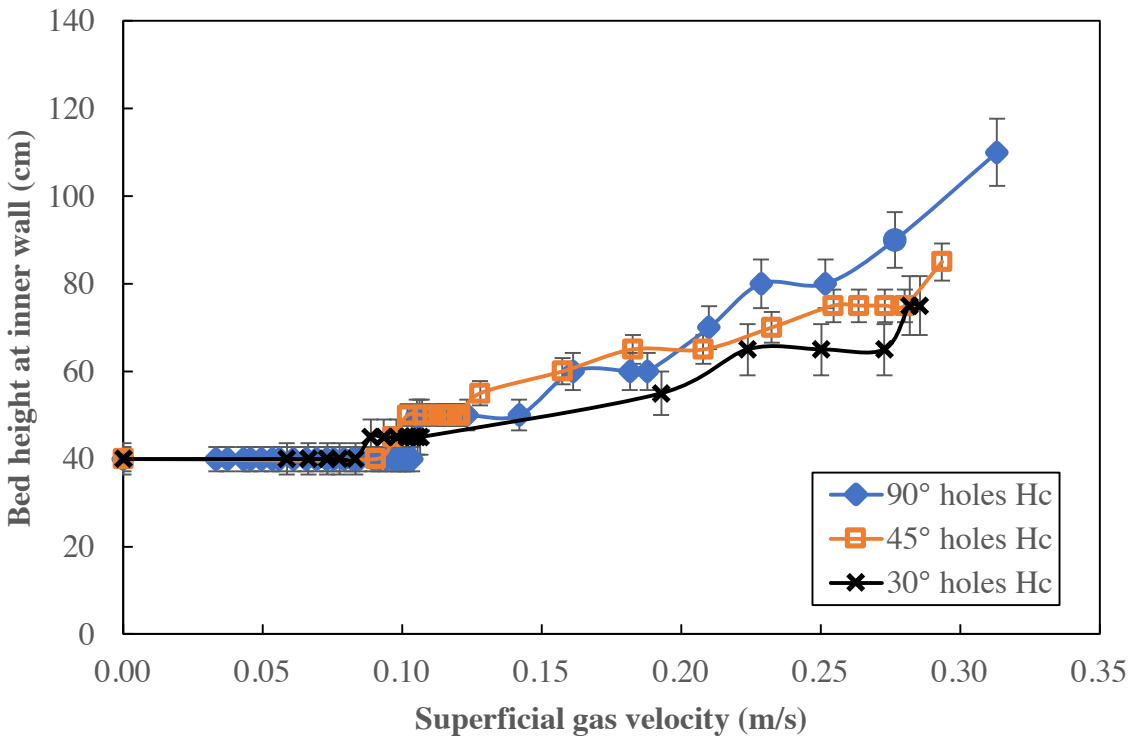

Figure 4-10 Bed expansion at inner wall for bed height of 40 mm

Figure 4-11 shows the difference in bed expansion between the outer wall and the inner wall. It is clearly seen that there was a higher difference for the 45°-hole distributor at higher superficial gas velocities. This is due to the jetting effect in the inner part of the distributor which caused swirling motion that extended as the superficial gas velocity increased. It can also be seen from the figure that the 30°-hole distributor started to expand at a lower superficial gas velocity compared to the 45°-hole distributor because of the same reason of air jetting that drove particles more towards the outer wall. The air jetting effects were more noticeable at steeper angles.

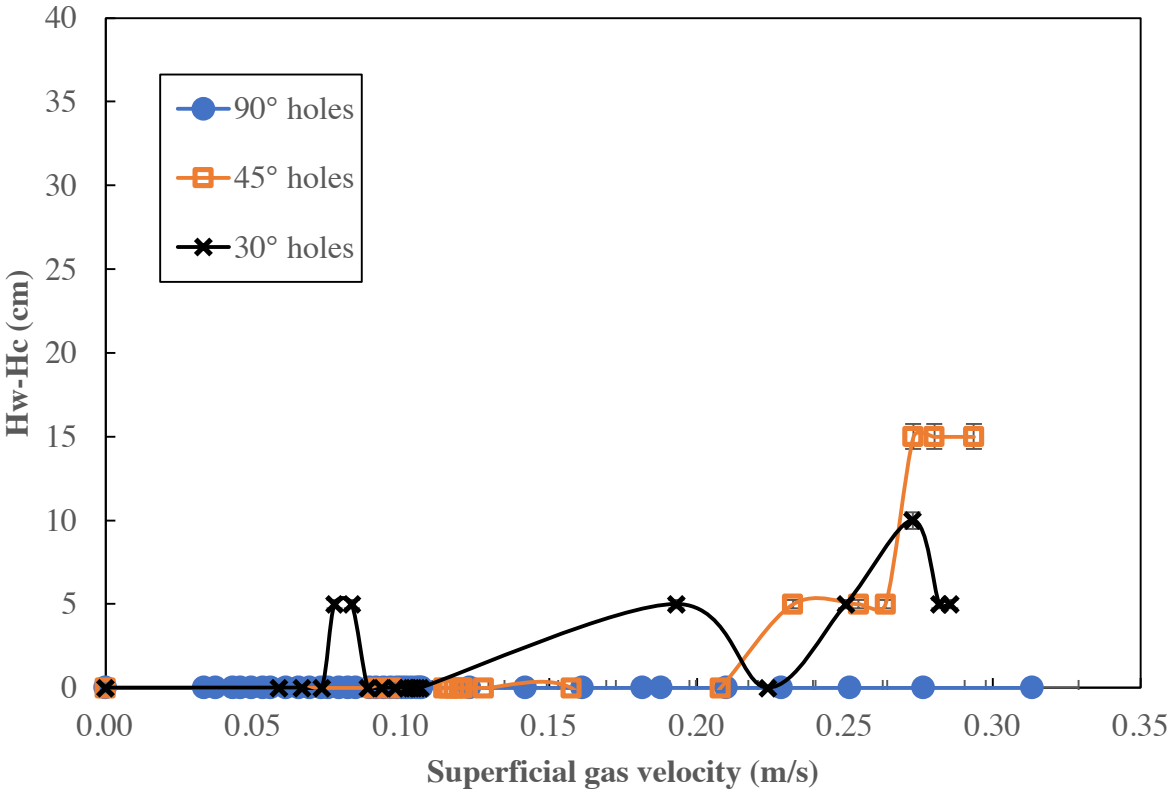

Figure 4-11 Bed expansion difference between outer and inner walls for bed height of 40 mm

Figures 4-12 and 4-13 show the bed expansion at the outer and inner walls for static bed height of 120 mm for the three distributors. At this static bed height, the effect of the holes angle was negligible.

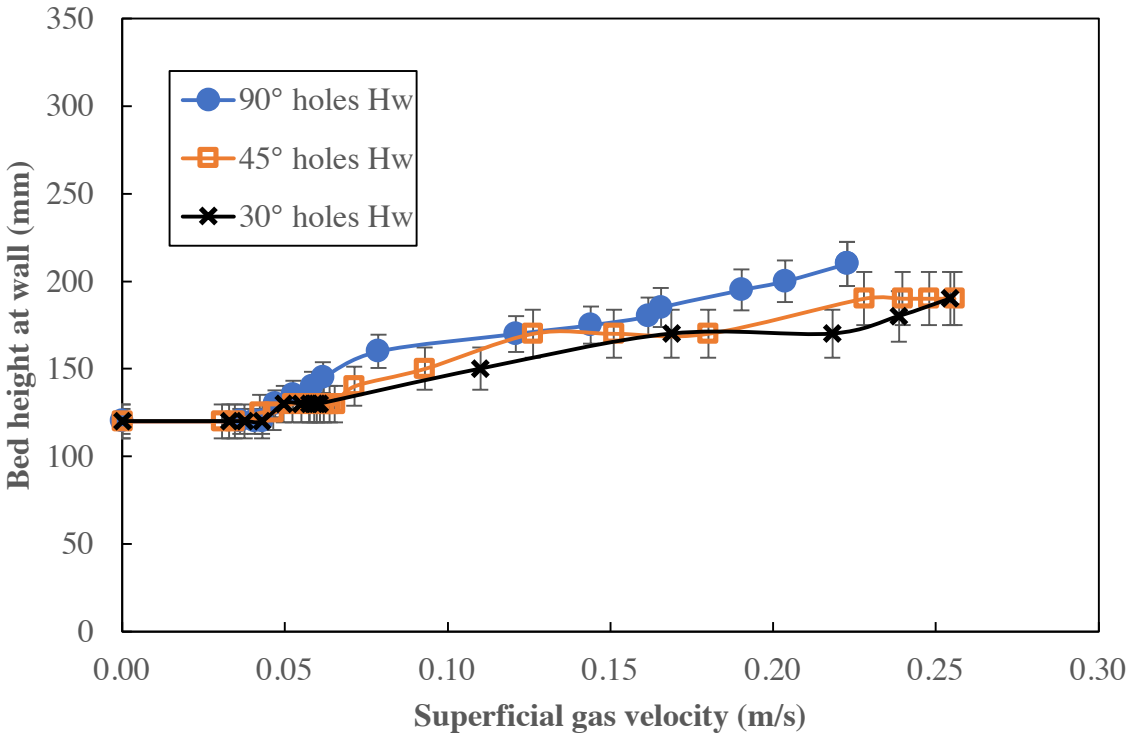

Figure 4-12 Bed expansion at outer wall for bed height of 120 mm

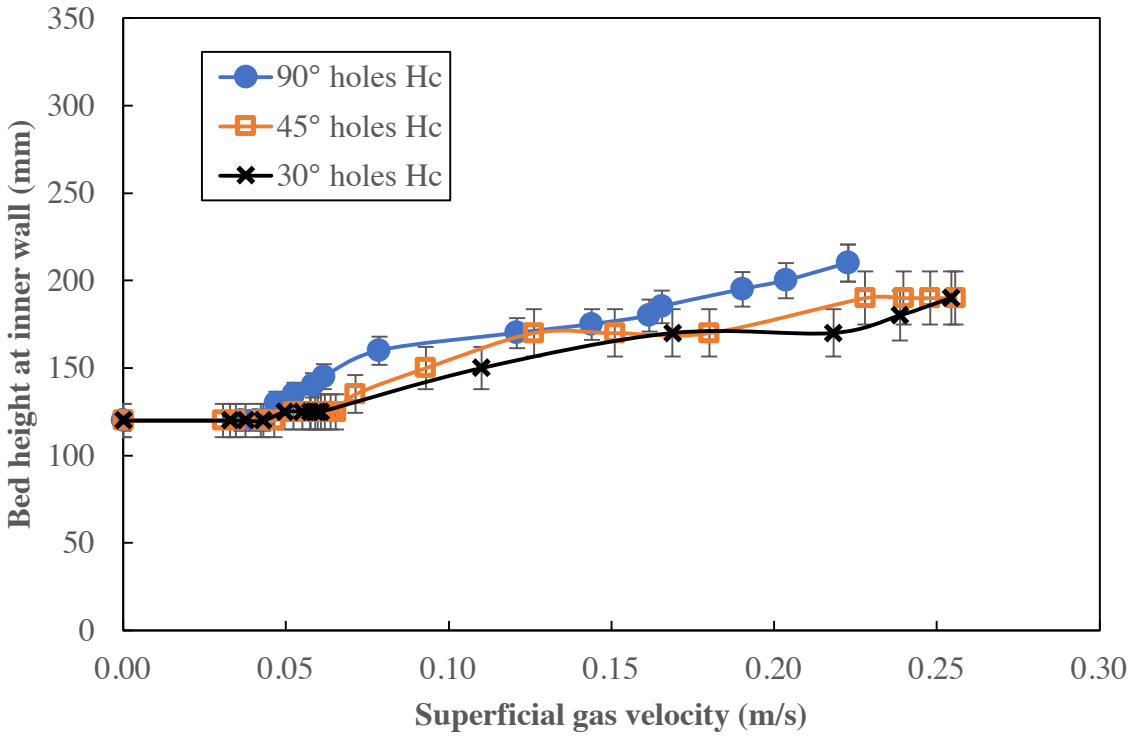

Figure 4-13 Bed expansion at inner wall for bed height of 120 mm

Similar results were also observed for the bed expansion at the inner wall. Figure 4-14 shows the difference in bed expansion between the outer and inner walls. All distributors showed little difference between the bed expansions at both locations, indicating little effect of the orifice inclination angle. This would mean that at this bed height, the fluidized bed performance was very close to a conventional fluidized bed. Overall, the effect of the orifice inclination angle on bed expansion was limited to shallow beds, i.e. static bed heights less than 120 mm.

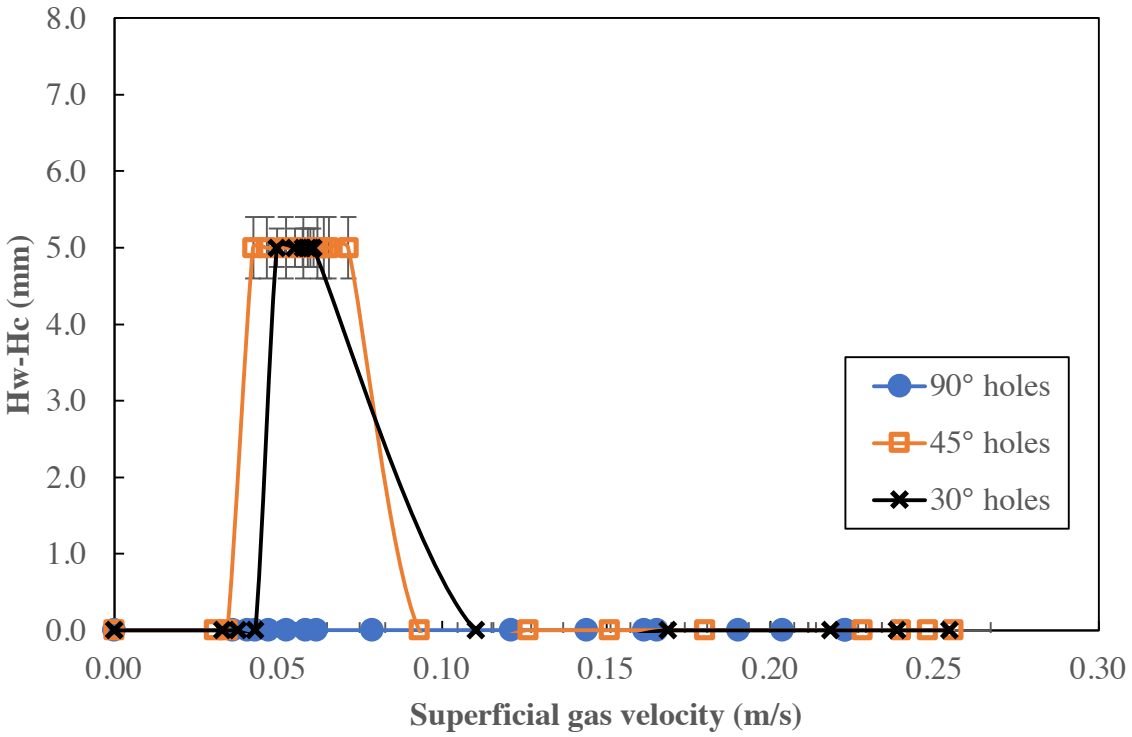

Figure 4-14 Bed expansion difference between outer and inner walls for bed height of 120 mm

4.1.5 Effects on minimum fluidization velocity

Three methods were used to determine the minimum fluidization velocity to examine the effect of the orifice inclination angle on it. The minimum fluidization velocity was first estimated using the empirical equations (4-1 and 4-2) provided by Wen and Yu (1966) at low Reynolds number which was independent of the orifice angle and bed height.

$$U_{mf} = \frac{d_p^2(\rho_s-\rho)g}{150\mu}\frac{\varepsilon_{mf}^3\phi^2}{(1-\varepsilon_{mf})} \qquad (4\text{-}1)$$

$$\varepsilon_{mf} = (14\phi)^{-1/3} \qquad (4\text{-}2)$$

Table 4-1 shows the minimum fluidization velocity with all parameters. The minimum fluidization velocity was also observed visually by recording the time when the particles

started to move. Finally, U_{mf} was estimated using the pressure drop-velocity curve in which the velocity at minimum fluidization corresponds to the one where the bed pressure drop flattens out (Refer to Appendix-C for illustration of graphical determination of U_{mf}).

Table 4-1 Minimum fluidization velocity from empirical equation of Wen and Yu (1966)

Variable	Value	Unit
Particle Diameter (d_p)	171	μm
Particle Density (ρ_s)	2635	kg/m^3
Air Density (ρ)	1.23	kg/m^3
Gravity constant (g)	9.8	m/s^2
Sphericity (ϕ)	1.0 (assumed value)	N/A
Voidage at minimum fluidization (ε_{mf})	0.41 (calculated from equation (4-2))	N/A
Air Viscosity (μ)	1.8 x 10^{-5}	$kg/(m.s)$
Minimum Fluidization Velocity (U_{mf})	0.034 (calculated from equation (4-1))	m/s

The minimum fluidization velocity was compared for all three distributors at two static bed depths (40 mm and 120 mm). Figures 4-15 and 4-16 present the results from the three methods discussed above. For a static bed height of 40 mm, both predicted and experimental values were very close for the 90°-hole distributor. The pressure drop-velocity curve method underestimated the minimum fluidization velocity, compared to the predicted value.

For a static bed height of 120 mm, all methods were very close. In addition, for the 90°-hole distributor, the minimum fluidization velocity was independent of bed height. The value estimated by the pressure drop-velocity curve was almost the same. However, for the inclined-hole distributors, the minimum fluidization velocity varied with the static bed height.

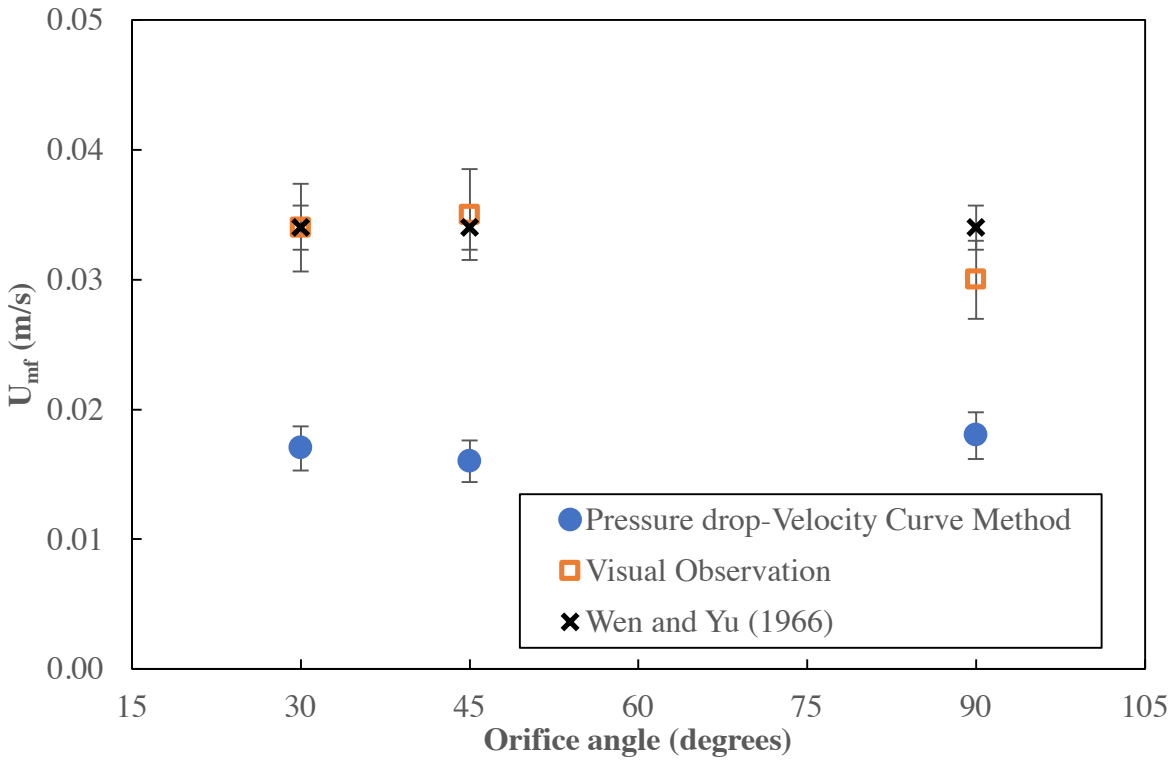

Figure 4-15 Minimum fluidization velocity for static bed height of 40 mm

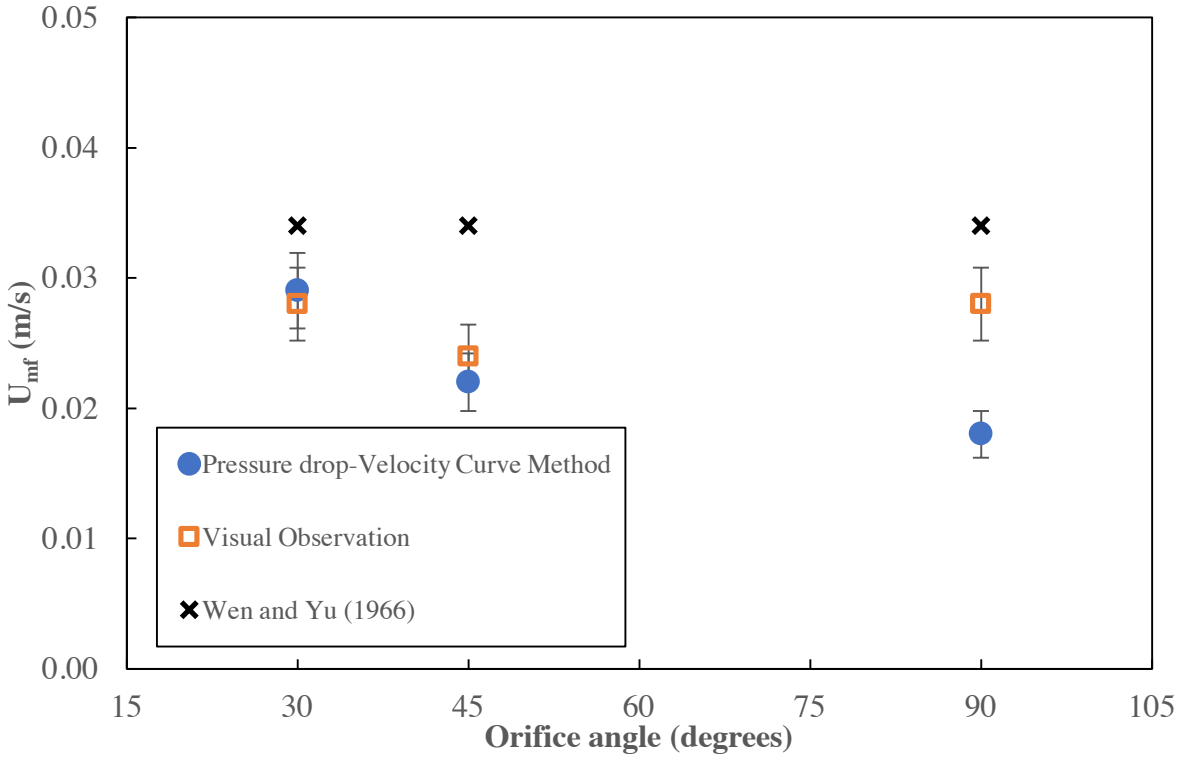

Figure 4-16 Minimum fluidization velocity for static bed height of 120 mm

4.2 Effects of static bed depth on hydrodynamics

The effects of the static bed depth on bed pressure drop, bed pressure drop fluctuations and minimum fluidization velocity were investigated.

4.2.1 Effects on bed pressure drop

The effects on bed pressure drop were studied for all three distributors. Four static bed heights were tested (40, 60, 90 and 120 mm). Figures 4-17, 4-18 and 4-19 present the results for the 30°, 45° and 90°-hole distributors, respectively.

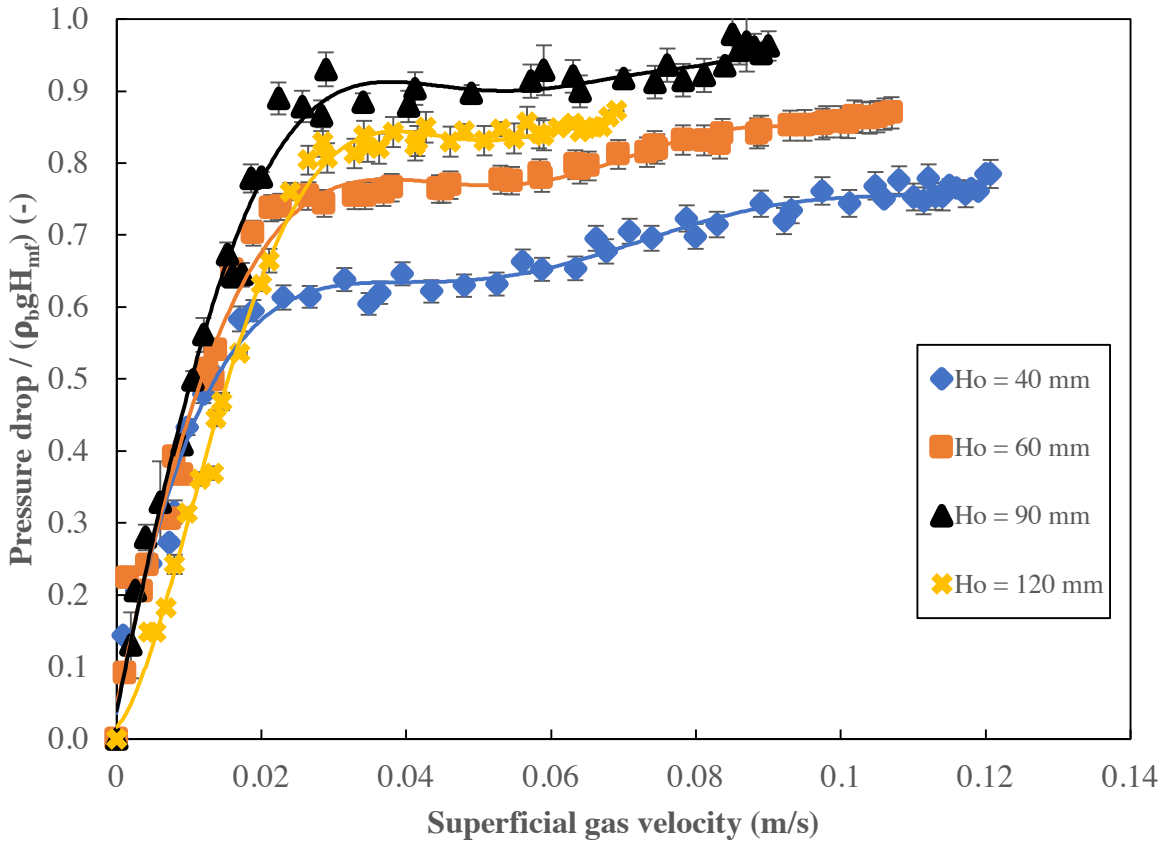

Figure 4-17 Normalized bed pressure drop vs. superficial gas velocity for different static bed depths and 30°-hole distributor

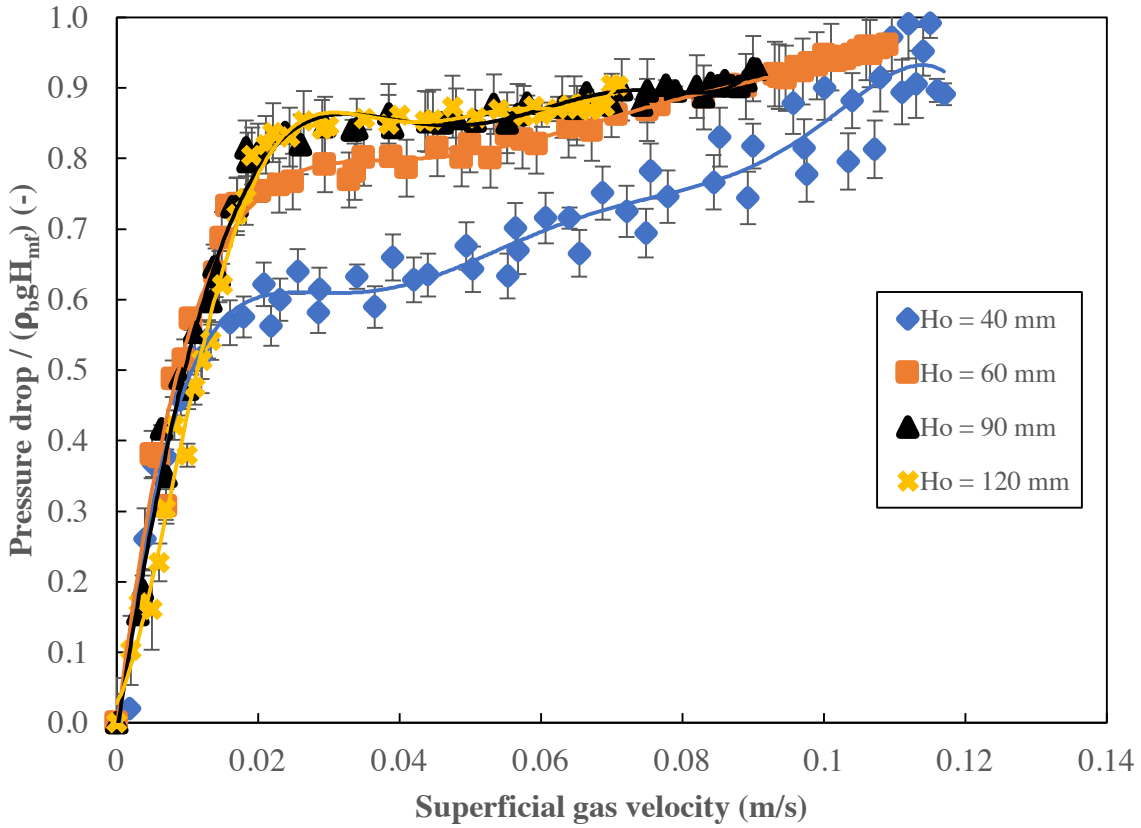

Figure 4-18 Normalized bed pressure drop vs. superficial gas velocity for different static bed depths and 45°-hole distributor

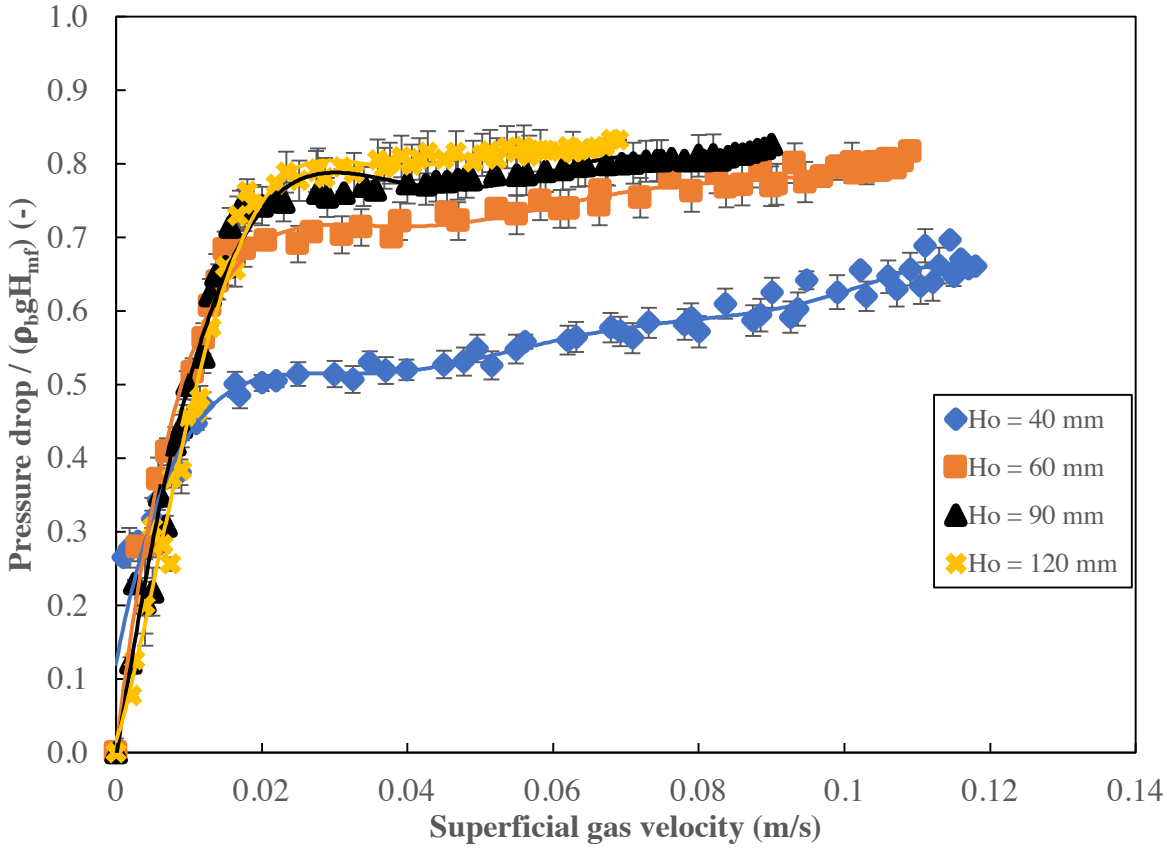

Figure 4-19 Normalized bed pressure drop vs. superficial gas velocity for different static bed depths and 90°-hole distributor

As the static bed depth increased, the bed pressure drop increased due to the increase in bed weight. All three distributors behaved in a similar manner except that the inclined-holes distributors had slightly higher bed pressure drop.

4.2.2 Effects on pressure drop fluctuations

Figures 4-20, 4-21 and 4-22 plot the results obtained for pressure drop fluctuations for the 30°, 45° and 90°-hole distributors. Pressure fluctuations increased with increasing static bed depth and increasing superficial gas velocity. Moreover, the fluctuations for the 30° and 45°-hole distributors were distinguished in such a way that it was clear that higher static bed depths had much higher pressure fluctuations because of the inclination and having more

space for bubbles to erupt. The fluctuations for lower superficial gas velocities were greater at higher static bed depths since bubbles had more space and time to rise before erupting at the bed surface. This was unlike the behaviour for the 90°-hole distributor in which fluctuations for lower superficial velocities were of similar magnitude.

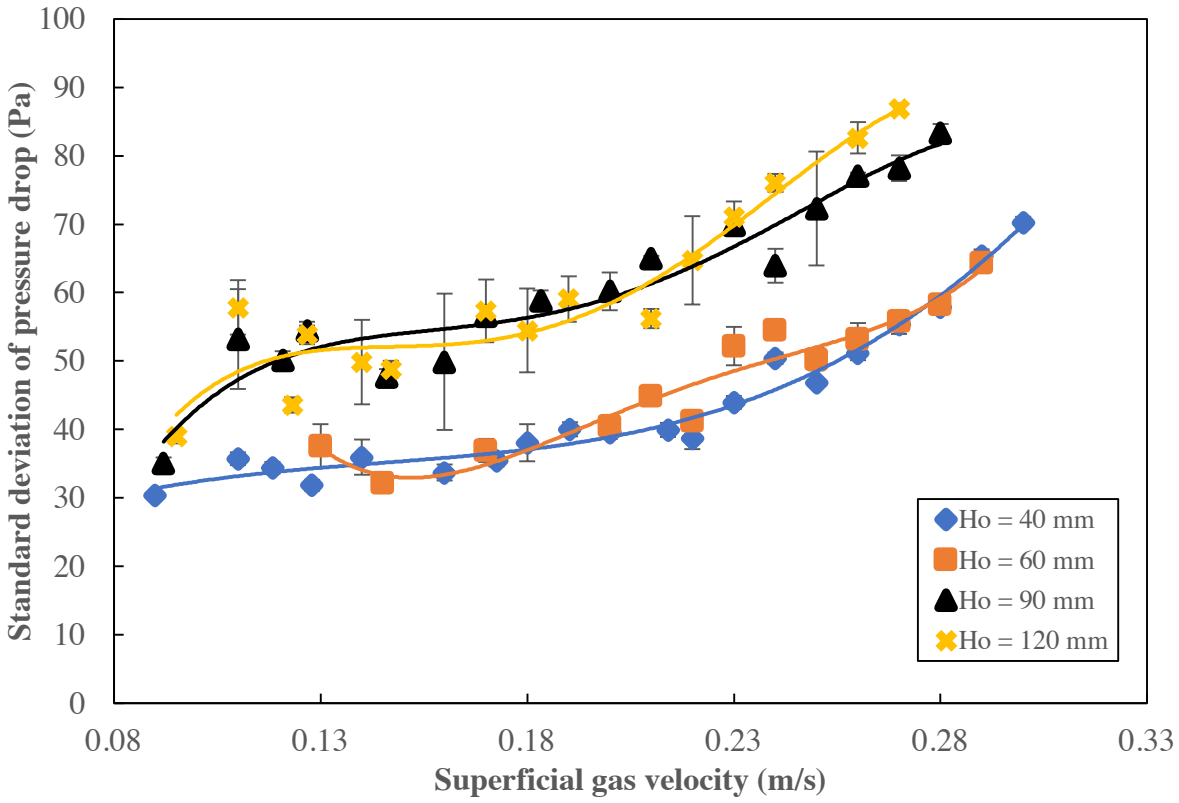

Figure 4-20 Pressure drop fluctuations for 30°-hole distributor for different static bed depths

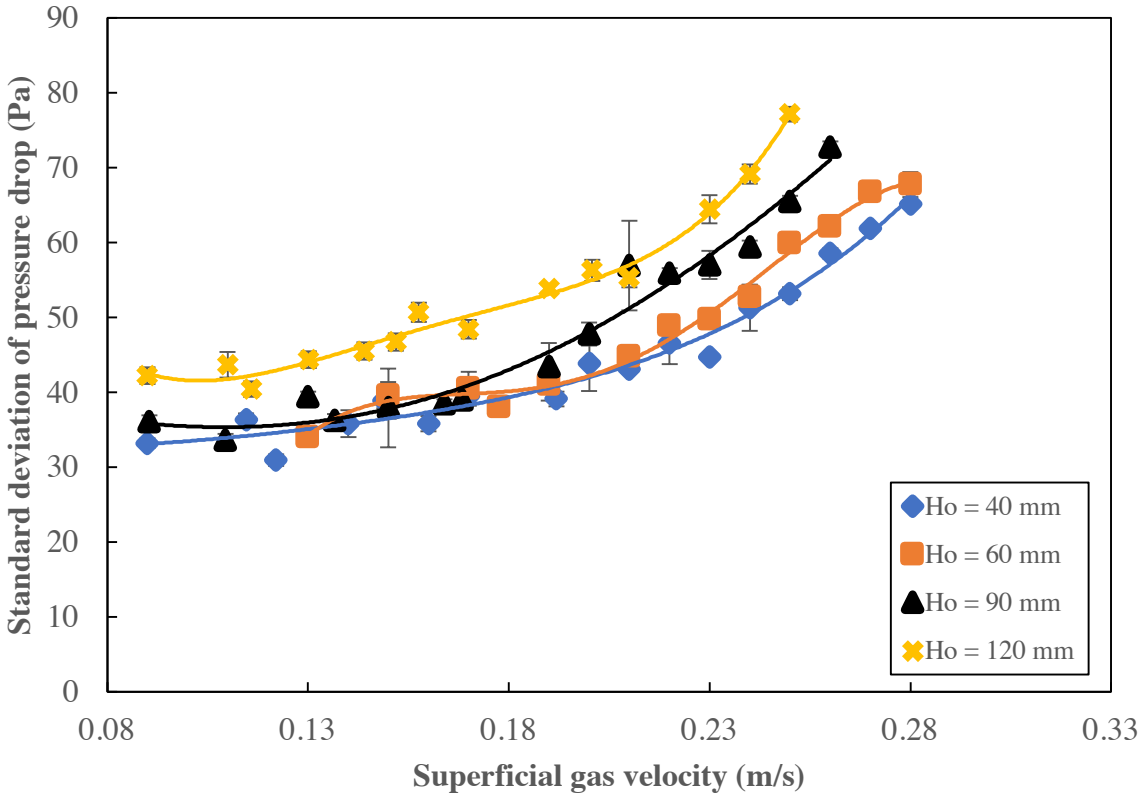

Figure 4-21 Pressure drop fluctuations for 45°-hole distributor for different static bed depths

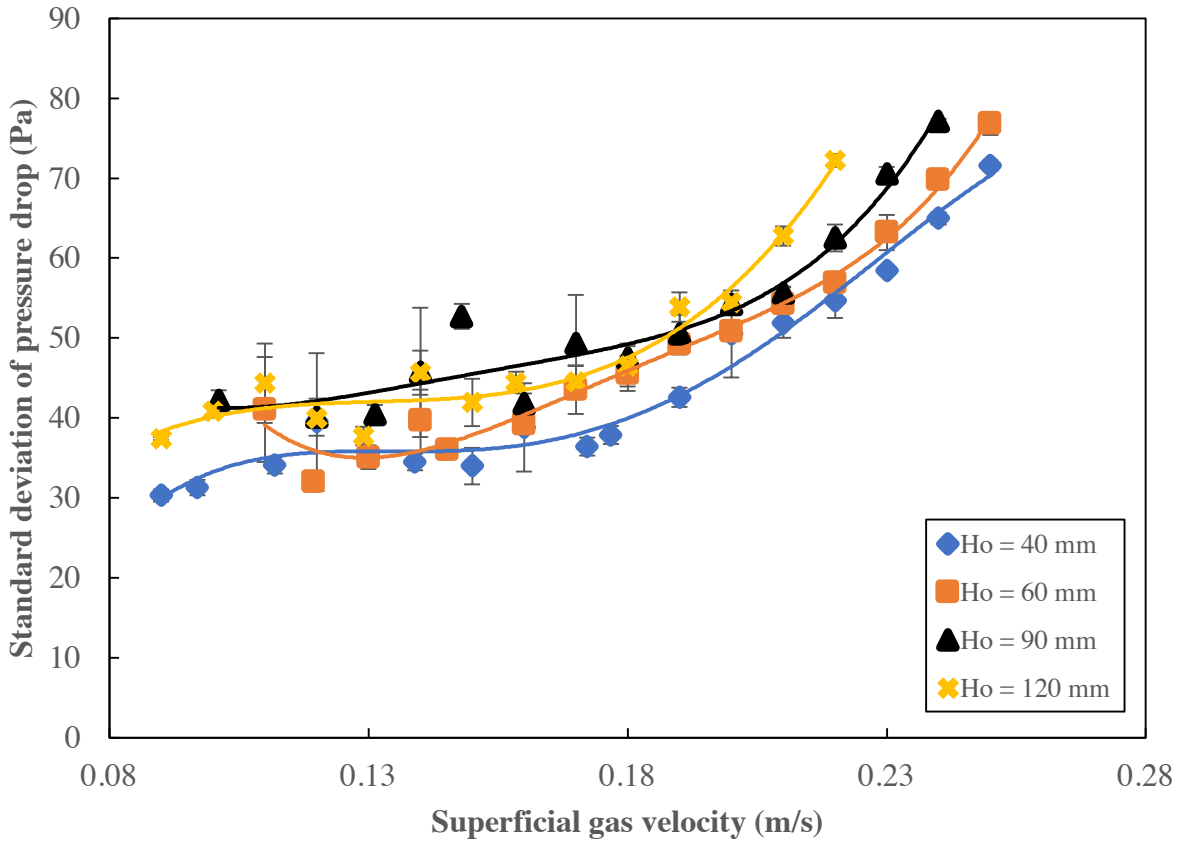

Figure 4-22 Pressure drop fluctuations for 90°-hole distributor for different static bed depths

4.2.3 Effects on minimum fluidization velocity

In a conventional fluidized bed, the minimum fluidization velocity is independent of the static bed height. The effect of bed height on the minimum fluidization velocity was investigated for the inclined-holes distributors. Figures 4-23, 4-24 and 4-25 compare the effects of static bed depths on minimum fluidization velocity based on several methods for all three distributors. The minimum fluidization velocity was determined as explained in section 4.1.5. Three methods were used, empirical correlation, visual observation and pressure drop-velocity curve. For the 90°-hole distributor, the minimum fluidization velocity did not change with static bed depth. However, the pressure drop-velocity curve showed an increase in the minimum fluidization velocity with increasing static bed depth which matched

the results reported by Sreenivasan et al. (2002) for the inclined-holes distributor. This change in minimum fluidization velocity with bed height for the inclined-holes distributors was attributed to the additional centrifugal force that is acting on the particles. The minimum fluidization velocity is the velocity when the bed materials are supported by their weight-minus-buoyancy.

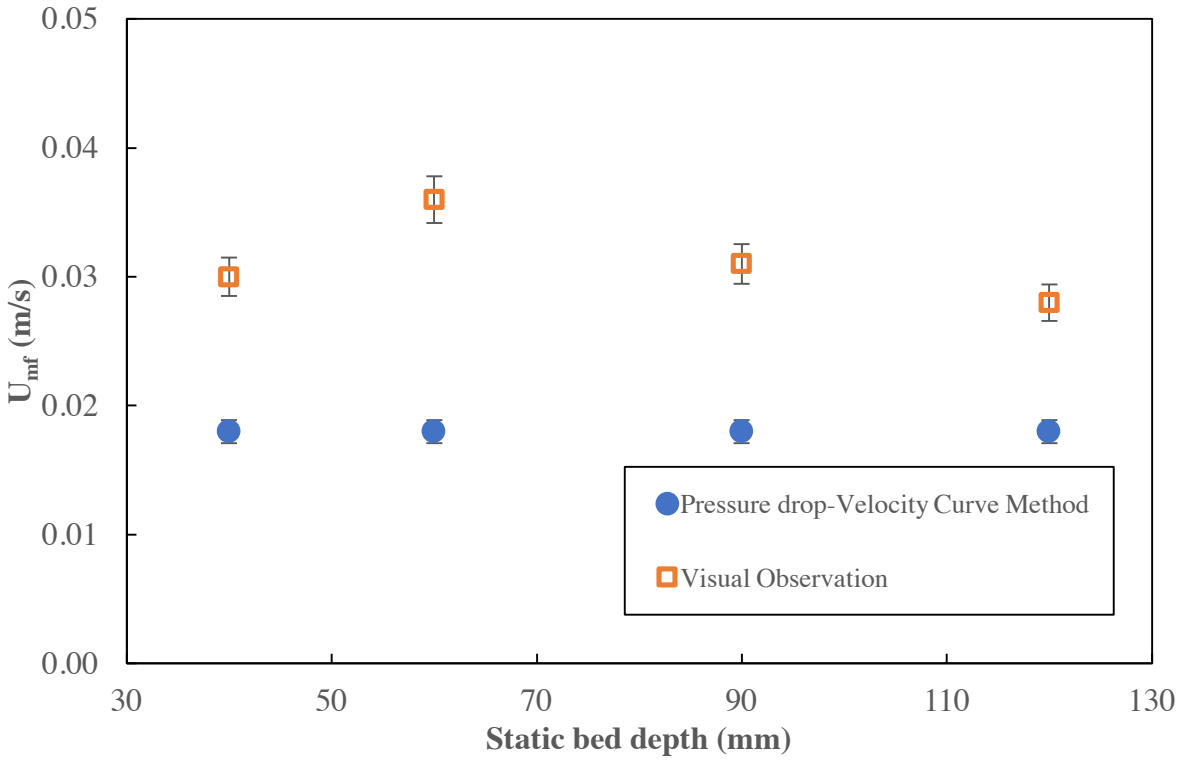

Figure 4-23 Effect of static bed depth on minimum fluidization velocity based on two methods for 90°-hole distributor

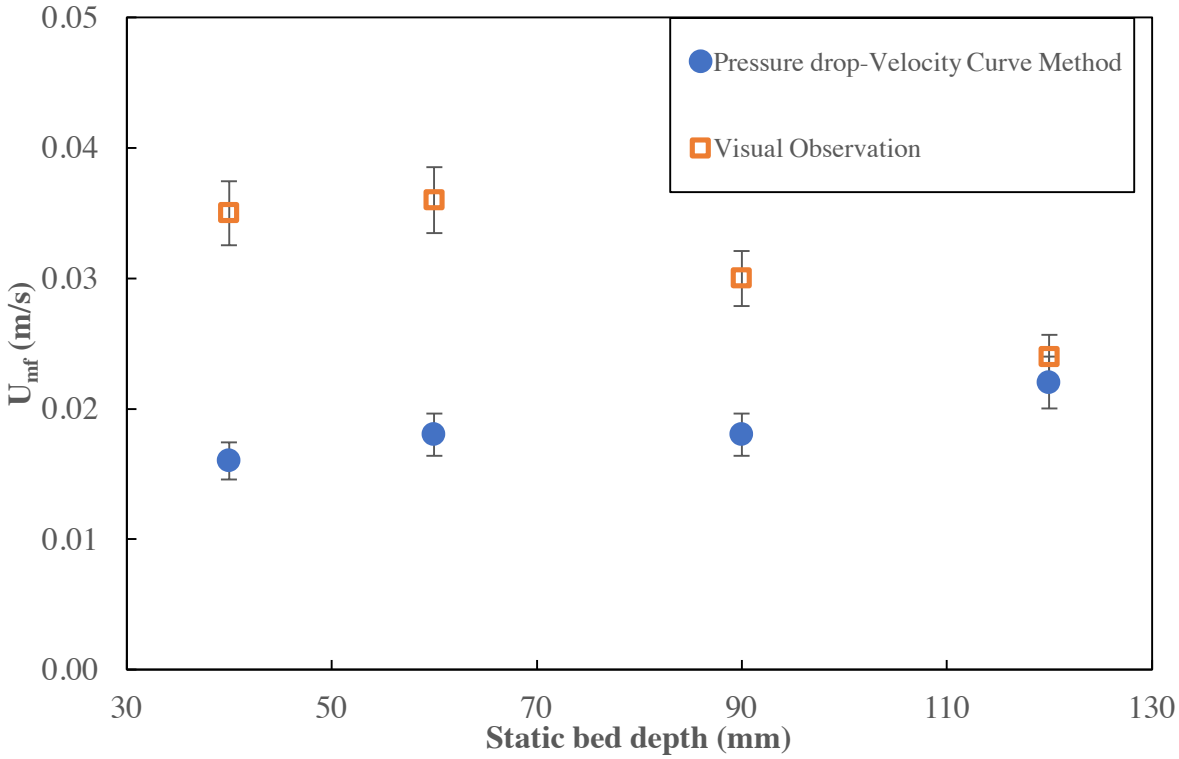

Figure 4-24 Effect of static bed depth on minimum fluidization velocity based on two methods for 45°-hole distributor

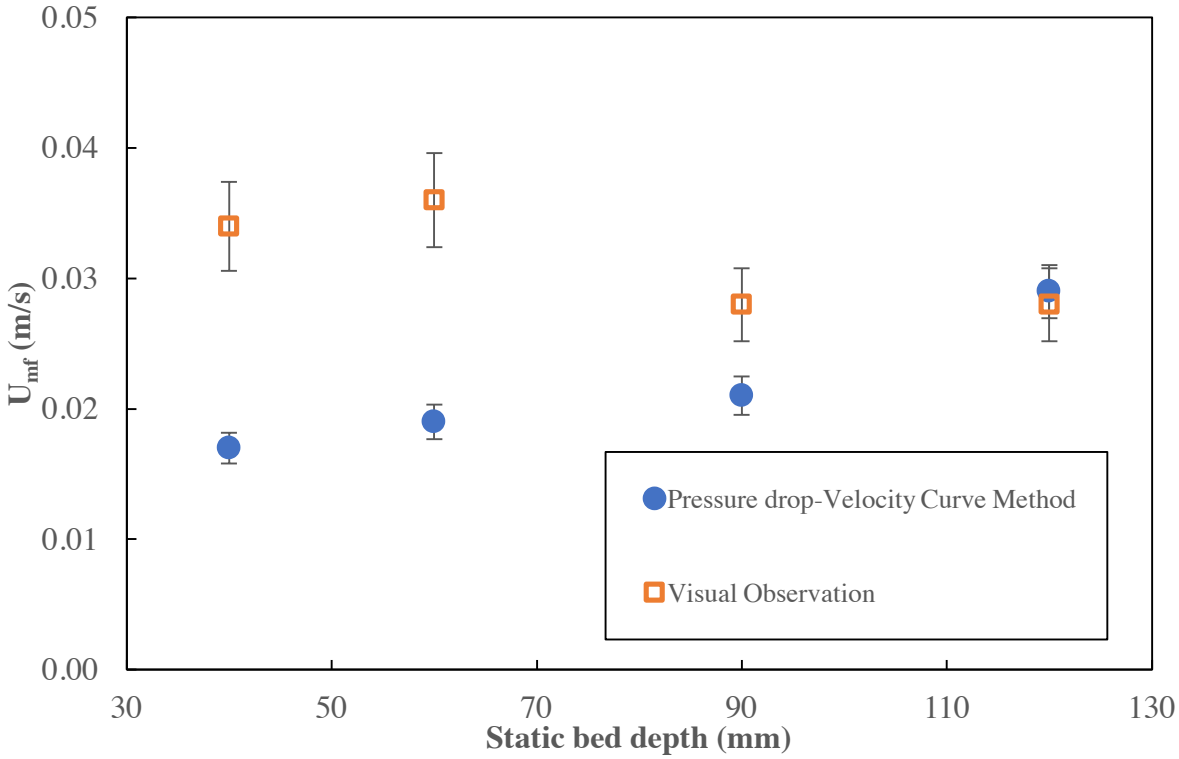

Figure 4-25 Effect of static bed depth on minimum fluidization velocity based on two methods for 30°-hole distributor

4.3 Effect of windbox packing on pressure drop

Windbox design could have an impact on the hydrodynamics of the fluidized bed. Therefore, the windbox was carefully packed with 25 mm plastic pall rings to ensure uniform spacing, and the bed pressure drop was measured and compared with an empty windbox. This was done for all three distributors to see what would be the effect of the packing on distributor pressure drop for an empty bed and bed pressure drop at a static bed depth of 60 mm with increasing superficial gas velocity. Figure 4-26 gives a photograph of the packing material.

Figure 4-26 Photo of 25 mm plastic pall rings packing

The results showed an increase in distributor pressure drop for an empty bed after installing the packing at lower superficial gas velocities (less than 0.1 m/s) which was expected since the packing introduced an additional pressure drop for the air flowing through it, which was evidenced by the measurement of the distributor pressure drop. However, the trend showed an opposite result for superficial gas velocities beyond 0.1 m/s. Figures 4-27, 4-28 and 4-29 present the distributor pressure drop for an empty bed measured for the 90°, 45° and 30°-hole distributors, respectively.

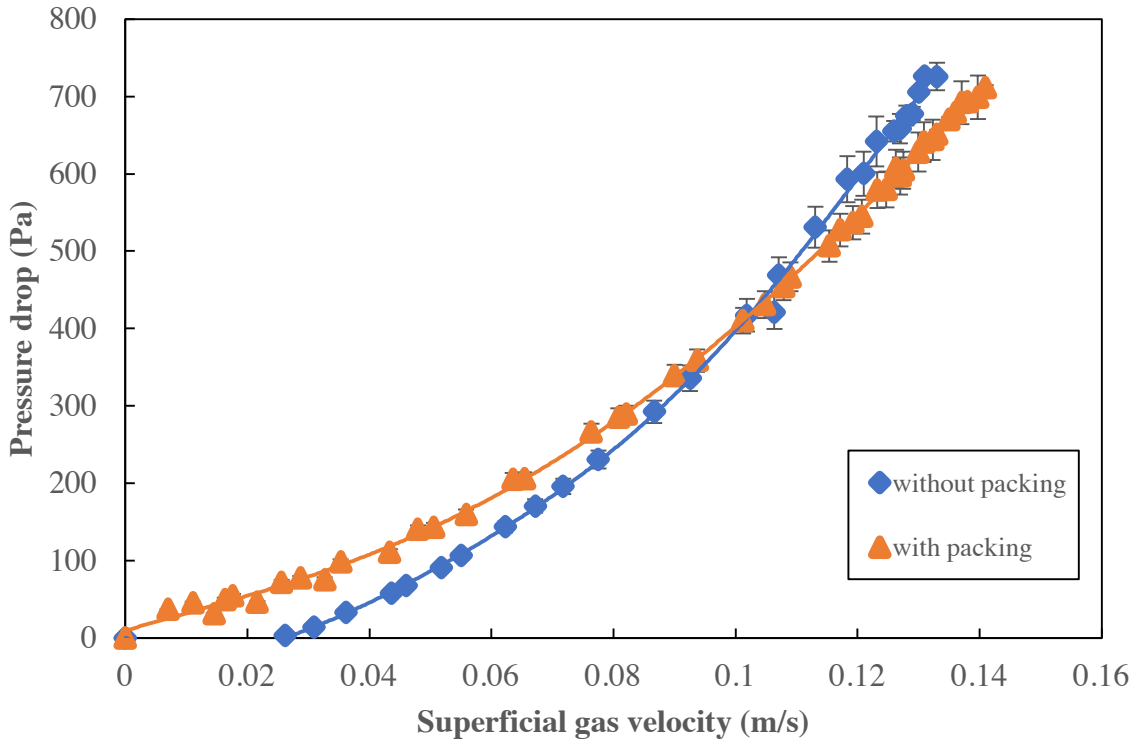

Figure 4-27 Effect of windbox packing on distributor pressure drop (empty bed) for 90°-hole distributor

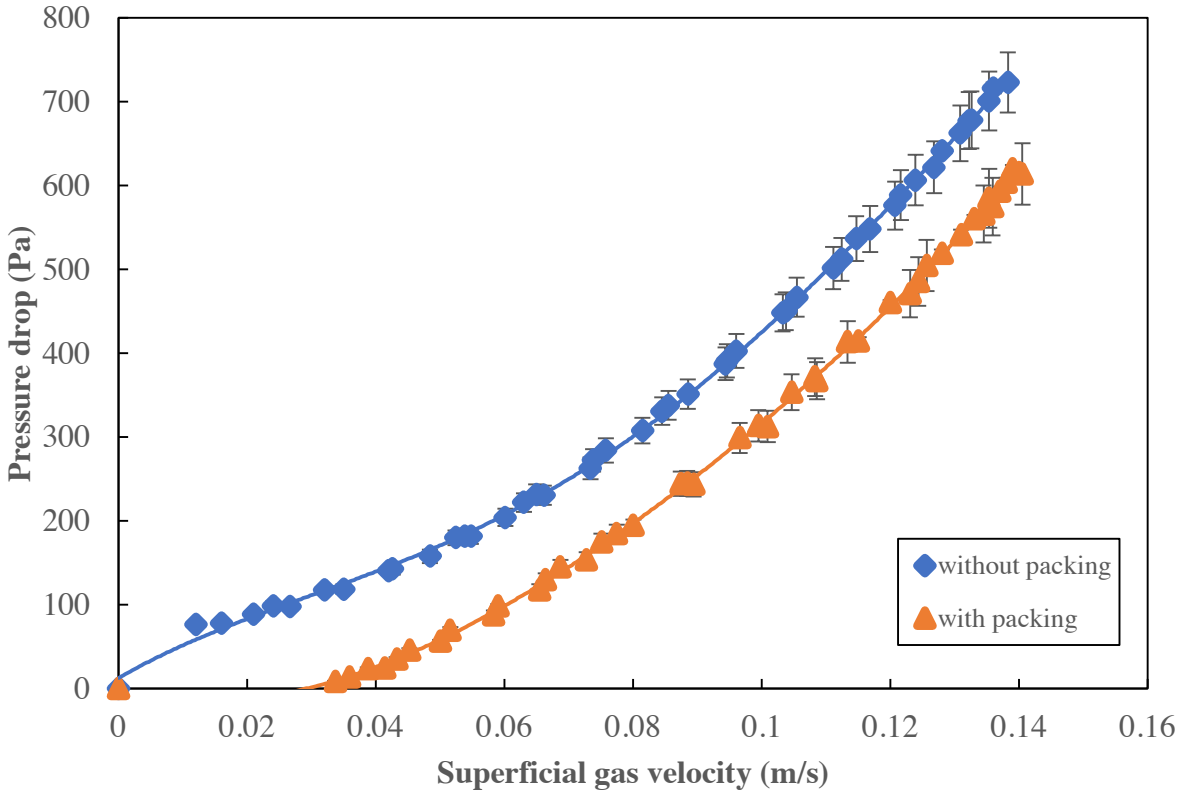

Figure 4-28 Effect of windbox packing on distributor pressure drop (empty bed) for 45°-hole distributor

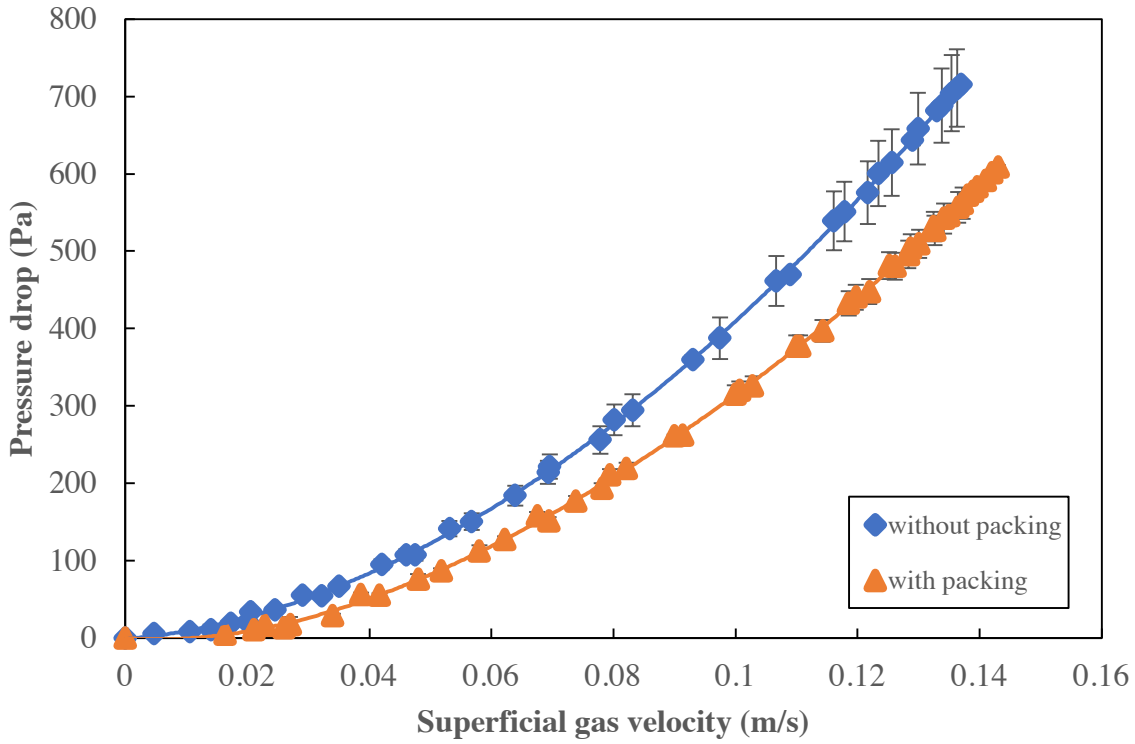

Figure 4-29 Effect of windbox packing on distributor pressure drop (empty bed) for 30°-hole distributor

With a static bed depth of 60 mm, the bed pressure drop was reduced when the packing was installed. This was because of the better air distribution underneath the distributor which improved the radial uniformity of fluidization gas flow. Figures 4-30, 4-31 and 4-32 compare the bed pressure drop for all three distributors at a static bed height of 60 mm with and without the packing.

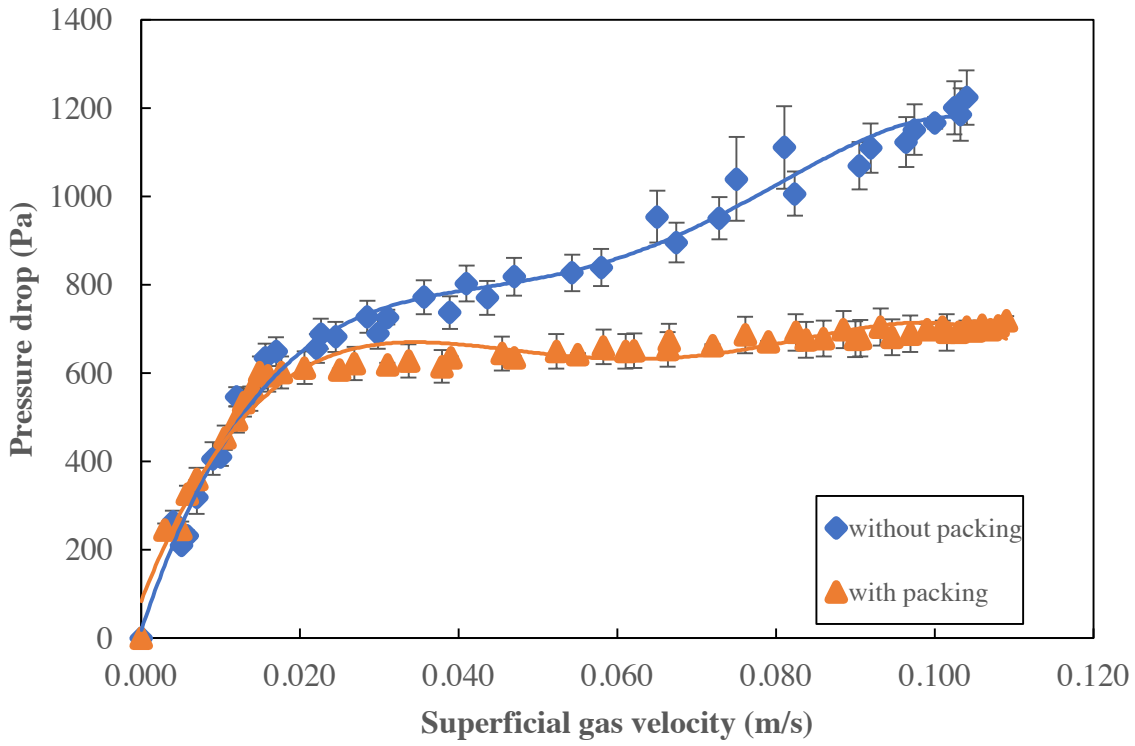

Figure 4-30 Effect of windbox packing on bed pressure drop for 90°-hole distributor for static bed depth of 60 mm

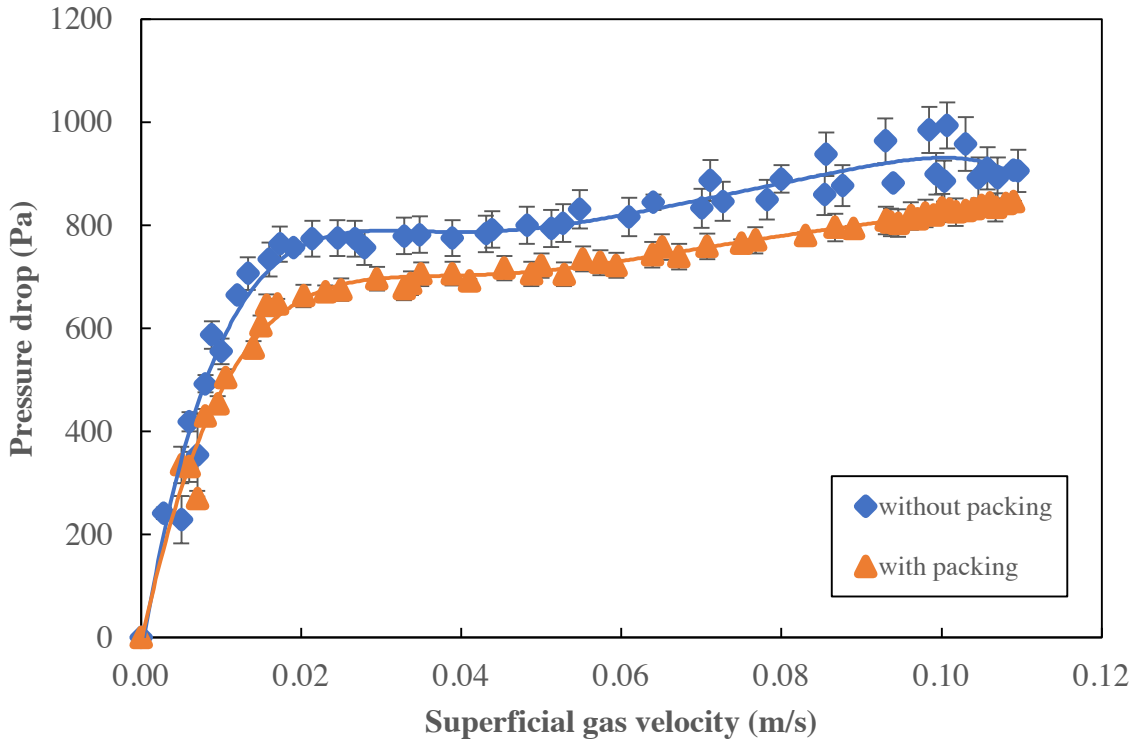

Figure 4-31 Effect of windbox packing on bed pressure drop for 45°-hole distributor for static bed depth of 60 mm

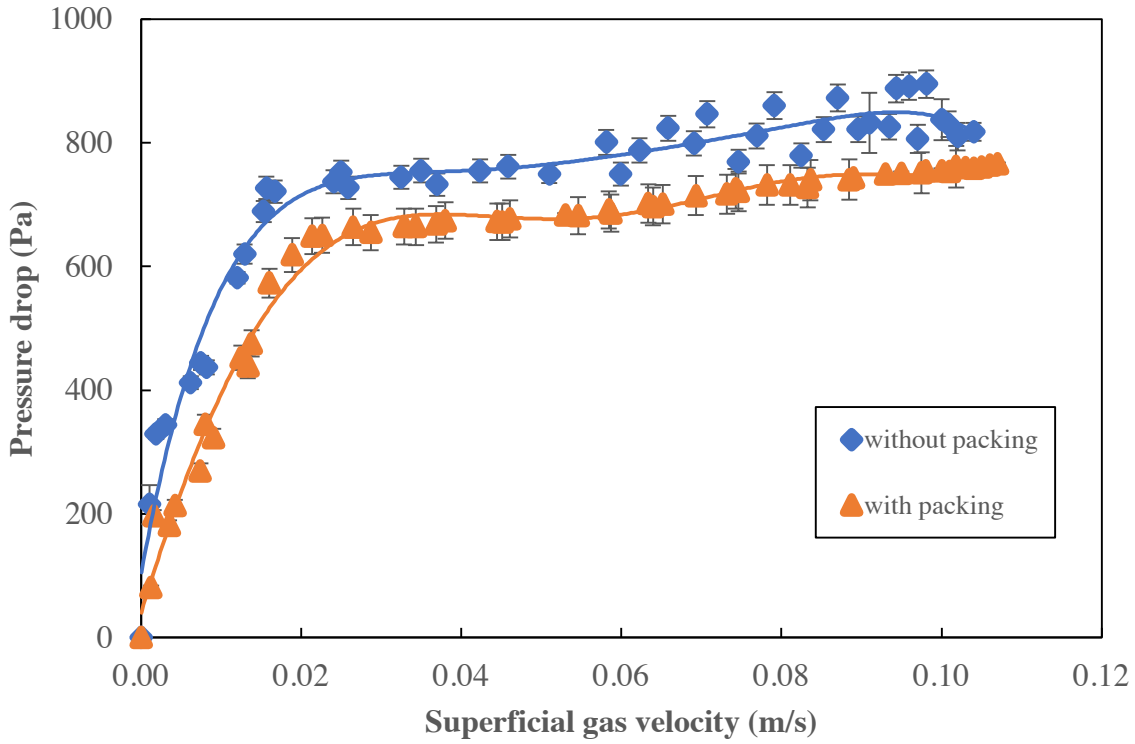

Figure 4-32 Effect of windbox packing on bed pressure drop for 30°-hole distributor for static bed depth of 60 mm

Chapter 5: Solids Mixing Study

5.1 Introduction

Solids mixing is important in characterizing fluidized bed reactors. Particles move in bubbling fluidized beds because of the presence of bubbles. They are carried upward by the wake of the bubbles and move downwards in regions where there are no bubbles (Kunii at el. 1991). Residence time distribution is one tool used to characterize solids mixing. In this chapter, the results obtained from solids mixing experiments are presented and discussed. Before moving forward to the results, a discussion is presented describing the solids mixing measurement system, tracer particles, tracer activation, detection and data treatment.

5.2 Measurement system, tracer particles activation and detection

Residence time distributions and local tracer concentrations were measured by activating the phosphorescent tracer particles at various locations in the fluidized bed. The tracer was activated by ultraviolet light directed downward produced by two lamps installed above the fluidized bed surface, as discussed in Chapter 3.

The tracer particles were borrowed from Coanda Research and Development Corporation. The tracer, called phosphorescent pigment, is yellowish in colour and has a particle density of 3600 kg/m^3 and a volume mean particle diameter of 76 microns. The tracer particles are composed of strontium silicate-aluminate oxide powder doped in Europium.

The tracer particles were activated while the bed of particles was stagnant. The top section of the bed was exposed to ultraviolet light using either or both lamps installed at the top of the column, directed downward onto the bed surface. The lamps were turned on using a switch located outside the fluidization column. For each set of data, the lamps were turned on for 12 min to ensure that the signals measured were independent of initial intensity. Once the tracer particles in the top layer were activated, the light was turned off and the air blower was simultaneously turned on to establish stable flow of air, which in turn ensured that the bed was fluidized quickly.

The air continued to flow for 2 min to capture the data, and then the air flow was turned off, signifying the end of data capturing. This led to a pulse input signal being detected at the first detector and a response signal at the second detector.

The tracer detection system consists of two 12 mm diameter single-fiber optical probes and two control boxes with photomultiplier and A/D converter. Two detectors were used for every mixing experiment. The column was covered by a black curtain to ensure that outside light did not interfere with the signals detected. Since the tracer particles decayed with time, a correction was required to correct the signal measured. To quantify the correction, the set-up was used as described in Chapter 3 where the tracer particles were activated for 12 min and left to decay. The decay curve is presented in Figure 3-7. The data were then fitted to a third order polynomial. Figure 5-1 presents the fitted decay curve data.

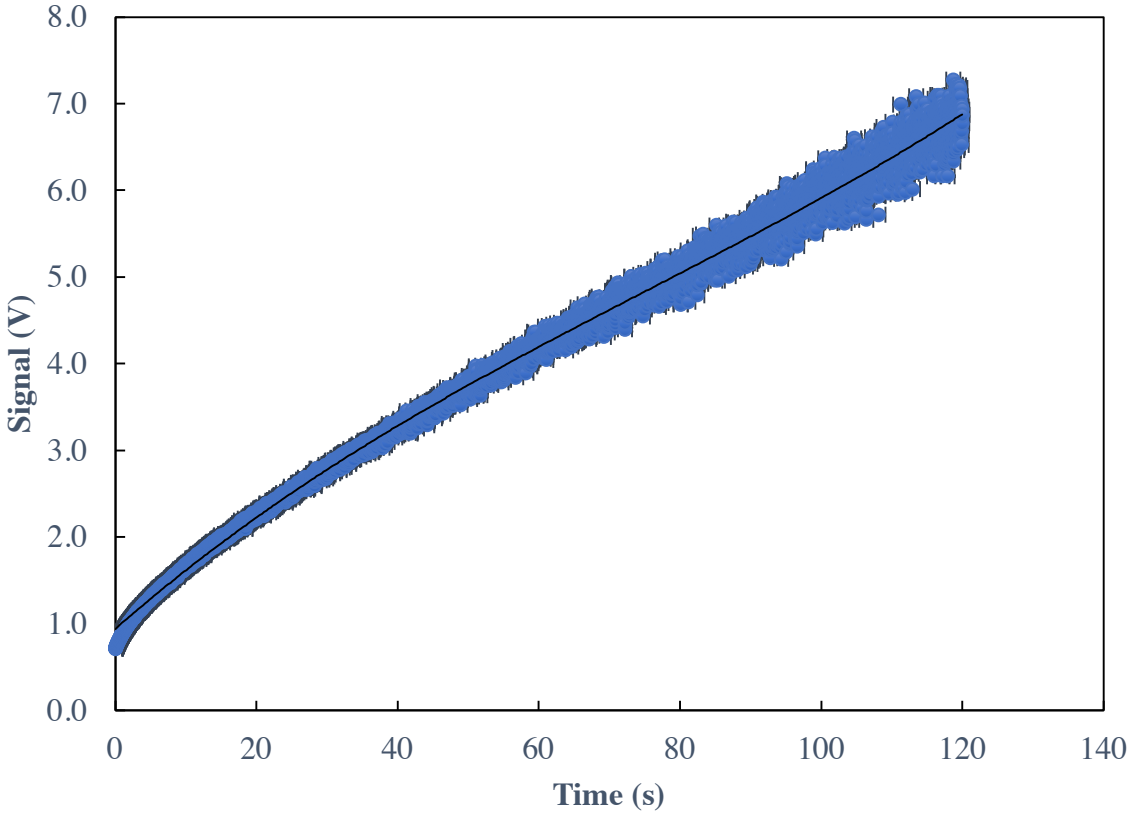

Figure 5-1 Decay curve fit

$$\frac{I_0}{I_{decay}(t)} = 2\times10^{-6}t^3 - 0.0004t^2 + 0.0713t + 0.9419 \qquad (5\text{-}1)$$

$$R^2 = 0.996$$

The captured data were treated by the following procedure:

1. Signals were loaded into an Excel file.
2. The time at which air flow was started was set to be t = 0.
3. The Signal baseline was adjusted to zero.
4. Signals were corrected for decay using equation (5-1).
5. Signals were smoothed using the Savitzky-Golay filter available in Matlab.

5.3 Axial solids mixing

It was assumed that axial solids mixing is independent and much faster than tangential solids mixing. To verify this assumption, the axial solids mixing was investigated for only the 90°-hole distributor. Figure 5-2 shows a diagram of the axial solids mixing experiment coordinates.

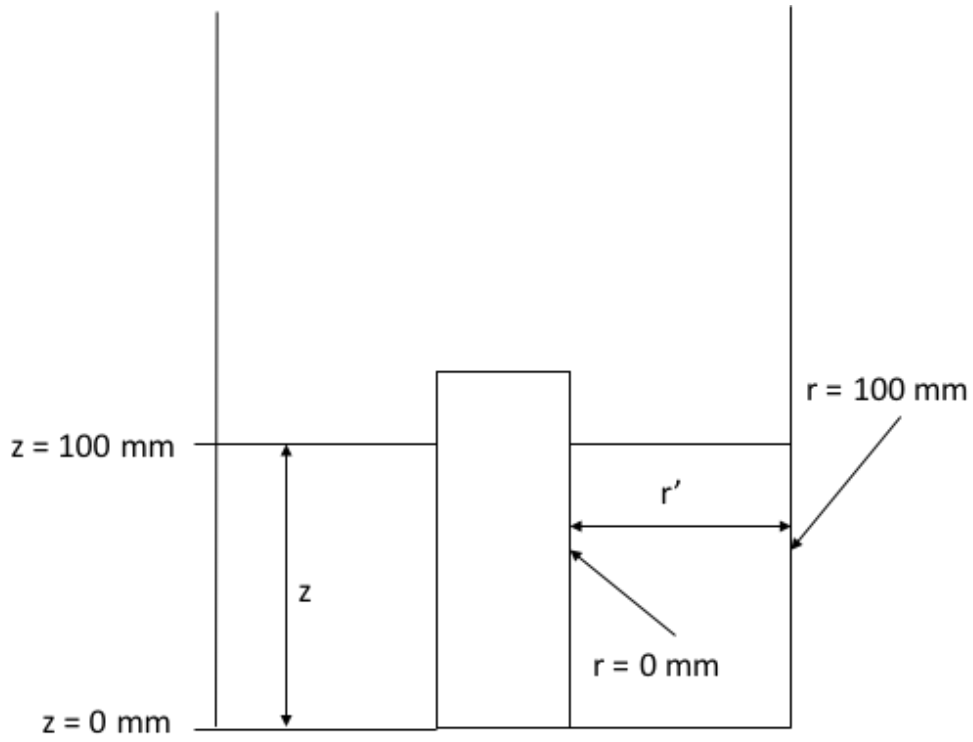

Figure 5-2 Axial solids mixing experiment diagram showing both axial and radial coordinates

The bed was operated at a static bed height of 100 mm with two probes installed at different axial positions (one at z = 50 mm and the other at z = 80 mm). Tracer particles were activated at the surface of the bed and once the air flow started, particles started to move. In this study, the turnover time was measured in addition to the dense phase downward velocity. Two superficial velocities were used and the probes were moved radially, with three radial positions analyzed (r = 25, r = 50 and r = 75 mm). Figure 5-3 illustrates the signals

obtained from both axial locations and at a radial position of 50 mm. The signals were normalized by dividing by the peak intensity for each probe and then corrected for decay.

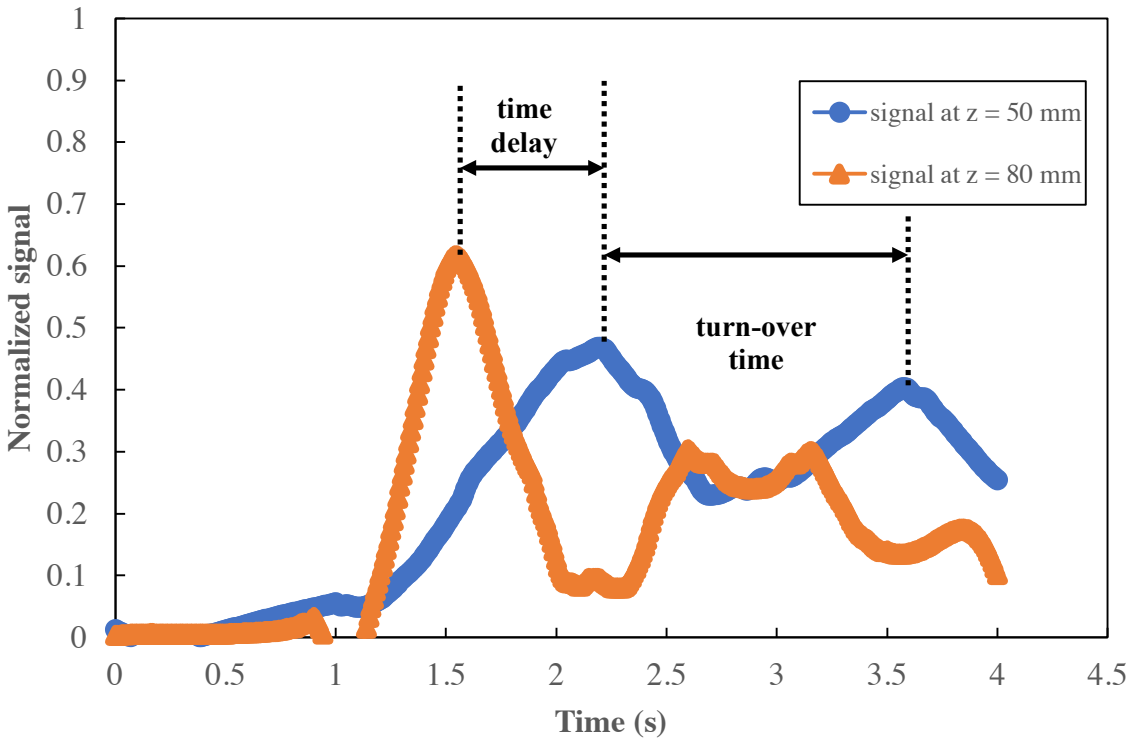

Figure 5-3 Normalized corrected tracer concentration for U=0.29 m/s and r = 50 mm

The results showed a sharp peak signal from the upper probe located at z = 80 mm and a little spreading for the lower probe located at z = 50 mm. However, the mixing was very difficult to quantify using the dispersion model since the solids movement was not identical in terms of showing good spreading. Therefore, another method was needed to quantify and characterize axial solids mixing.

Geldart (1997) correlated the reliance of overall mixing rate (R_m) with the product of four terms: bulk density of dense phase, fraction of bed solids moving upward, mean upwards velocity and bed cross-sectional area. He also defined the turnover time as the time required to turn over the bed once. A simple calculation is presented in equations (5-2) and (5-3) in

which the turnover time is related to the height at minimum fluidization, the bubble wake fraction, the drift fraction, the deviation from the two-phase theory (Y) and minimum fluidization velocity.

$$Turnover\ time\ (\tau_T) = \frac{H_{mf}}{(\beta_w + 0.38\beta_d)Y(U - U_{mf})} \qquad (5\text{-}2)$$

$$Y = 2.27\ Ar^{-0.21} \qquad (5\text{-}3)$$

Both wake and drift fractions values depend on gas and particle properties which are represented by the Archimedes number according to Geldart (1997).

The turnover time was measured from the data collected using the autocorrelation between two consecutive peaks. Three repeated measurements were taken at each superficial gas velocity. The measured turnover time was compared with prediction from Geldart (1997) equations (5-2) and (5-3) in which the turnover time was defined to be the ratio of mass of powder to the mass circulation rate. Table 5-1 presents the values used for equation (5-2).

Table 5-1 Geldart (1997) turnover time estimation

Variable	Value	Unit
H_{mf}	0.1	m
β_w	0.3*	-
β_d	0.85*	-
Y	0.86**	-
U	0.17, 0.23 and 0.24	m/s
U_{mf}	0.013***	m/s

*found from Geldart (1997) graph relating to Archimedes number

**calculated from equation (5-3)

***calculated from Wen and Yu (1966) empirical correlation

There was good agreement between calculated turnover time and the predicted value. This indicated that equation 5-2 was able to estimate the turnover time for the fluidized bed with the 90°-hole distributor. Figure 5-4 presents the turnover time calculated vs. predicted.

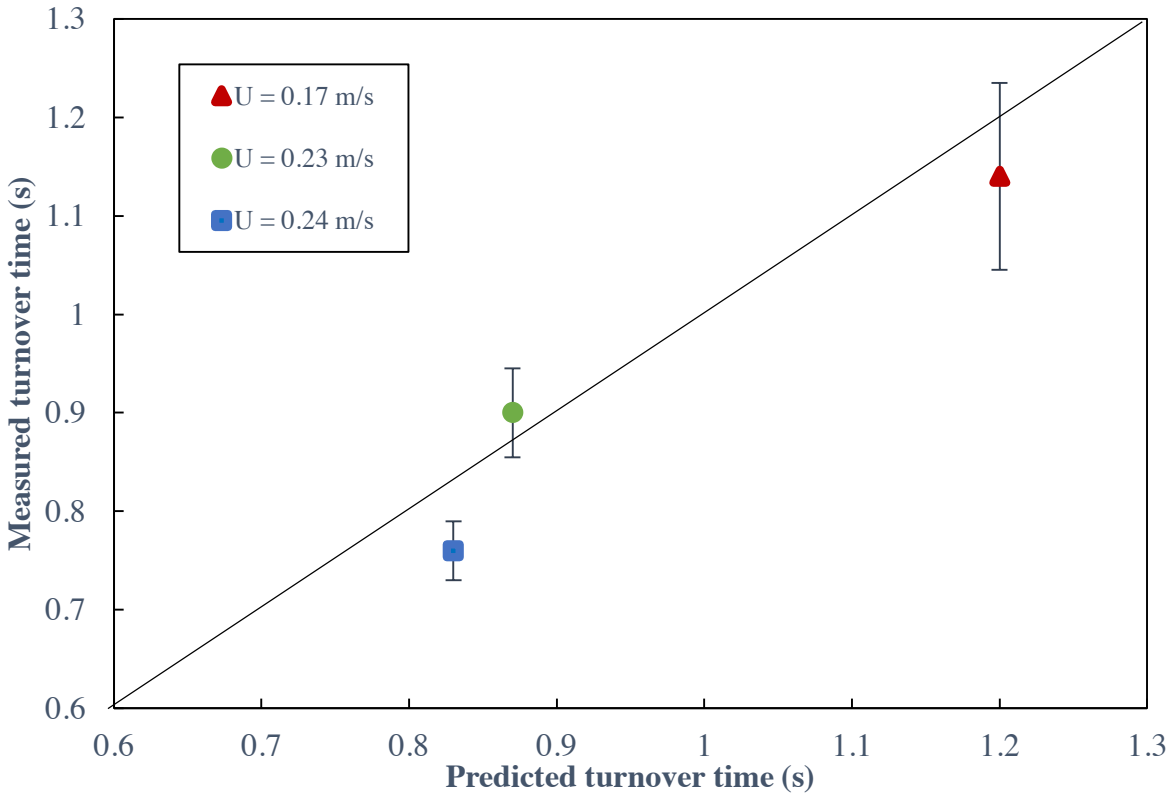

Figure 5-4 Measured turnover time for axial solids mixing vs. time predicted by Geldart (1997) equation (5-2)

Another parameter that was measured to characterize the axial solids mixing was the dense phase downward velocity (U_s). Two methods were used to estimate U_s. First, the velocity was calculated from the bubbling bed model equations given by Kunii et al. (1991):

$$U_s = \frac{f_w \delta U_b}{1-\delta-f_w \delta} \qquad (5\text{-}4)$$

$$\delta = \frac{U}{U_b} \tag{5-5}$$

$$U_b = 0.711\sqrt{gD_b} \tag{5-6}$$

$$D_b = D_{be} - (D_{be} - D_{b0})e^{\left(-0.3\frac{z}{D_T}\right)} \tag{5-7}$$

$$D_{b0} = \frac{1.38}{g^{0.2}}\left[\frac{A}{N_{or}}\left(U - U_{mf}\right)\right]^{0.4} \tag{5-8}$$

$$D_{be} = 1.64\left[A\left(U - U_{mf}\right)\right]^{0.4} \tag{5-9}$$

Second, the velocity was obtained from the time delay between the two probes by cross-correlation of the signals obtained from the probes and the distance between the probes. The cross-correlation function available in Matlab was used, since the manual determination of peaks was troublesome and could lead to errors. Three repeated measurements were taken for two superficial gas velocities. Figure 5-5 compares the predicted and measured dense phase downward velocities.

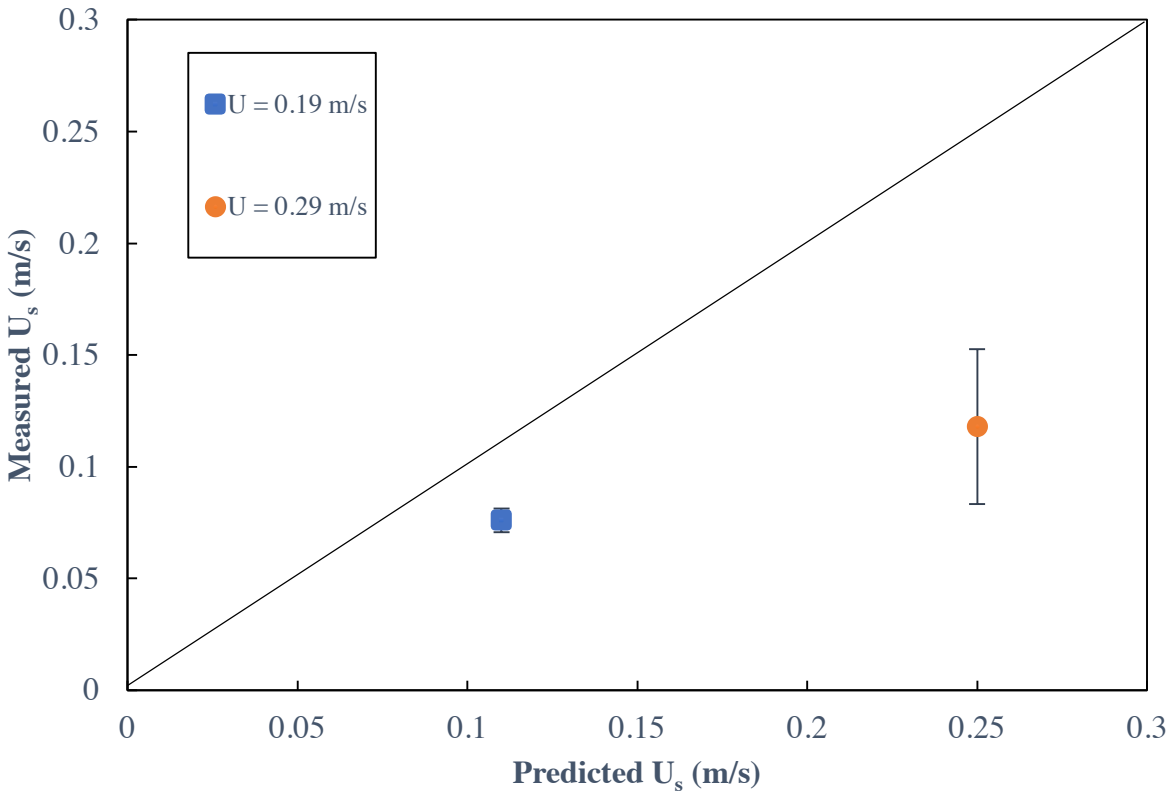

Figure 5-5 Dense phase downward velocity measured vs. predicted

The measured velocity was much less than the predicted value for both superficial gas velocities. This was investigated using video recording to check what was happening. The video indicated that there was a major impact of the probes on the dense phase downward velocity. Particles were not moving downward at the same rate everywhere along the annulus. Therefore, using a video recording taken during the same period as in the tracer experiment, the velocity was calculated by recording the time particles passed the probes location and by knowing the distance between the two probes. In this case, the probes were removed to see their effect on the particle motion. Figure 5-6 presents the findings with the probes removed after three repeated measurements. The results confirm that probes did indeed reduce the measured dense phase downward velocity.

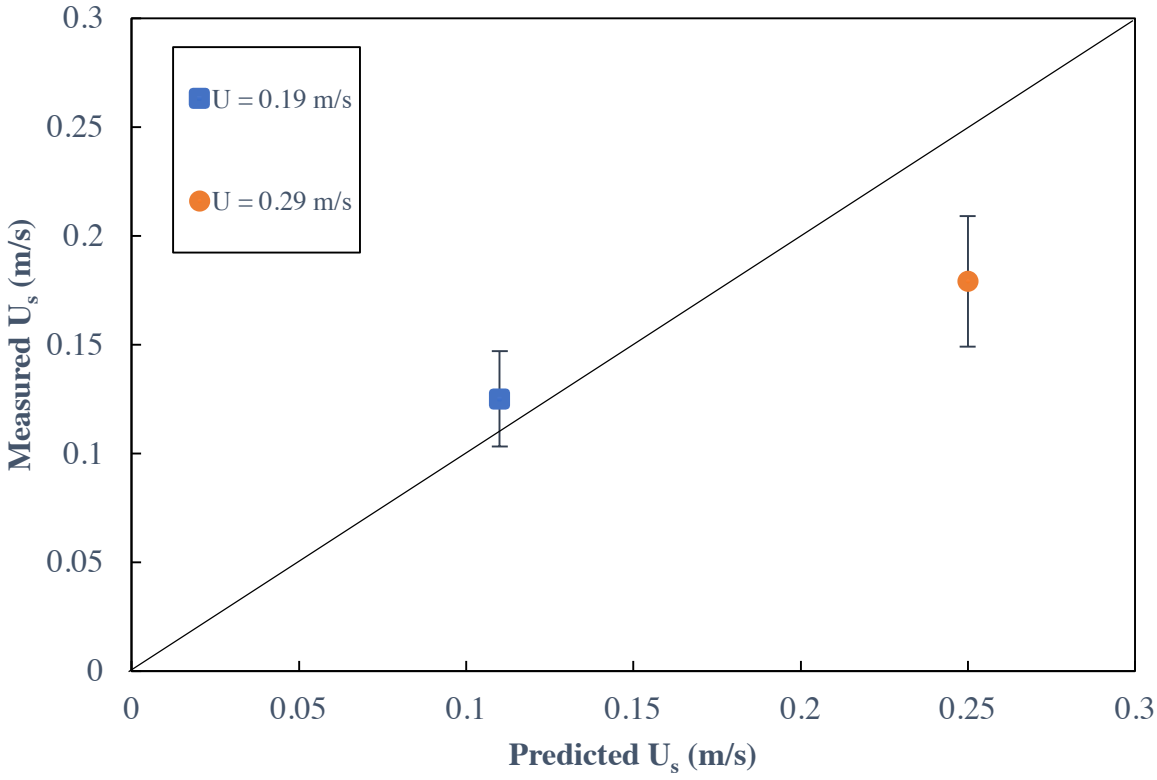

Figure 5-6 Dense phase downward velocity measured without probes vs. predicted

5.4 Tangential solids mixing

All three distributors were tested to determine the tangential mixing behaviour. Three tangential positions were chosen, together with three radial positions across the annulus. Figure 5-7 shows a top view of the fluidized bed surface illustrating the coordinates.

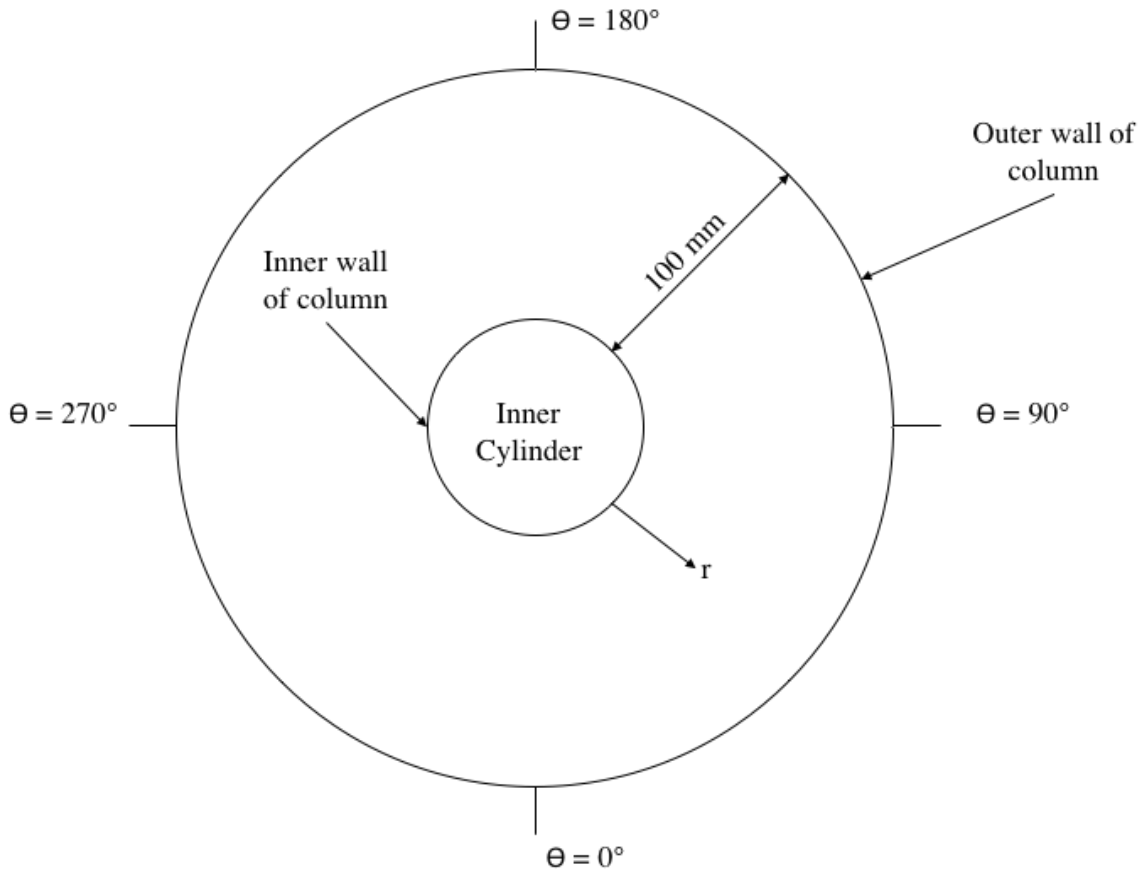

Figure 5-7 Top view of fluidized bed surface highlighting both radial and tangential coordinates

The bed was operated at a static bed height of 100 mm. The tracer particles were activated using two ultraviolet lamps, both directed downward from above, illuminating one sector of the bed surface (between $\theta = 270°$ and $\theta = 0°$ in Figure 5-7). Two detectors were used simultaneously, one as an input and the other to detect the output signal. The bed was also operated at two superficial gas velocities. The signals were normalized by dividing by the peak intensity for each probe.

Starting with the 90°-hole distributor, Figure 5-8 shows the normalized tracer concentration corrected for decay, at a superficial gas velocity of 0.17 m/s and at r = 50 mm. Tracer was detected first at the input detector, and then a peak was detected at the second detector. The cross-correlation function available in Matlab was used to estimate the time delay between

the signals from the first and second detectors and, knowing the tangential distance, the tangential particle velocity was estimated for the 90°-hole distributor.

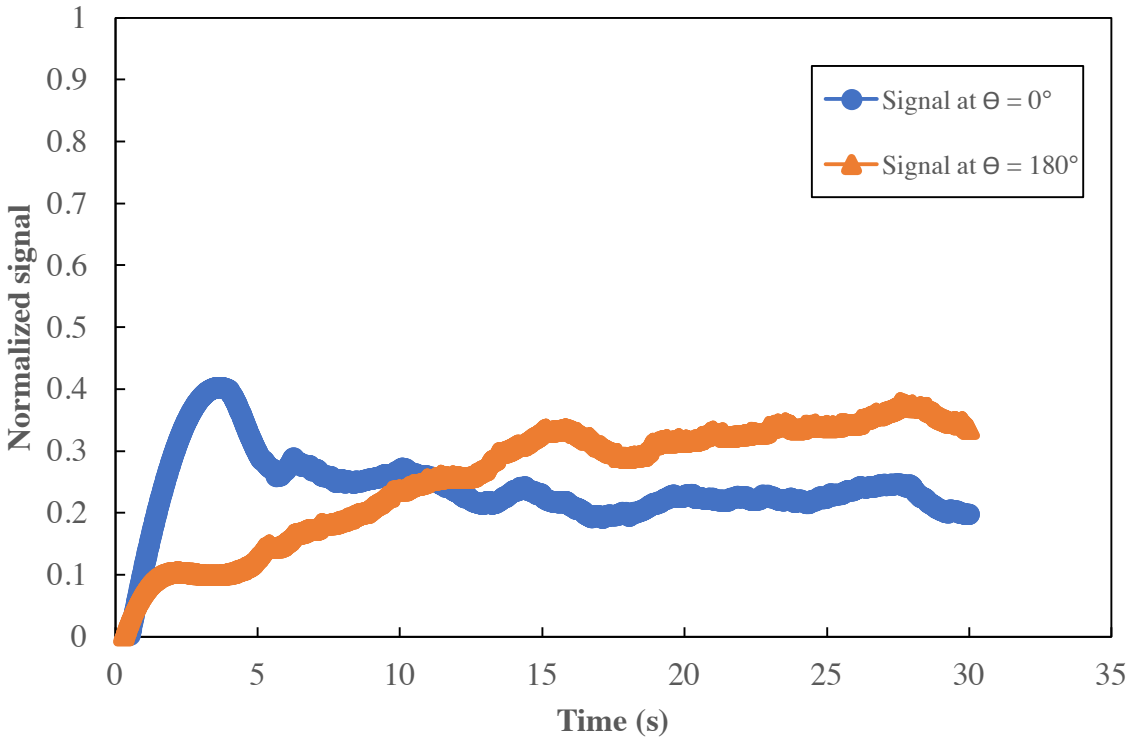

Figure 5-8 Normalized corrected tracer concentrations for 90°-hole distributor, U = 0.17 m/s and r = 50 mm

A similar trend was observed when the bed was operated at a superficial velocity of 0.24 m/s with the results shown in Figure 5-9.

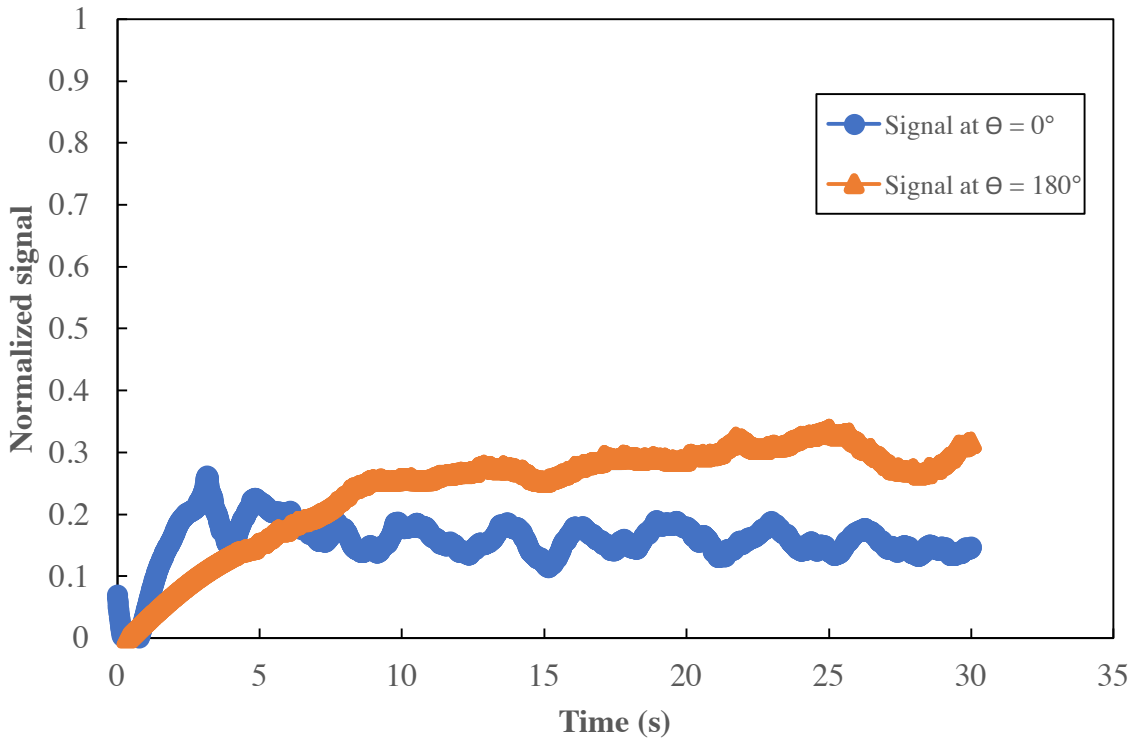

Figure 5-9 Normalized corrected tracer concentrations for 90°-hole distributor, U = 0.24 m/s and r = 50 mm

The results obtained from the cross-correlation of the two signals, showed that the tangential particle velocity for the 90°-hole distributor was around 3.3 and 3.5 mm/s when operating at superficial gas velocities of 0.17 and 0.24 m/s, respectively.

Figures 5-10 and 5-11 show the corresponding results for the 45° and 30°-hole distributors. The tangential particle velocity was estimated for both distributors. The tangential particle velocity profile showed an increase in magnitude with increasing radial position so that the tangential particle velocity near the outer wall was higher than near the inner wall. In addition, as expected, the tangential particle velocity was the highest for the 30°-hole

distributor followed by the 45°-hole and then the 90°-hole distributor. Figure 5-12 presents the tangential particle velocity profiles for the 30°-hole distributor, while Figure 5-13 shows the tangential profiles for the 45°-hole distributor.

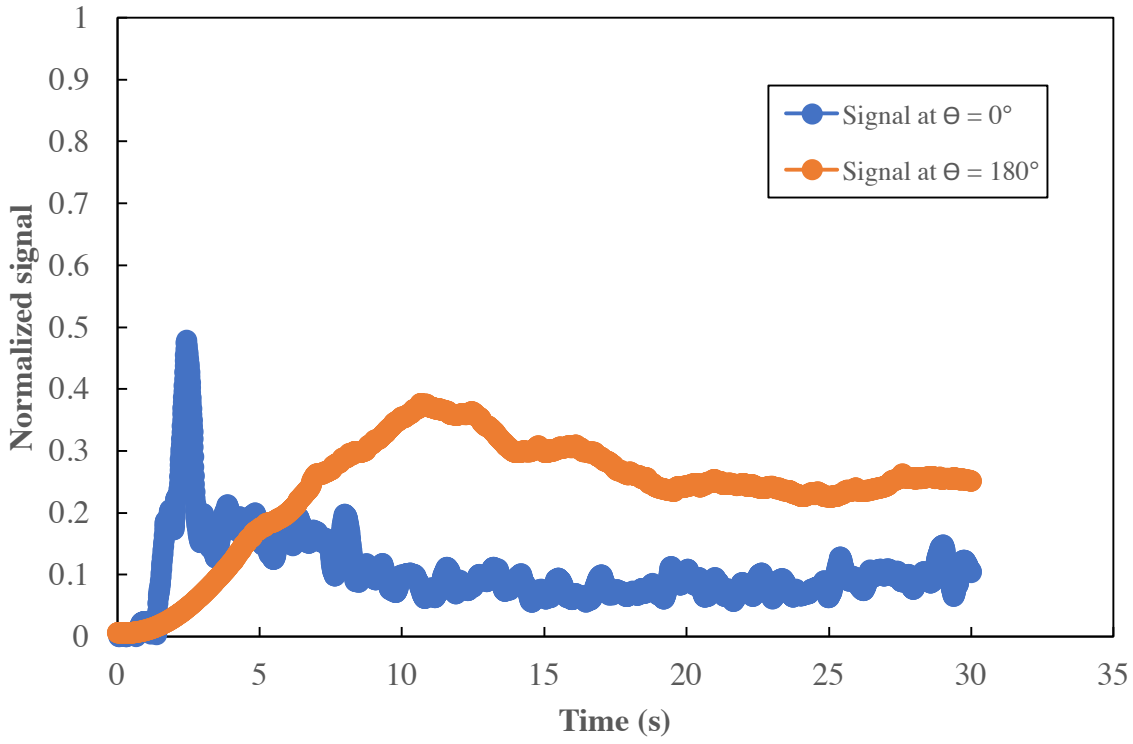

Figure 5-10 Normalized corrected tracer concentrations for 45°-hole distributor, U = 0.17 m/s and r = 50 mm

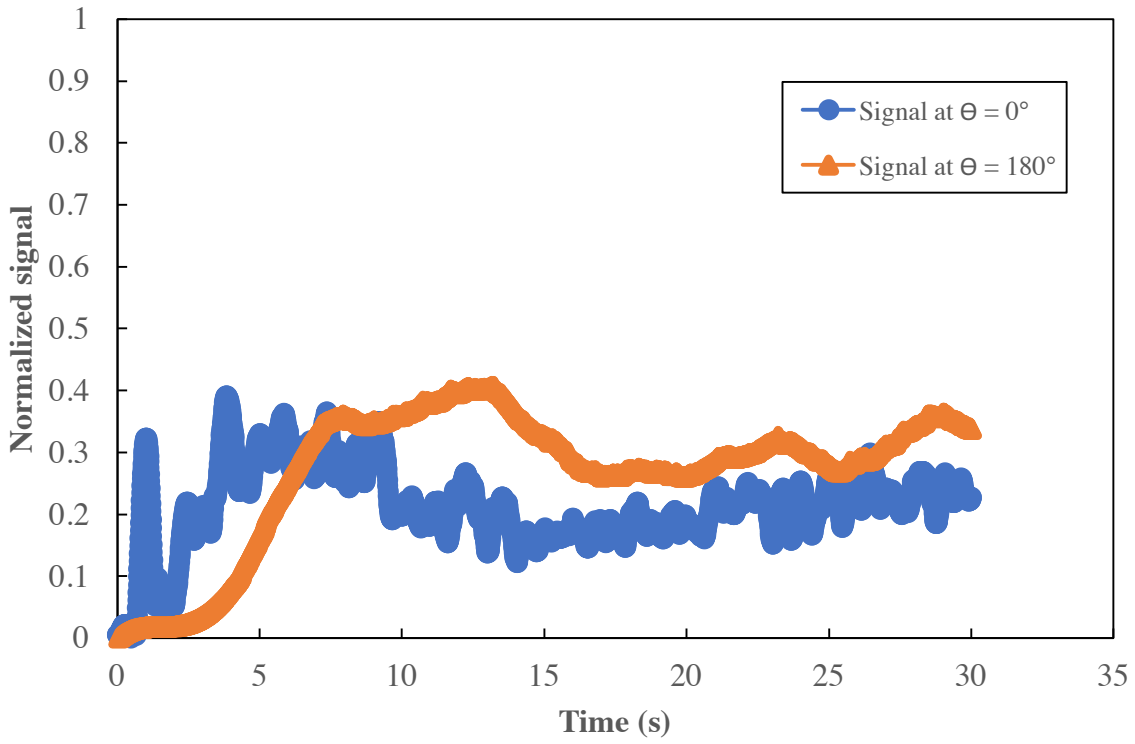

Figure 5-11 Normalized corrected tracer concentrations for 30°-hole distributor, U = 0.17 and r = 50 mm

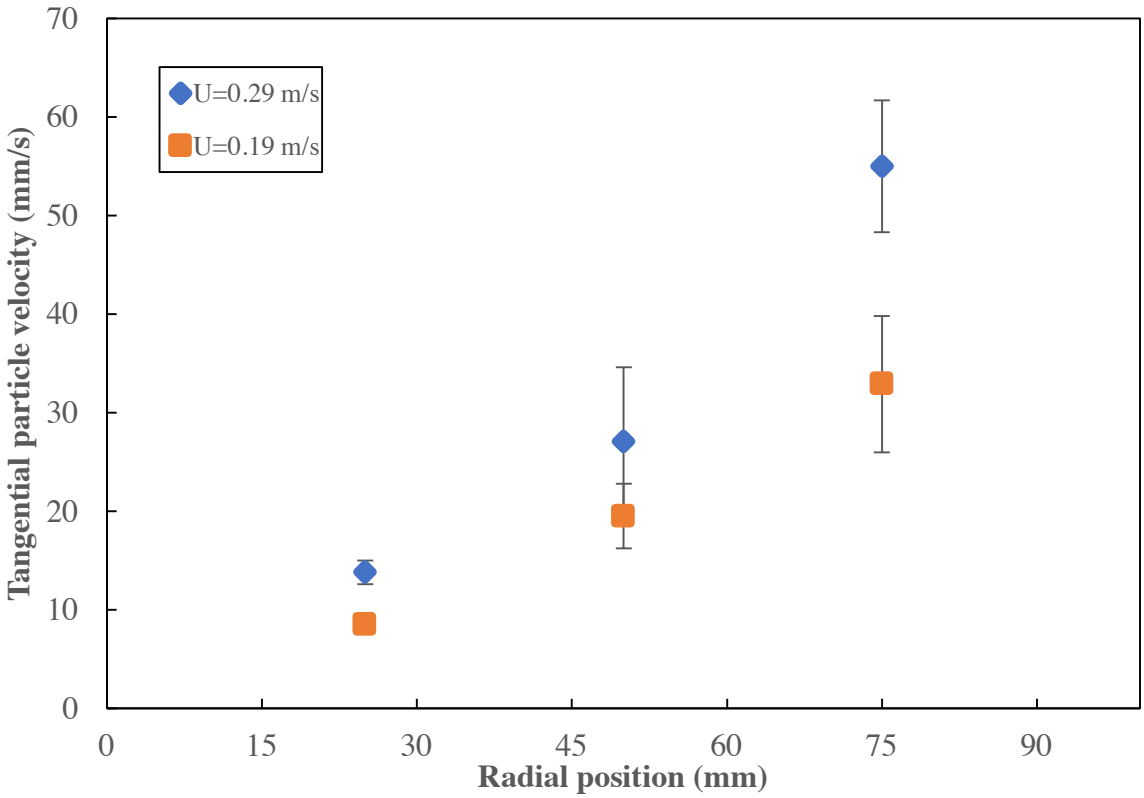

Figure 5-12 Tangential particle velocity profiles for 30°-hole distributor between θ = 0°and θ = 180°

The angular velocity was also calculated and was found to increase with increasing radial position as well. The angular velocity is determined as the ratio of the tangential velocity to radial distance measured from the centre of the distributor (i.e. r +$R_{\text{inner cylinder}}$). Figures 5-12b shows the angular velocity profile for the 30°-hole distributor.

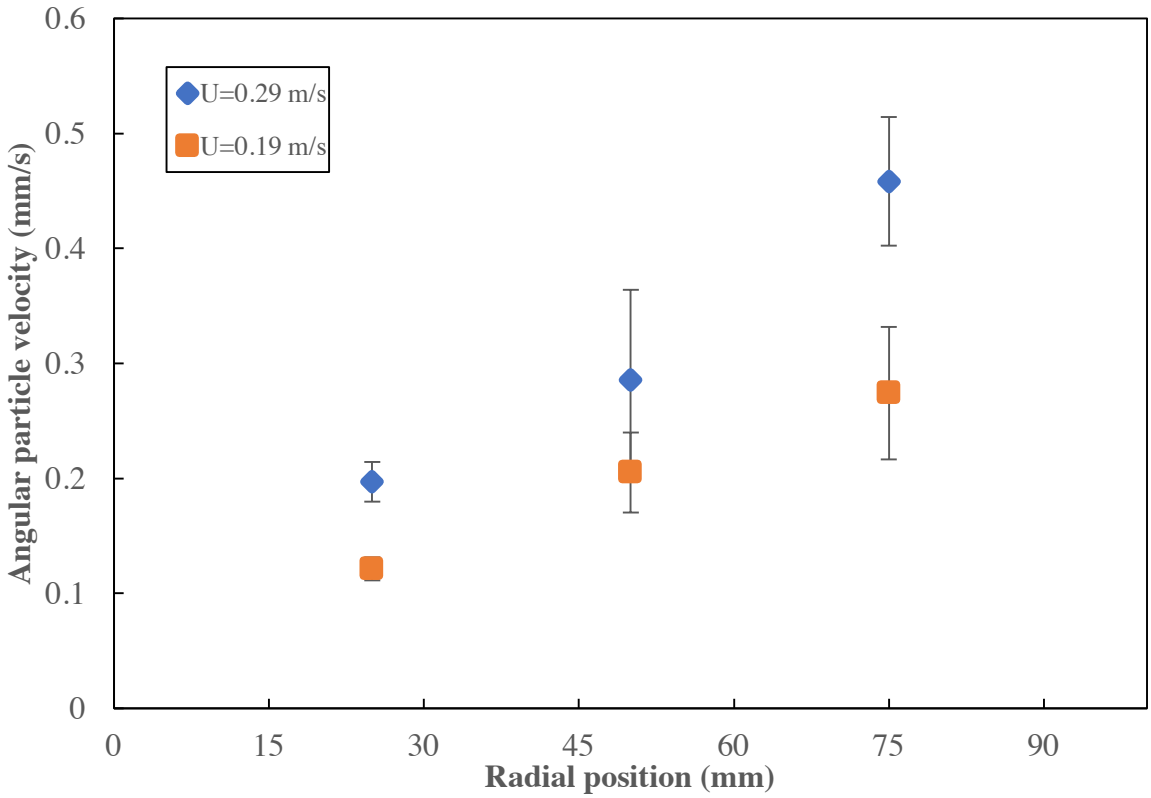

Figure 5-12b Angular particle velocity profiles for 30°-hole distributor between θ = 0°and θ = 180°

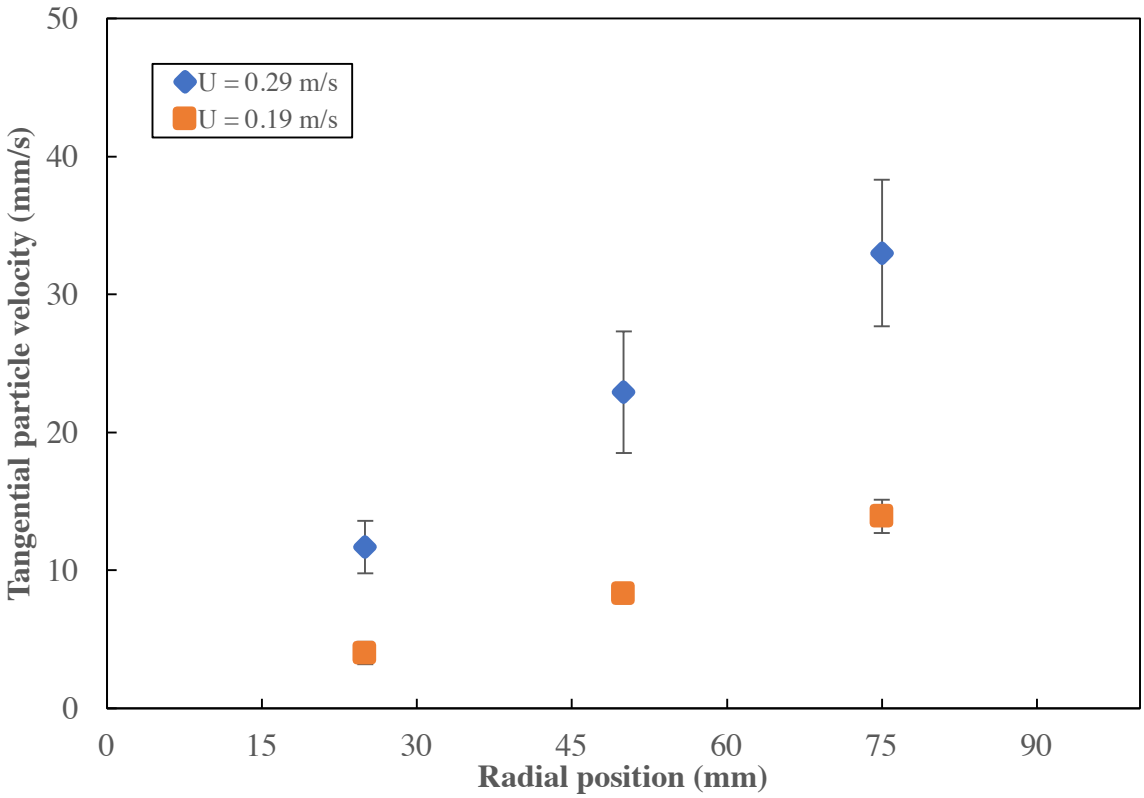

Figure 5-13 Tangential particle velocity profiles for 45°-hole distributor between θ = 0°and θ = 180°

In addition, Figure 5-14 presents the effect of orifice angle on the tangential particle velocity measured at r = 50 mm for two superficial gas velocities. The figure clearly shows the higher velocities for the 30°-hole distributor, as expected.

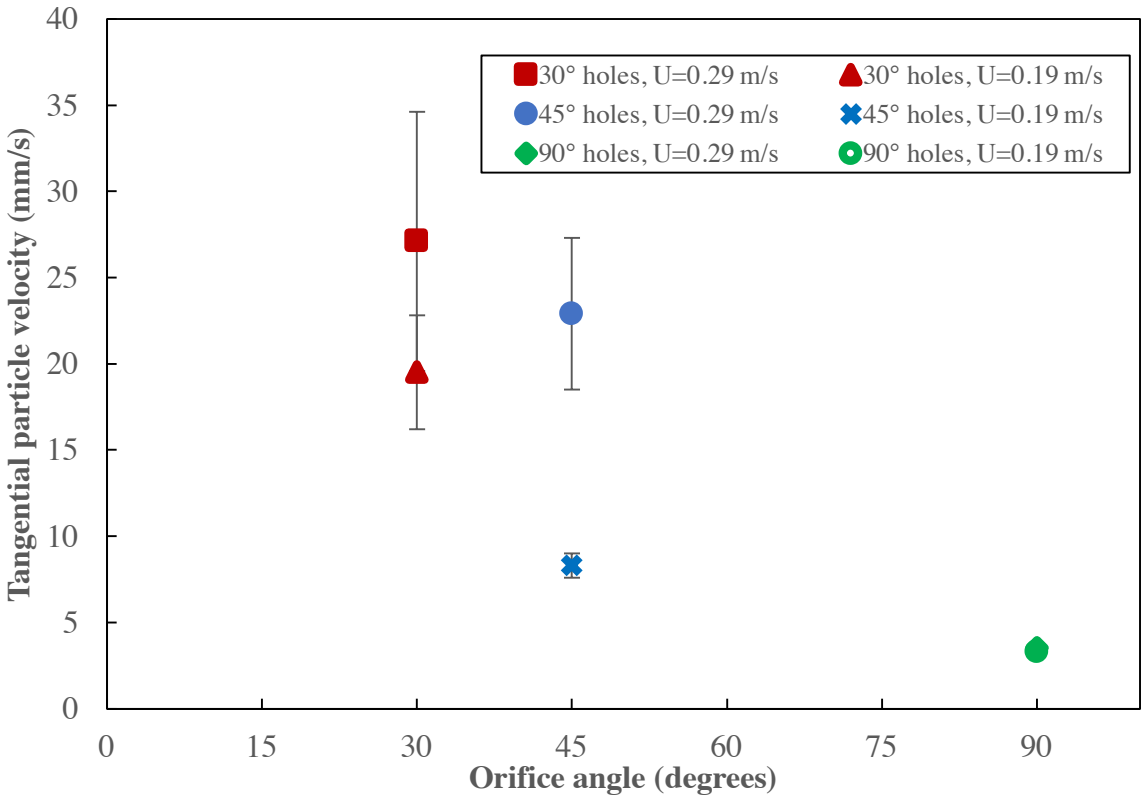

Figure 5-14 Effect of orifice angle on tangential particle velocity at r = 50 mm and between θ = 0°and θ = 180°

In order to describe the tangential mixing of solids in the fluidized bed, the one-dimensional dispersion model (equation 5-10) was used (Fogler, 2006). In this model, the tangential dispersion was used with the axial dispersion neglected, because the axial mixing is assumed to be much faster than tangential mixing. The first peak input signal spread as the tracer was measured at the output detector. Using the residence time distribution, the Peclet number was estimated for all three distributors to quantify the tangential mixing.

$$\mathfrak{D}_t \frac{1}{r^2}\frac{\partial^2 C}{\partial \theta^2} - \frac{1}{r}\frac{\partial (UC)}{\partial \theta} = \frac{\partial C}{\partial t} \qquad (5\text{-}10)$$

The system was assumed to have open-open boundary since there was a large distance between the inlet and the input probe as well as a large distance between the outlet and the

output probe. The solution of the dispersion model equation in terms of variance and mean residence time was used to solve for the Peclet number (Pe) with equation (5-11) taken from (Fogler, 2006) as the solution:

$$\frac{\Delta\sigma^2}{\Delta t_m^2} = \frac{2Pe+8}{Pe^2+4Pe+4} \qquad (5\text{-}11)$$

where the Peclet number defined by equation (5-12) is a function of the superficial gas velocity, dispersion coefficient and tangential distance (L) (Fogler, 2006):

$$Pe = \frac{UL}{D_t} \qquad (5\text{-}12)$$

Both the variance and the mean residence time were calculated from the RTD data. First, the RTD function E(t) was determined from the tracer concentrations data according to the following equation (Fogler, 2006)

$$E(t) = \frac{C(t)}{\int_0^\infty C(t)dt} \qquad (5\text{-}13)$$

C(t) is the tracer concentration data captured by the detectors. Once the RTD function E(t) is evaluated for all t, the first moment of the RTD function E(t), is calculated. The first moment is simply the mean residence time and is calculated using equation (5-14) (Fogler, 2006):

$$t_m = \int_0^\infty t.E(t)dt \qquad (5\text{-}14)$$

The variance was also calculated according to (Fogler, 2006) using equation (5-15):

$$\sigma^2 = \int_0^\infty (t - t_m)^2 E(t)dt \qquad (5\text{-}15)$$

In addition, the dispersion model solution was compared with the mechanistic model based on the Davidson (1961) bubble for horizontal movement of solids as proposed by Kunii and Levenspiel (1991). Their model for Geldart A and B solids was used with $\alpha = 1$, as it was assumed in their model for Group A particles, where α is a function of bubble size, cloud thickness and bubble density in the bed, as shown in

$$D_h = \frac{3}{16}\frac{\delta}{1-\delta}\frac{\alpha^2 U_{mf} D_b}{\varepsilon_{mf}} \qquad (5\text{-}16)$$

where D_b is the bubble diameter calculated from equation (5-7). Figure 5-15 shows the effect of orifice inclination angle on the Peclet number. Tangential mixing was higher (i.e., Pe was lower) for steeper orifice angle at a higher superficial gas velocity (0.29 m/s). For the lower superficial gas velocity (0.19 m/s), the tangential mixing was almost the same for all three distributors.

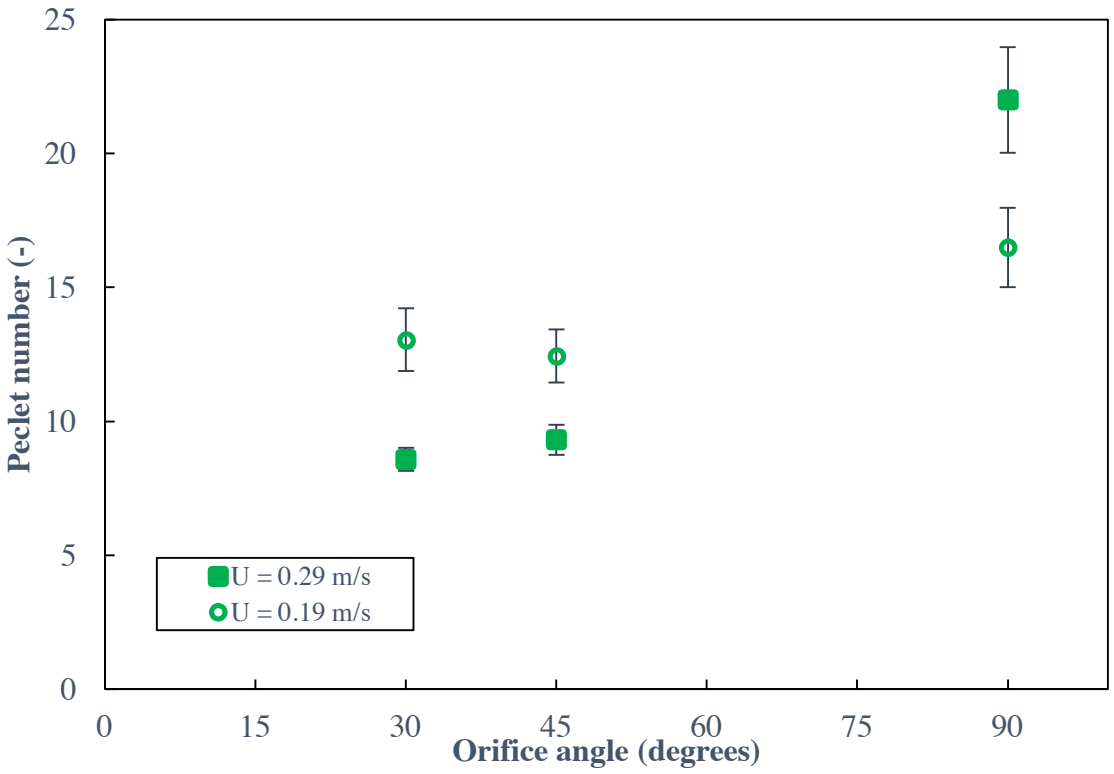

Figure 5-15 Effect of orifice angle on tangential solids mixing

Figure 5-16 shows how our experimentally measured tangential dispersion coefficient compared to the horizontal dispersion coefficient calculated from the Kunii and Levenspiel (1991) model. The tangential dispersion estimated was much higher, indicating poor agreement between their model and the experimental data.

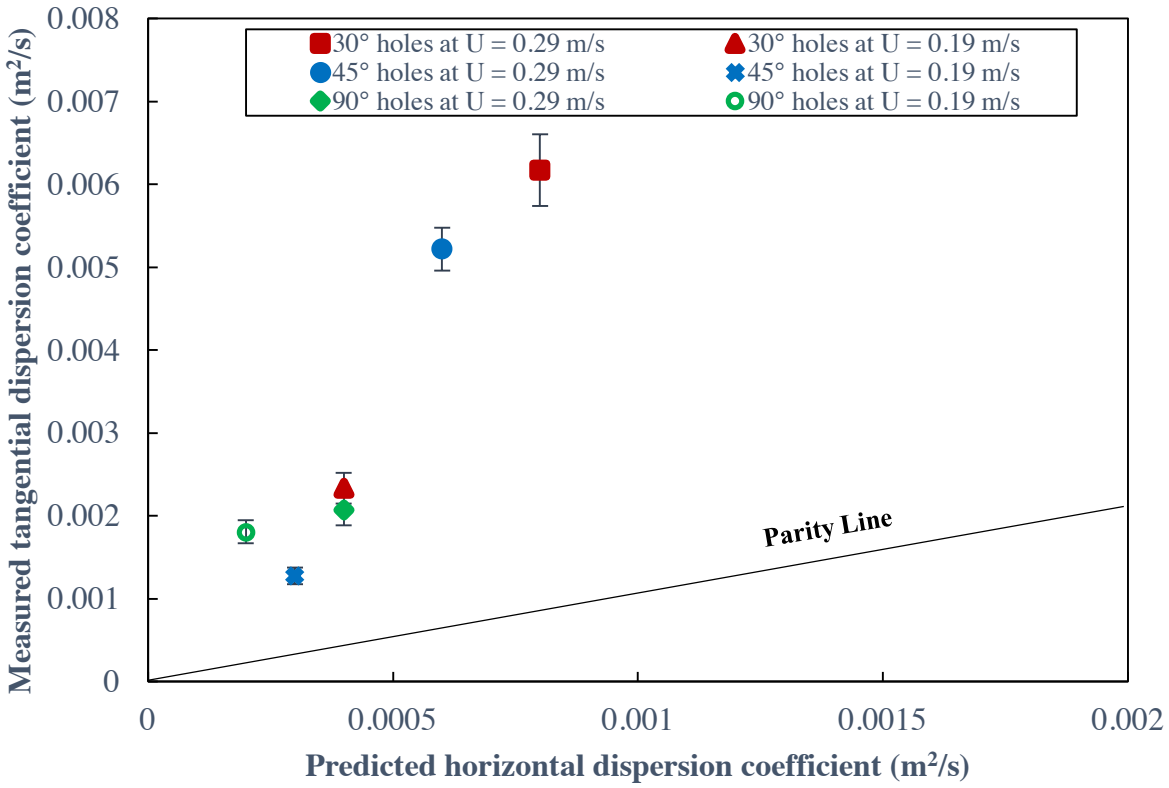

Figure 5-16 Comparison of our experimental tangential dispersion coefficient with horizontal dispersion coefficient from Kunii and Levenspiel (1991) with $\alpha = 1$

Chapter 6: Conclusions

Three distributors were designed and fabricated, all with the same specifications except for the orifice inclination angle. The angles were vertical (90°), 45° and 30°. Two bed materials were used, glass beads and phosphorescent particles, belonging to Groups A and B in the Geldart classification. Two studies were conducted, a hydrodynamic study and a solids mixing study. In the hydrodynamic study, the effects of orifice inclination angle, static bed height and windbox packing were investigated. In the solids mixing study, the axial solids mixing was investigated for the 90°-hole distributor using phosphorescent tracer particles and by estimating the bed turnover time and dense phase downward velocity. In addition, tangential solids mixing was studied for all three distributors using the phosphorescent tracer particles to measure the residence time distribution to estimate the tangential dispersion coefficient and the tangential particle velocity using the dispersion model. The major findings from this research and future research needs are summarized below.

6.1 Major conclusions

The major findings from the hydrodynamic study were as follows:

1. For a given superficial gas velocity, the distributor pressure drop was lower for the 45°-hole and 30°-hole distributors than the 90°-hole distributor. The magnitude was around 10% less than for the 90°-hole distributor at the same superficial gas velocity.
2. Bed pressure drop was lowest for the 90°-hole distributor.
3. There was no clear difference between the 45°-hole and 30°-hole distributors in terms of bed pressure drop.
4. Bed pressure drop fluctuations were highest for the 90°-hole distributor, indicating larger bubbles.

5. In a shallow bed, bed expansion was highest for the 90°-hole distributor followed by the 45°-hole and then the 30°-hole distributor.
6. In a deep bed, bed expansion was virtually the same for all three distributors.
7. The minimum fluidization velocity was highest for the 30°-hole distributor followed by the 45°-hole and then the 90°-hole distributor.
8. Static bed height had an impact on the minimum fluidization velocity for the inclined-holes distributors. The pressure fluctuation method showed a drop in minimum fluidization velocity with increasing static bed height. The pressure drop-velocity curve method showed the opposite.
9. Installing coarse windbox packing improved air distribution which in turn improved the radial flow distribution.

The major conclusions from the solids mixing study were as follows:

1. Turnover time for the 90°-hole distributor could be estimated based on the bubbling bed model equations.
2. Probes and ports in this study interfered with the solids mixing by reducing the dense phase downward velocity by ~40%.
3. The tangential particle velocity increased with increasing radius in the annulus. The velocity was higher near the outer wall of the column and lower near the inner wall.
4. Tangential particle velocity was highest for the 30°-hole distributor followed by the 45°-hole and then the 90°-hole distributor.
5. Both inclined distributors (30° and 45° holes) resulted in greater tangential mixing than the 90°-hole distributor.

6.3 Suggestions for future work

In this research project, the bed expansion was estimated visually. It is recommended that for future work, a more appropriate method such as using axial pressure profiles. In addition, this study did not investigate the radial mixing. It is recommended to measure the particle velocity along the radial position by using fiber optical probes directed along the distributor area to measure radial particle velocities at different radial positions. Moreover, the middle hollow cylinder radius could influence the bed hydrodynamics, which should be studied. Also, in the current column setup, there were too many intrusive ports that influenced the solids mixing. It is thus recommended to design a column of few ports to investigate solids mixing and effects of orifice angle especially for shallow beds. Finally, the orifice inclination angles that were chosen were not steep enough to create high magnitudes of swirling. It is recommended to study different designs of distributors with steeper angles such as 15°.

References

Baba, T., M. Nakajima, S. Morooka, and H. Matsuyama. 1984. A new measuring system for flow patterns of solid particles in gas-solid fluidized bed. Journal of Chemical Engineering of Japan 17 (3): 275-9.

Collin, A., K. -E Wirth, and M. Stroeder. 2009. Characterization of an annular fluidized bed. Powder Technology 190 (1): 31-5.

Davidson, J.F., 1961, in Symposium on fluidization – discussion, Trans. Instn. Chem. Engrs.. 39. 230-232.

Felipe, C. A. S., and S. C. S. Rocha. 2007. Prediction of minimum fluidization velocity of gas–solid fluidized beds by pressure fluctuation measurements — analysis of the standard deviation methodology. Powder Technology 174 (3): 104-13.

Fogler, H. 2006. Elements of chemical reaction engineering. 4th ed. Upper Saddle River, NJ: Prentice Hall PTR.

Ghaly A.E., K.N. Macdonald. 2012. mixing patterns and residence time determination in a bubbling fluidized bed system. American Journal of Engineering and Applied Sciences 5 (2): 170-83.

Geldart, D. 1973. Types of gas fluidization. Powder Technology 7 (5): 285-92.

Geldart, D. (1997). Mixing in fluidized beds. In Chemistry and Chemical Engineering. Mixing in the process industries (2nd ed., pp. 62-78).

Goswami, S., B. Jayashre, J. Samantray, D. Gupta, and H. Pant. 2014. Measurement of mixing time and holdup of solids in gas–solid fluidized bed using radiotracer technique. Journal of Radioanalytical and Nuclear Chemistry 302 (2): 845-50.

Harris, A. T., J. F. Davidson, and R. B. Thorpe. 2002. A novel method for measuring the residence time distribution in short time scale particulate systems. Chemical Engineering Journal 89 (1): 127-42.

Kaewklum, R., V. I. Kuprianov, and P. L. Douglas. 2009. Hydrodynamics of air–sand flow in a conical swirling fluidized bed: A comparative study between tangential and axial air entries. Energy Conversion and Management 50 (12): 2999-3006.

Kaewklum, R., and V. I. Kuprianov. 2010. Experimental studies on a novel swirling fluidized-bed combustor using an annular spiral air distributor. Fuel 89 (1): 43-52.

Karri, S. 2003. "Gas Distributor and Plenum Design in Fluidized Beds" Chapter 6 In Handbook of fluidization and fluid-particle systems. Vol. 91 New York: Marcel Dekker.

Kojima, T., K. Ishihara, Y. Guilin, and T. Furusawa. 1989. Measurement of solids behaviour in a fast fluidized bed. Journal of Chemical Engineering of Japan 22 (4): 341-6.

Kroger, D., E. K. Levy, and J. C. Chen. 1979. Flow characteristics in packed and fluidized rotating beds. Powder Technology 24 (1): 9-18.

Kumar, V., M. F. Batcha and V.R. Raghavan. 2011. Study of the fluid dynamic performance of distributor type in torped type reactors. Engineering Transaction 6 (1): 70-5.

Kunii, D., and O. Levenspiel. 1991. Fluidization engineering. 2nd ed. Boston: Butterworth-Heinemann.

Liu, D., and X. Chen. 2012. Quantifying lateral solids mixing in a fluidized bed by modeling the thermal tracing method. AIChE Journal 58 (3): 745-55.

Miin, C.S., S.A. Sulaiman, V.R. Raghavan, M.R. Heikal, and M.Y. Naz. 2015. Hydrodynamics of multi-sized particles in stable regime of a swirling bed. Korean Journal of Chemical Engineering 32 (11): 2361-7.

Mohideen, M.F., B. Sreenivasan, S.A. Sulaiman, and V.R. Raghavan. 2012. Heat transfer in a swirling fluidized bed with geldart type-D particles. Korean Journal of Chemical Engineering 29 (7): 862-7.

Morooka, S., K. Kusakabe, N. Ohnishi, F. Gujima, and H. Matsuyama. 1989. Measurement of local fines movement in a fluidized bed of coarse particles by a fluorescent tracer technique. Powder Technology 58 (4): 271-7.

Naz, M., and S. Sulaiman. 2016. PTV profiling of particles motion from the top and side of a swirling fluidized bed. Journal of Instrumentation 11: P05019.

Ouyang, F., and O. Levenspiel. 1986. Spiral distributor for fluidized beds. Industrial & Engineering Chemistry Process Design and Development 25 (2): 504-7.

Pallarès, D., F. Johnsson. 2006. A novel technique for particle tracking in cold 2-dimensional fluidized beds—simulating fuel dispersion. Chemical Engineering Science 61 (8): 2710-20.

Perry, R. H., and D.W. Green. 2008. Perry's chemical engineers' handbook. 8th ed. New York: McGraw-Hill.

Ran, X., F. Wei, Z. Wang, and Y. Jin. 2001. Lateral solids dispersion in a high-density riser with swirling air flow. Powder Technology 121 (2): 123-30.

Sreenivasan, B., and V.R. Raghavan. 2002. Hydrodynamics of a swirling fluidised bed. Chemical Engineering & Processing: Process Intensification 41 (2): 99-106.

Takahashi, T., Z. Tanaka, A. Itoshima, and L.T. Fan.1984. Performance of a rotating fluidized bed. Journal of Chemical Engineering of Japan 17 (3): 333-6.

Wen, C. Y., and Y. H. Yu. 1966. A generalized method for predicting the minimum fluidization velocity. AIChE Journal 12 (3): 610-2.

Yang, T., and X. Bi. 2009. Novel fluidized bed reactor for integrated NOx adsorption-reduction with hydrocarbons. Environmental Science & Technology 43 (13): 5049-53.

Yudin, A., S. Anuar, and A. Oumer. 2016. Improvement on particulate mixing through inclined slotted swirling distributor in a fluidized bed: An experimental study. Advanced Powder Technology 27 (5): 2102-11.

Appendix A: Distributor designs

The distributors were designed and fabricated in-house. They were made of Plexiglas. They were designed to have a target pressure drop of 2500 Pa for a bed depth of 150 mm. The pressure drop was calculated according to Karri (2003):

$$\Delta P = Kg\rho L \qquad \text{A-1}$$

Where K = 0.3. The gas velocity through the holes were then calculated according to Karri (2003) as:

$$U_h = C_d\sqrt{\frac{2\Delta P}{\rho_g}} \qquad \text{A-2}$$

The orifice coefficient C_d depends on the plate thickness and the hole pitch. The plate thickness was chosen to be 9.5 mm due to limited time for ordering from the workshop. Square pitch design was used to calculate the holes pitch length according to Karri (2003) using the following equation:

$$L_h = \frac{1}{\sqrt{N_d}} \qquad \text{A-3}$$

To start, the orifice discharge coefficient was assumed to be 0.77 according to Karri (2003) and from that number, the holes' gas velocity was calculated to be equal to 49 m/s. The volumetric flow rate was given by the capacity of the air blower. Since the blower capacity is very large because the column was designed for turbulent fluidization, an experiment was done to determine the least flow rate to be used. It was determined to be at ¼ of the blower's capacity and was equal to 106 cubic meters per hour. Table A-1 shows the design calculations.

Table A-1 Distributor design calculations

Distributor design for Q = 106 N m^3 / h					
Hole diameter (mm)	Number of holes (#)	Hole density (holes/m^2)	Square pitch length (mm)	t/d_h	C_d, calculated
1.6	303	4589	14.8	6	0.79
2.4	135	2040	22.1	4	0.79
3.2	76	1147	29.5	3	0.79

The number of holes was calculated from Karri (2003) as follows:

$$N = \frac{1.14}{d_h^2} \qquad \text{A-4}$$

Several hole diameters were chosen depending on the drill sizes available at the workshop. From the holes' diameter, the number of holes was determined. The final holes' diameter was chosen to be 3.18 mm with 76 holes. A hollow cylinder was then placed in the middle of the distributor covering some of the holes. The diameter of the cylinder was chosen so that the annulus width formed was 100 mm. The total number of holes was then determined to be 60 holes.

Appendix B: Pressure transducers calibration procedure

The pressure transducers were calibrated using a previously calibrated digital manometer. The calibration took place using the fluidized bed reactor set-up. First, the digital manometer was used to measure the pressure drop across the distributor with no flow to establish the zero reference point. Then, the air flow was turned on and the digital manometer was used instead of the pressure transducers to read the pressure drop across the distributor. Several trials were made to obtain the calibration curve as shown in Figures B-1 and B-2.

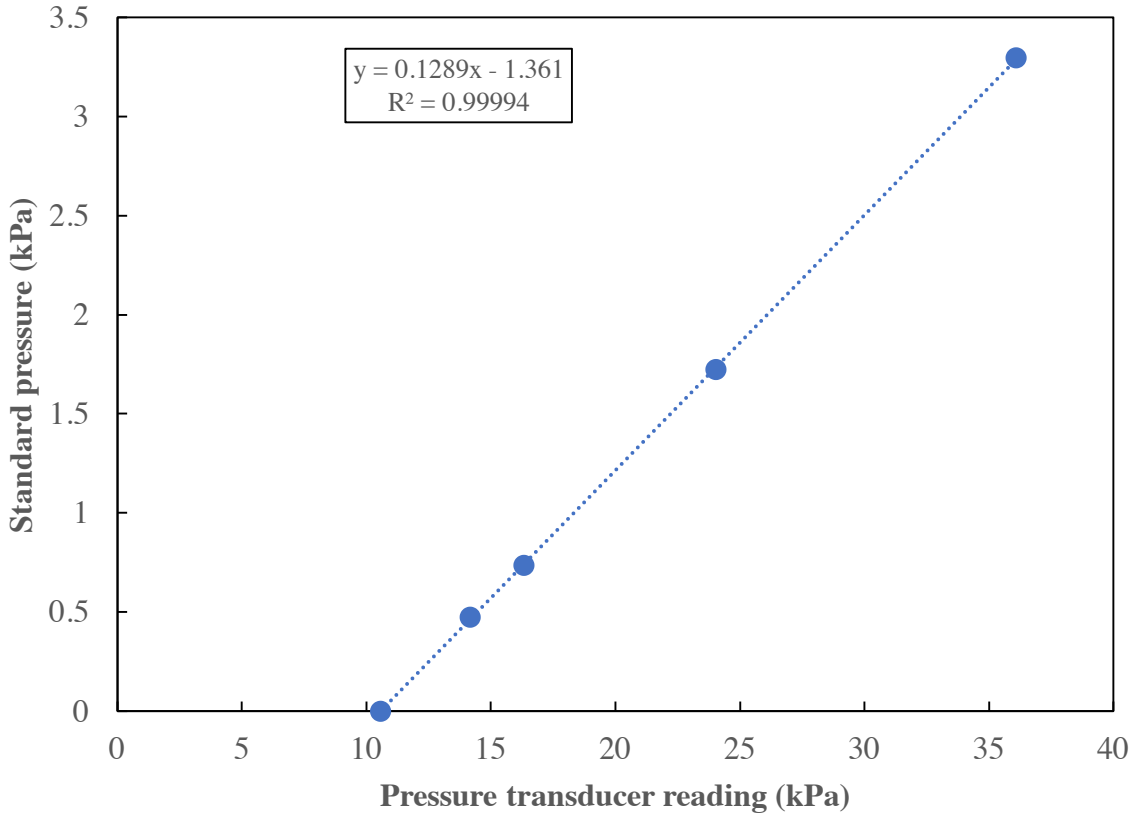

Figure B-1 Pressure transducer calibration for distributor pressure drop

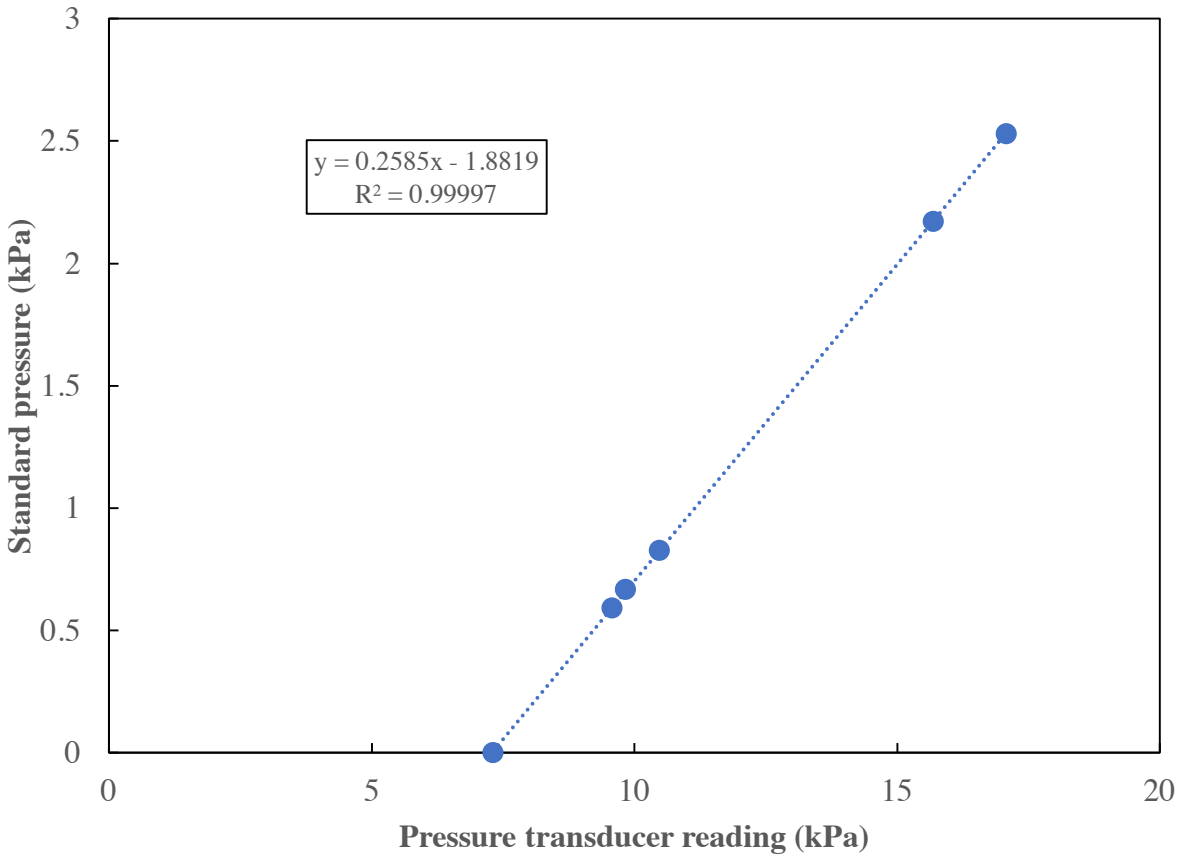

Figure B-2 Pressure transducer calibration for orifice

Appendix C: Graphical determination of U_{mf}

The minimum fluidization velocity (U_{mf}) was determined using the pressure drop-velocity curve method. The minimum fluidization velocity is defined as the velocity at which the bed pressure drop flattens out and is nearly equal to the bed weight-minus buoyancy. Figure C-1 illustrates graphically how to determine of the minimum fluidization velocity.

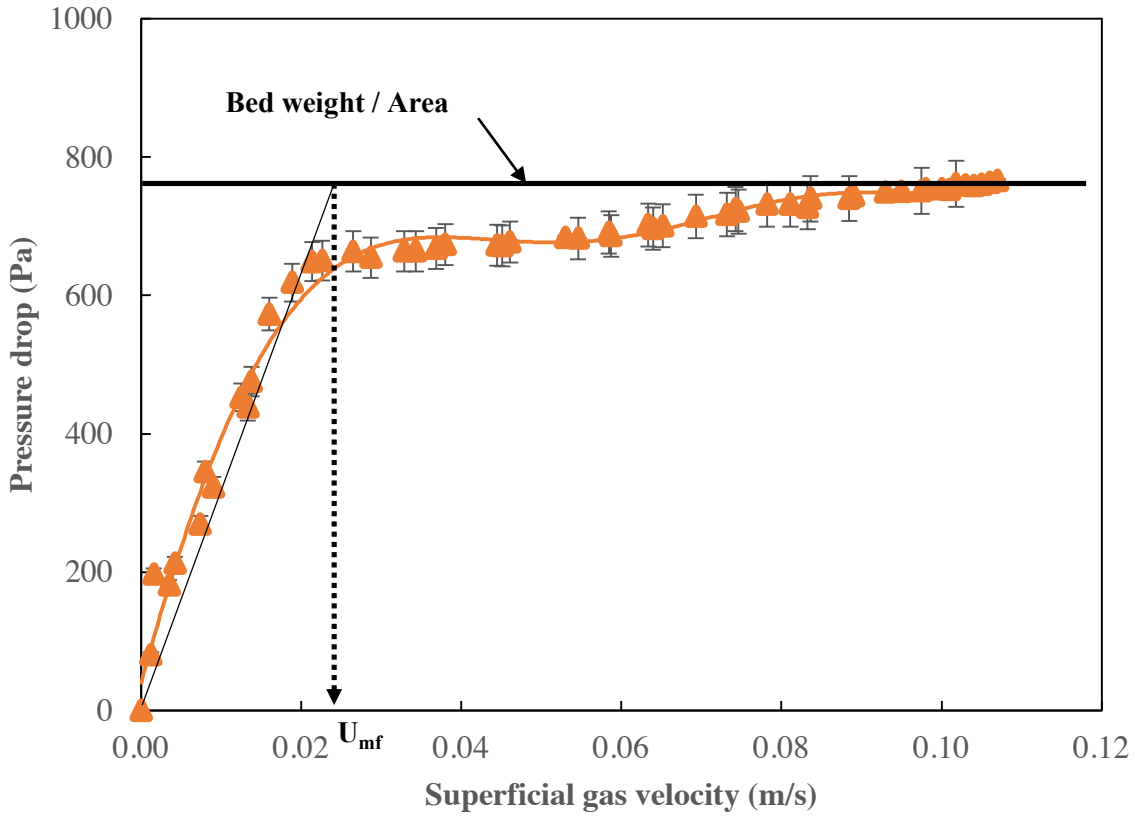

Figure C-1 Illustration of U_{mf} graphical determination